VILNIUS UNIVERSITY
CENTER FOR NATURAL SCIENCES AND TECHNOLOGY

Darius
GAILEVIČIUS

Photonic Crystals for Manipulation of Spatial Propagation of Light Beams

DOCTORAL DISSERTATION

Natural sciences
Physics N 002

VILNIUS 2019

This dissertation was written between 2015 and 2019 at Vilnius University.

Academic supervisor:
Prof. Dr. Roaldas Gadonas (Vilnius University, Natural sciences, Physics, N 002, from 1st of October 2015 to 9th of April 2019.)
Prof. Habil. Dr. Kęstutis Staliūnas (ICREA Research Professor at Universitat Politècnica de Catalunya (UPC), Natural sciences, Physics, N 002, from 10th of April 2019.)

Dissertation Defence Panel:

Chairman – **Prof. habil. dr. Audrius Dubietis** (Vilnius University, Natural sciences, Physics, N 002).
Members:
dr. Andrejus Michailovas (Center For Physical Sciences And Technology, Natural sciences, Physics, N 002)
Prof. habil. dr. Valdas Sirutkaitis (Vilnius University, Natural sciences, Physics, N 002).
habil. dr. Gintaras Valušis [Center For Physical Sciences And Technology, Natural sciences, Physics, N 002]
Prof. dr. Mikas Vengris (Vilnius University, Natural sciences, Physics, N 002).

The dissertation shall be defended at a public meeting of the Dissertation Defence Panel at 10:00 on 30th of September 2019 in Auditorium 306 of the Vilnius University Laser Research center. Address: Sauletekio al. 10, 306 aud., Vilnius, Lithuania, tel. +370 5 236 6005; e. mail info@itpc.vu.lt

The text of this dissertation can be accessed at the libraries of Vilnius University Library, as well as on the website of Vilnius University: www.vu.lt/lt/naujienos/ivykiu-kalendorius

VILNIAUS UNIVERSITETAS
FIZINIŲ IR TECHNOLOGIJOS MOKSLŲ CENTRAS

Darius
GAILEVIČIUS

Fotoniniai kristalai šviesos pluoštų erdviniam sklidimui valdyti

Disertacija rengta 2015–2019 metais Vilniaus universiteto Lazerinių tyrimų centre.

Mokslinis vadovas:

Prof. Dr. Roaldas Gadonas (Vilniaus universitetas, fiziniai mokslai, fizika, N 002, vadovavo nuo 2015 m. spalio 1 d. iki 2019 m. balandžio 9 d.)

Prof. Habil. Dr. Kęstutis Staliūnas (ICREA, „Universitat Politècnica de Catalunya" (UPC), N 002, vadovavo nuo 2019 m. balandžio 10 d.)

Gynimo taryba:

Pirmininkas – **Prof. habil. dr. Audrius Dubietis** [Vilniaus universitetas, fiziniai mokslai, fizika, N 002]

Nariai:

dr. Andrejus Michailovas [Fizinių ir technologijos mokslų centras, fiziniai mokslai, fizika, N 002]

Prof. habil. dr. Valdas Sirutkaitis [Vilniaus universitetas, fiziniai mokslai, fizika, N 002]

habil. dr. Gintaras Valušis [Fizinių ir technologijos mokslų centras, fiziniai mokslai, fizika, N 002]

Prof. dr. Mikas Vengris [Vilniaus universitetas, fiziniai mokslai, fizika, N 002]

Disertacija ginama viešame Gynimo tarybos posėdyje 2019 m. rugsėjo mėn. 30 d. 10 val. fizikos fakulteto lazerinių tyrimų centro 306 auditorijoje. Adresas: Sauletekio al. 10, 306 aud., Vilnius, Lietuva,, tel. +370 5 236 6005; el. paštas info@itpc.vu.lt.

Disertaciją galima peržiūrėti Vilniaus universiteto bibliotekoje bibliotekose ir VU interneto svetainėje adresu: https://www.vu.lt/naujienos/ivykiu-kalendorius

Acknowledgements

The immense scope of my academic endeavors would have been not possible without the support of the academic community of our Vilnius University's Laser Research Center and all of my coauthors. Also, I want to acknowledge my previous supervisor Prof. Habil. Dr. Roaldas Gadonas for the great academic freedom he allowed me and my current supervisor for Prof. Habil. Dr. Kęstutis Staliūnas for guiding me through my scientific carrier.

I thank Femtika UAB for allowing me access to their facilities and resources to complete the Bessel - DLW experiments.

I thank Light Conversion UAB for the help in maintaining our fs-laser sources well beyond what could have been expected otherwise.

Thanks to my senior colleagues and highly qualified researchers dr. Vytautas Purlys and dr. Martynas Peckus with whom we worked closely together on the topic of photonic crystal filtering.

I acknowledge dr. Viktor B. Taranenko from the National Academy of Sciences of Ukraine for his exceptional knowledge and expertise in experimental laser physics that he shared with me during our collaboration.

Thanks to senior colleagues and highly qualified researchers dr. Mangirdas Malinauskas, dr. Sima Rekštytė, prof. Vygantas Mizeikis and prof. Saulius Juodkazis with whom we collaborated on projects that, although not part of this dissertation, bore fruit as great research results.

Thanks to dr. Akvile Zabiliūtė-Karaliūnė for a well made initial LaTeX dissertation template.

Thanks to Laser Research Center's Optician Šarūnas Jablonskas for preparing multiple samples for my experiments.

Thanks to Kristina Babrauskaitė for proofreading and providing helpful advice on the summary part of my manuscript.

Thanks to Nail Garejev for helping me navigate the formalities of the Ph.D. process.

Finally, I thank my parents Rimas and Genė Gailevičiai and brother Gediminas Verbauskas for supporting me all these years.

A lot of my research was partly funded by different grants from the Research Council of Lithuania, including travel grants and an additional stipend.

Contents

List of abbreviations

1D	one-dimensional
2D	two-dimensional
3D	three-dimensional
AR	anti-reflective
BAS	Broad Aperture Semiconductor (laser)
BPM	Beam-propagation method
CCD	Charge coupled device
CW	Continuous-wave (laser operation regime)
DLW	Direct laser writ(e/ing)
FAC	Fast-axis Collimator
FDTD	Finite difference time domain (method)
fs	femtosecond
FWHM	Full width at half maximum
HeNe	Helium Neon (laser)
HR	highly-reflective
IR	infrared (range or wavelength)
Nd:YAG	neodymium-doped yttrium aluminum garnet; Nd:Y3Al5O12
PBG	Photonic bandgap
PhC	Photonic Crystal
RCWA	Rigorous Coupled Wave Analysis
SEM	scanning electron microscope
TE	transverse electric (polarization)
TEM	transmissive electro-magnetic (mode)
TM	transverse magnetic (polarization)
UVFS	ultra-violet grade fused silica
VCSEL	Vertical-cavity surface-emitting laser
VECSEL	Vertical-external-cavity surface-emitting laser
VIS	visible (range or wavelength)

Introduction

Photonics is a term currently understood to mean the generation, handling and detection of optical radiation. My work here generally centers around a specific area of photonics associated with periodic structures, in particular, spatially periodic concerning the refractive index of a structure. This periodicity, in other words, the order is the reason for many interesting light-matter interaction effects. Nature has already made use of these in the form of pigmentless iridescent colors of the peacock's tail [1] or blue morpho butterfly [2] *etc.* To begin with, the name of those periodically modulated refractive index structures is "Photonic crystal" (abbrev. PhC). The refractive index can be modulated along any possible direction is space, from 1-dimensional examples, where the pattern is repeated, as the name implies in one direction, to 3-dimensional. Periodicity is not enough for interesting interactions as the PhC lattice must also be on the scale of the wavelength λ of interest and often be oriented in the right direction. To recognize these conditions, where there is no absorption is not trivial.

Photonic crystals, are celebrated for their properties in the frequency domain, such as frequency bandgaps and slow light effect [3, 4], however, they can also affect the spatial beam propagation, causing such peculiarities as the negative refraction [5, 6], anomalous diffraction (flat lensing) [7, 8], and, most importantly for the present work – spatial (angular) filtering. The spatial filtering by PhCs is based on the angular bandgaps [9, 10] and angular quasi-bandgaps [11, 12], and does not require the access to the far-field domain of resonating field unlike with conventional filtering techniques by confocal lens arrangements.

Both cases are explored here in my thesis, beginning with the problem of producing such structures so they can be examined, expanding the theory of how can they be improved, and finally testing how the electromagnetic field behaves in a positive feedback system, such as a laser cavity.

Goal of the dissertation

By using the numerical and available micro-fabrication techniques to produce and characterize Photonic crystal filters with well understood properties to be applicable in laser cavities.

Novelty and importance of the work

1. A new method for forming Laue regime PhC spatial filters using a Bessel beam based direct laser write approach was developed to overcome PhCs length limitations.

2. Bragg regime Photonic crystals have been experimentally shown to facilitate a spatial filtering effect in the visible range.

3. The axisymmetric geometry photonic crystals with linear modulation of the longitudinal period were demonstrated. It was shown, that the far-field filtering band angle-width is improved by a factor of two.

4. It was experimentally demonstrated that non-linear *vs.* linear chirped modulation of the longitudinal periods (chirp) improves the transmission profile for two-dimensional Laue regime photonic crystals for spatial light filtering.

5. A microchip laser combined with an intra-cavity axisymmetric photonic crystal spatial filter has been demonstrated featuring an increased beam brightness by a factor of three.

6. A broad area emitting external cavity semiconductor laser combined with an intra-cavity photonic crystal spatial filter has been demonstrated to feature enhanced beam brightness.

Statements to defend

1. 2D Photonic crystals arranged in the Laue regime for spatial filtering can be realized using a Bessel beam DLW approach, therefore removing the experimental limitation of the number of longitudinal periods and consequently increasing the achievable filtering angular bandwidth to $\sim$4° in the visible and 6° in the infrared operational wavelength regimes.

2. 2D Photonic crystals, arranged in the transmission Bragg regime as conformal thin-film dielectric layers deposited on a periodically modulated 1D relief grating template, show detectable signs of spatial filtering through a stop-gap mechanism in the visible regime.

3. 3D axisymmetric Photonic crystals arranged in the Laue regime for spatial filtering for the VIS ($\lambda = 633$ nm) wavelength range can be realized using a Gaussian beam DLW approach to have a longitudinal period linear chirp structure that due to a change of the central filtering angle along the PhC structure results in an increased from 17 mrad to 43 mrad angular filtering interval.

4. 2D Photonic crystals that are arranged in the Laue spatial filtering geometry and are fabricated using the DLW method have non-trivial longitudinal period length (interlayer distance) chirp variations, wherein such variations that match selected far-field intensity transmission (filtering) profiles can be discovered using the numeric gradient and genetic optimization algorithms.

5. 3D axisymmetric photonic crystals arranged in the Laue regime for spatial filtering can produce an increase in the observed beam brightness of an axially pumped continuous-wave operation Nd:YAG laser by a factor of 3 by introducing a far-field domain intensity transmission profile that suppresses the higher-order resonant cavity transverse modes.

6. The emitted beam brightness of an external cavity single emitter broad-edge emitting semiconductor IR laser ($\lambda = 970$ nm) can be increased at least by a factor of 1.5 by an intracavity 2D photonic crystal Laue regime spatial filter that introduces a far-field domain angular loss profile for slow-axis plane suppressing the higher-order resonant cavity transverse modes.

Layout of the dissertation

The dissertation is segmented in 4 main parts, or chapters. The first part introduces the reader to the terms that I preferred to use, the second new finding on new types of PhCs by media and fabrication method, the third part to the solution of tuning the geometry of Laue PhC filters and the fourth demonstrating new types of lasers with integrated PhCs.

Contribution of the author

The main co-authors of the research results presented in the Thesis are prof. dr. R. Gadonas, prof. dr. K. Staliūnas, dr. V. Purlys, dr. M. Peckus, PhD student L. Grinevičiūtė, dr. Tomas Tolenis., Master student Ceren Babayt, dr. Carsten Bree, PhD student Sandeep Gawali.

Contribution of thesis author is further noted in accordance to the list of Thesis papers.

A1: sample fabrication, characterization, data analysis, numeric modeling, drafting the figures, preparing the manuscript in equal part with the co-authors.

A2: sample fabrication, characterization, data analysis, development of numeric model, simulations, drafting the figures, preparing the manuscript in equal part with the co-authors.

A3: sample fabrication, characterization (microscope, wet-etching), drafting the figures and preparing the manuscript in equal part with the co-authors.

A4: sample fabrication, characterization, data analysis, development of numeric model, simulations, drafting the figures, preparing the manuscript in at least in by 1/3.

A5: development of the initial numeric model (limited to BPM implementation).

A6: substrate (grating template) preparation/replication, single pass focused beam characterization, preparing the manuscript in equal part with the co-authors. It is notable here that junior colleagues had exceptional roles: Ceren Babayt performed the FDTD calculations, and Lina Grinevičiūtė performed the thin-film deposition experimtents, AFM characterization.

A7: fabrication system adaptation, sample fabrication, characterization, data analysis, drafting 3/4 of the figures, preparing the manuscript in equal part with the co-authors. Notable that dr. V. Purlys designed and tested the first implementation of the Bessel-DLW system.

A8: fabrication system adaptation, sample fabrication, single-pass regime characterization. It is notable here that junior colleague: Sandeep Gawali, performed the experiments on the laser cavity.

Approbation of the research results

This section presents the lists of papers, patents and conferences related to the dissertation. In the doctoral dissertation the following papers.

List of papers and patents related to the dissertation

A1 D. Gailevicius, V. Purlys, L. Maigyte, M. Peckus, and K. Staliunas, "Chirped axisymmetric photonic microstructures for spatial filtering," J. Nanophotonics **8**(1), 084094 (2014).

A2 D. Gailevičius, V. Purlys, L. Maigytė, E. Gaižauskas, M. Peckus, R. Gadonas, and K. Staliūnas, "Femtosecond direct laser writing of photonic spatial filters in soda–lime glass," Lith. J. Phys. **55**(3), 1–5 (2015).

A3 D. Gailevicius, V. Koliadenko, V. Purlys, M. Peckus, V. Taranenko, and K. Staliunas, "Photonic Crystal Microchip Laser," Sci. Rep. **6**(1), 34173 (2016).

A4 D. Gailevičius, V. Purlys, M. Peckus, R. Gadonas, and K. Staliunas, "Spatial Filters on Demand Based on Aperiodic Photonic Crystals," Ann. Phys. **529**(8), 1700165 (2017).

A5 C. Brée, D. Gailevičius, V. Purlys, G. G. Werner, K. Staliunas, A. Rathsfeld, G. Schmidt, and M. Radziunas, "Chirped photonic crystal for spatially filtered optical feedback to a broad-area laser," J. Opt. **20**(9), 095804 (2018).

A6 L. Grineviciute, C. Babayigit, D. Gailevičius, E. Bor, M. Turduev, V. Purlys, T. Tolenis, H. Kurt, and K. Staliunas, "Angular filtering by Bragg photonic microstructures fabricated by physical vapour deposition," Appl. Surf. Sci. **481**, 353–359 (2019).

A7 D. Gailevičius, V. Purlys, and K. Staliunas, "Photonic Crystal Spatial Filters Fabricated by Femtosecond Pulsed Bessel Beam," arXiv:1908.02842 [physics.app-ph] (2019). (Submitted for peer review to Optics Letters)

A8 S. Gawali, D. Gailevičius, G. Gerre-Werner, V. Purlys, C. Cojocaru, J. Trull, J. Montiel-Ponsoda, and K. Staliunas, "Photonic crystal spatial filtering in broad aperture diode laser," arXiv:1906.05242 [physics.optics] (2019). (Submitted for peer review in Applied Physics Letters)

List of conference contributions related to the dissertation

B1 <u>Darius Gailevičius</u>, Lina Grinevičiūtė, Vytautas Purlys, Tomas Tolenis, Roaldas Gadonas, Kestutis Staliunas, Photonic crystals for visible wavelength via physical vapour deposition, 11th International Conference on Photo-Excited Processes and Applications – ICPEPA 11, September 10-14, 2018, Vilnius, Lithuania. Poster presentation.

B2 <u>D. Gailevicius</u>, V. Koliadenko, V. Purlys, M. Peckus, V. Taranenko, K. Staliunas, "Microchip Laser based on a Photonic Crystal", Laser Precision Microfabrication Symposium 2017, Toyama, Japan, 2017. Oral presentation.

B3 <u>D. Gailevicius</u>, V. Purlys, M. Peckus, R. Gadonas, K. Staliunas, "Beam shaping with optimized photonic crystals from Chirp to Numeric Design", Laser Precision Microfabrication Symposium 2017, Toyama, Japan, 2017. Oral presentation.

B4 <u>Darius Gailevičius</u>, Vytautas Purlys, Martynas Peckus, Roaldas Gadonas, Kestutis Staliunas, "Beam shaping with numerically optimized photonic crystals", SPIE Photonics West, San Francisco, USA, 2017. Oral presentation.

B5 <u>D. Gailevicius</u>, V. Koliadenko, V. Purlys, M. Peckus, V. Taranenko, K. Staliunas, "Photonic crystal microchip laser", SPIE Photonics West, San Francisco, USA, 2017. Oral presentation.

B6 <u>D. Gailevicius</u>, V. Purlys, L. Maigyte, E. Gaizauskas, M. Peckus, R. Gadonas, K. Staliunas, Asymmetric 2D spatial beam filtering by photonic crystals, SPIE Photonics Europe 2016, Brussels, Belgium, April 2016. Oral presentation.

B7 <u>D. Gailevicius</u>, V. Purlys, L. Maigyte, M. Peckus, R. Gadonas, K. Staliunas, "Beam Shaping with Axisymmetric Photonic Crystals", Open Readings 2015, Vilnius. Poster presentation.

B8 <u>D. Gailevicius</u>, V. Purlys, M. Peckus, E. Gaizauskas, L. Maigyte, K. Staliunas, "Direct femtosecond laser writing of photonic crystal based spatial filters in soda lime glass", 15th International Symposium on Laser Precision Microfabrication, Vilnius, Lithuania, 2014 June. Poster presentation.

List of papers not included as part of the dissertation

C1 L. Maigyte, V. Purlys, J. Trull, M. Peckus, C. Cojocaru, D. Gailevičius, M. Malinauskas, and K. Staliunas, "Flat lensing in the visible frequency range by woodpile photonic crystals," Opt. Lett. **38**(14), 2376 (2013).

C2 V. Purlys, L. Maigyte, D. Gailevičius, M. Peckus, M. Malinauskas, and K. Staliunas, "Spatial filtering by chirped photonic crystals," Phys. Rev. A **87**(3), 033805 (2013).

C3 V. Purlys, L. Maigyte, D. Gailevičius, M. Peckus, R. Gadonas, and K. Staliunas, "Super-collimation by axisymmetric photonic crystals," Appl. Phys. Lett. **104**(22), 221108 (2014).

C4 V. Purlys, L. Maigyte, D. Gailevičius, M. Peckus, M. Malinauskas, R. Gadonas, and K. Staliunas, "Spatial filtering by axisymmetric photonic microstructures," Opt. Lett. **39**(4), 929 (2014).

C5 S. Rekštytė, T. Jonavičius, D. Gailevičius, M. Malinauskas, V. Mizeikis, E. G. Gamaly, and S. Juodkazis, "Nanoscale Precision of 3D Polymerization via Polarization Control," Adv. Opt. Mater. **4**(8), 1209–1214 (2016).

C6 L. Jonušauskas, D. Gailevičius, L. Mikoliūnaitė, D. Sakalauskas, S. Šakirzanovas, S. Juodkazis, and M. Malinauskas, "Optically Clear and Resilient Free-Form μ-Optics 3D-Printed via Ultrafast Laser Lithography," Materials (Basel). **10**(1), 12 (2017).

C7 D. Gailevičius, V. Padolskytė, L. Mikoliūnaitė, S. Šakirzanovas, S. Juod-kazis, and M. Malinauskas, "Additive-manufacturing of 3D glass-ceramics down to nanoscale resolution," Nanoscale Horizons **4**(3), 647–651 (2019).

1.   Conceptual overview

Photonics is a term currently understood to mean the generation, handling and detection of optical radiation. My work here generally centers around a specific area of photonics associated with periodic structures, in particular, spatially periodic concerning the refractive index of a structure. This periodicity, in other words – order, is the reason for many interesting light-matter interaction effects. Nature has already made use of these in the form of pigment-less iridescent colors of the peacock's tail [1] or blue morpho butterfly [2] *etc.* The selective interaction between radiation of a particular wavelength and the periodic structure is the key here. In my thesis, I will demonstrate how these structures can be made, understood and used for a particular industrial application.

Photonic crystals

To begin with, the name of those periodically modulated refractive index structures is "Photonic crystal" (abbrev. PhC). The refractive index can be modulated along any possible direction is space, from 1-dimensional examples, where the pattern is repeated, as the name implies in one direction, to 3-dimensional. Periodicity is not enough for interesting interactions as the PhC lattice must be on the scale of the wavelength λ of interest and often be oriented in the right direction. To recognize these conditions, where there is no absorption is not trivial.

Historically speaking, the first example of such structure was a crystalline mineral examined by Lord Rayleigh. The mineral was correctly recognized to have particular optical transmission and reflection properties not due to absorption, but due to its periodic structure [13]. A particular reflection appeared, when for a particular observed wavelength, the lattice constant was of half-wavelength ($\lambda/2 \approx d$). Following this discovery, it took a century for the nomenclature of Photonic crystal to be born in the context of structures modulated in three dimensions [14, 15]. The property of interest that characterizes these structures is most often called the photonic-bandgap.

1.1. The photonic bangap and spatial filtering

Photonic crystals, besides their celebrated properties in the frequency domain, such as frequency bandgaps and slow light effects [3, 4], can also affect the spatial beam propagation, causing such peculiarities as the negative refraction [5, 6], anomalous diffraction (flat lensing) [7, 8], and importantly for the present work – spatial (angular) filtering. The spatial filtering by PhCs is based on the angular bandgap PhCs [9, 10] and angular quasi-bandgaps PhC [11, 12], and does not require the access to the far-field domain of resonating field like with conventional filtering techniques by a confocal lens arrangement.

Spatial (or angular) filtering is frequently used to improve the spatial quality of light beams by removing the undesired angular or far-field components of the radiation. Conventional design for spatial filtering comprises a confocal system of lenses with a diaphragm of appropriate diameter positioned in the confocal plane, blocking the undesired angular components of the spatial spectrum [16]. Such a configuration extends over at least two focal lengths of both lenses and is of a relatively large size – it could hardly be used in micro- or nano-scale photonic devices. Other, more sophisticated arrangements for spatial filtering are based on liquid–crystal cells [17], utilization of thin-film interfaces [18], anisotropic media [19], metallic grids [20], *etc.* have not resulted in widespread technological applications. Recently, an alternative approach to spatial filtering has been suggested, which is based on the propagation of light beams through photonic crystals (PhCs) — materials with a periodic modulation of the refractive index on a wavelength scale [21, 9, 22, 10]. PhC based spatial filters are potentially advantageous due to their relatively small size as compared to the conventional spatial filters, which could enable the integration of such filters into micro-optical devices or micro-laser resonators.

These filters are based on the well-known property of PhCs – photonic bandgaps, i.e., forbidden frequency ranges at which light waves cannot propagate [15]. The PhCs, thus in general, can provide frequency (chromatic) filtering, eliminating (reflecting) specific frequency components from the incident radiation. Similar to the chromatic bandgaps (complete photonic bandgaps), angular bandgaps (partial photonic bandgaps or stopgaps) can also appear in PhCs, which can be engineered in such a way that for a given frequency only on- and around- axis waves are allowed to propagate. Angular filtering has been shown in two- and three-dimensional (2D and 3D) PhCs in the microwave and infrared spectral range [21, 9, 22, 10]. Most simple mechanisms of spatial filtering by PhCs are based on angular band gaps, which appear if a condition related to a longitudinal modulation period: $d_{||} \lesssim \lambda/2$, is met. However, despite the enormous progress in micro and nano-structure fabrication technologies, the latter condition was still difficult to fulfill in the visible and near-infrared ranges. Perhaps, this is the reason why the spatial filtering

by angular band gaps has never been before experimentally demonstrated in optics. However, indeed such a filter has been realized and is further elaborated on in section 2.3.
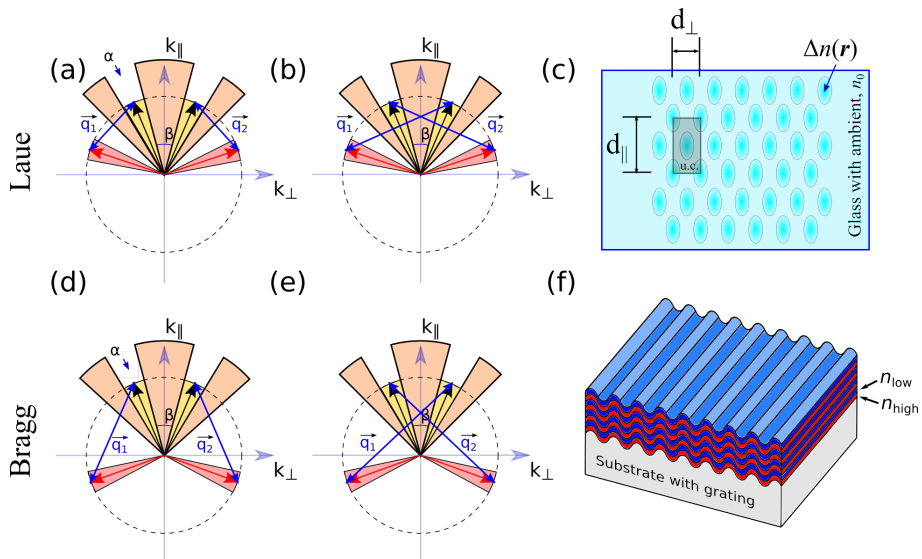
Figure 1.1: Illustration of spatial filtering in a 2D PhC: Laue mechanism of resonant wave scattering in a gapless configuration for first order same sign $\pm|\alpha| \implies \pm|\beta|$ (a) and opposite sign $\mp|\alpha| \implies \pm|\beta|$ (b) deflection and the corresponding model lattice structure (c); Bragg mechanism for first order same sign $\pm|\alpha| \implies \pm|\beta|$ (d) and opposite sign $\mp|\alpha| \implies \pm|\beta|$ (e) reflection and corresponding model lattice structure (f). Filtering occurs when the waves in the yellow triangle, centered around the α, incidence zones get into resonant scattering condition with PhC lattice wave vectors $\vec{q_{1,2}} = (q_\perp, q_\parallel)$. u.c. - denoted the unit cell, $\Delta n(\mathbf{r})$ - the spatial refractive index distribution.

As an alternative to the spatial filtering based on the angular band gaps, a mechanism of PhC based spatial filtering was proposed with the PhCs arranged in a gapless (or quasi angular bandgap) configuration [23]. In the latter case, a deflection of the angular components of radiation in the forward direction is observed (see fig. 1.1). The gapless spatial filtering can be obtained for substantially larger longitudinal periods of modulation $d_{||} > \lambda/2$; hence, current fabrication techniques can be applied more efficiently. Such kind of filtering has been recently demonstrated experimentally in different 3D configurations using PhCs with a rectangular symmetry in transverse space [11, 24], as well as photonic structures with axisymmetric rings [25, 26]. The gapless filtering has been recently proposed also to clean atomic ensembles on Bose-Einstein condensates [27].

1.2. Principles

To help the reader better understand the physical mechanism of how such a filter works, I will outline the terms and principles of two types of filters: Laue and Bragg. The terminology used here was proposed in ref. [12]. The directionally selective structures that have longitudinal periods larger than the wavelength $\lambda/2 < d_z$ will be referred to as operating in the Laue regime. The term here is used in analogy to forward X-Ray diffraction in crystalline materials (Laue diffraction [28]), however, reserved for the optical context [29]. Following this train of thought, I define the Bragg regime for the case of $\lambda/2 \gtrsim d_z$ in the same crystallographic X-Ray diffraction that produces strong reflections for particular angles of incidence from periodic structures [30]. This basically corresponds to the case of said optical photonic bandgap structures, but it should be easier to grasp in the sense of constructive and destructive interference, probably, more usual for my reader.

The lattice system of interest here (at least for the 2D case) is the centered rectangular (orthorhombic). Both relevant cases of such lattice and scattering mechanism is illustrated in fig. 1.1. Such a lattice can be characterized by the lattice wave-vector in k-space (reciprocal space): $\mathbf{q} = \{q_\perp, q_\parallel\}$. There are alternative notations for said components such as $q_\perp \equiv q_x \equiv q_y \equiv q_r$ and $q_\parallel \equiv q_z$ (along optical axis) depending on the context. The wave-vector components are associated with the lattice constants as $q_\perp = 2\pi m_\perp/d_\perp$ and $q_\parallel = 2\pi m_\parallel/d_\parallel$. The values m are such that $m_\perp \in \mathbb{Z}, m_\parallel \in \mathbb{N}$. Resonant scattering for an incident plane wave $\mathbf{k}_1$ with the wavenumber $\|\mathbf{k}\| = 2\pi n_0/\lambda_{\mathrm{air}}$ by the PhC structure into some allowed $\mathbf{k}_2$ occurs, if the momentum and energy are conserved (elastic scattering):

$$k_{\parallel 1} + q_\parallel = k_{\parallel 2}, \tag{1.1a}$$

$$k_{\perp 1} + q_\perp = k_{\perp 2}, \tag{1.1b}$$

$$k_{\parallel 1}^2 + k_{\perp 1}^2 = k^2, \tag{1.1c}$$

$$k_{\parallel 2}^2 + k_{\perp 2}^2 = k^2. \tag{1.1d}$$

Considering only forward propagation and first order scattering $m_\perp, m_\parallel = 1$ scattering will occur when at the filtering angle α into the angle β:

$$k_{\perp 1} = -\frac{q_\perp}{2} \pm \frac{q_\parallel}{2}\sqrt{-\frac{q_\parallel^2 + q_\perp^2 - 4k^2}{q_\parallel^2 + q_\perp^2}}, \tag{1.2a}$$

$$k_{\perp 2} = \frac{q_\perp}{2} \pm \frac{q_\parallel}{2}\sqrt{-\frac{q_\parallel^2 + q_\perp^2 - 4k^2}{q_\parallel^2 + q_\perp^2}}. \tag{1.2b}$$

$$\alpha_{\text{filtr.}} = \arcsin(k_{\perp 1} n_0 / k). \tag{1.2c}$$

$$\beta_{\text{difr}} = \arcsin(k_{\perp 2} n_0 / k). \tag{1.2d}$$

These equations hold for both cases (Laue and Bragg). However, knowing the resonant angles for a particular wavelength is not enough. The remaining question concerns how the energy is transferred between coupled waves in the PhC as a beam propagates. For the Bragg regime reflection causes the field to decays exponentially, in Laue filters the energy is transferred in a non-trivial way. The interaction between two coupled waves for both cases is shown in fig. 1.2.
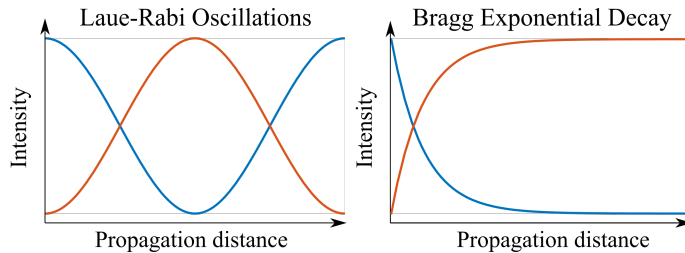
Figure 1.2: The diffracted waves in Laue configuration propagate in a forward direction and result in periodic energy exchange between the zero and first diffraction orders, whereas the waves in a Bragg configuration reflect backward, and thus result in an exponential decay (and correspondingly the stop-bands) of the incident wave intensity.

1.2.1. Laue regime filters

The PhC filters so far were designed and fabricated to work in Laue diffraction regime, where the waves diffract predominantly in a forward direction as schematically illustrated in fig. 1.1 (a,b). In general, the Laue regime occurs for $d_z > \lambda$. In this case, no full photonic bandgap exists. As the wave propagates through the PhC, the periodic revivals called Rabi oscillations occur between the zero- $(m_\perp, m_\parallel = 0)$ and first- $(m_\perp, m_\parallel = 1)$ diffracted orders.

The advantage of proposed Laue spatial filtering is that it requires relatively low refractive index modulation (of the order of 10^{-2} and less), which is around two orders lower compared to Bragg cases [10, 9, 22, 21]. Such low index modulation suggests the possibility for the inscription of such PhCs into the bulk of transparent materials, such as glass, by using direct femtosecond laser write (DLW) technique [31, 32]. However, this technique typically allows for lower values of refractive index modulation (10^{-3}). Too low values impose other restriction, mainly, as explained below, on the necessary PhC lengths for efficient operation. Therefore, a careful choice of processing parameters must be made in order to optimize it.

Due to the fact that relatively small transversal periods (of an order of 1 and 2 micrometers for 2D and 3D axisymmetric PhCs, respectively) were used in the multilayer structures, the formation of successive layers can modify the previous one and induce tension in the area of further successive layer fabrication. This makes it difficult to characterize such structures using conventional methods, such as phase contrast microscopy. The solution is using a characterization method based on the so-called s-coefficient, which is a phenomenological constant and allows the characterization of periodic structures without knowing its specific details (such as amplitude Δn_{max} of refractive index modulation, profile of refractive index change, size of the modified regions or, more particularly, the longitudinal size of the modifications Δl). The s - coefficient can be interpreted as the scattering coefficient of one crystalline longitudinal period of the structure and expressed by (see Thesis paper **A2** Appendix A and B or Thesis paper **A4** Note 1 in Supporting information for a detailed derivation):

$$s = \pi^{3/2} \Delta n_{max} \Delta l / 2\lambda_0, \tag{1.3}$$

and as it was shown in [24], can be used as a tool for determining the most appropriate crystal geometry for available laser processing parameters for a given application. For example, if for given PhC fabrication conditions the value of s is known, and a particular application requires a 100% intensity depletion for an arbitrary input beam along a predefined filtering angle α, then the number of PhC periods N needed to achieve the best result can be estimated following the relation $s \times N \approx 1.5$. In addition, approximate line width could be determined, which follows the relation $w \approx 50\sqrt{s}$ mrad. Similarly, controlling s might also be beneficial for other applications, *e.g.* axisymmetric super-collimation [33] or flat lensing [34].

To simulate the behavior of Laue PhCs, multiple methods can be used. The beam propagation method (BPM) is the preferred choice [35, 36]. It is used when diffractive homogeneous space propagation can be evaluated separately from scattering from an infinitely thin phase grating, which, in this case, applies to one crystal layer. It is simple, requires low computational resources, and its use is justified as long as the refractive index modulation depth is low $\Delta n < 10^{-2}$ (reflections can be ignored) and longitudinal period length is greater than the wavelength of operation so as $n_0 d_z / \lambda \geq 7.2$ as outlined in Thesis Paper **A2** Appendix A.

Applying the method is relatively simple. Consider the electric field vector **E** polarized along the "bars" of the PhC (Transverse Magnetic polarization). The electric field is defined as $\mathbf{E}(x, z, t) = \mathbf{E}(x, z) \exp i\omega t$, with a complex amplitude $E(x, z) = A(x, z) \exp i\phi(x, z)$. The problem to be solved is determining how the complex envelope $A(x, z)$ (under the slow varying envelope approximation) changes from the input $A(x, z = 0) \implies \mathbf{A}_0$ to the output facet

$A(x, z = 2Nd_{z/2}) \implies \mathbf{A}_N$ of a PhC having N periods or $2N$ layers. The layers are spaced in the longitudinal direction by half of the period length for a non-chirped structure $d_z/2 = d_{z/2}$. To get the result numerically the following procedure needs to be applied in an iterative manner:

$$\mathbf{A}_j = \mathcal{F}^{-1} \left(\mathbf{P} \mathcal{F}(\mathbf{S} \mathbf{A}_{j-1}) \right), j = 1, 2, ..., 2N. \tag{1.4}$$

$\mathcal{F}$ and $\mathcal{F}^{-1}$ are the discrete Fourier and inverse Fourier transform operators. S is the scattering operator (space-dependent or inhomogeneous operator). It can be defined as $\mathbf{S} = \exp(isM_j)$ [1]. As the refractive index pattern can take many forms M_j can be defined in a multitude of ways, but here it is approximated to be of a harmonic profile $M_j = (-1)^j \cos(2\pi x/d_x)$. $\mathbf{P}$ is the homogeneous space propagation (diffraction) operator. Following traditional formalism it is defined for the paraxial case, however, the paraxial dispersion can be substituted with the spherical dispersion term and it gives better correspondence experimental results[2]: $\mathbf{P} = \exp\left(id_{z/2}\sqrt{(k^2 - k_x^2)}\right)$. A flow chart to visualize the implementation of eq. 1.4 is given in fig. 1.3.

If the PhC layer structure is more complicated and known, then eq. 1.4 can be adapted. In the simplest case, the layer must be divided to m sublayers. m is the sublayer step number for a thickness of $d_{z/2}/m$. Then the scattering coefficient also must be scaled $s \to s/m$, to avoid incorrectly modeling m times more efficient PhCs. Then propagation and scattering operators $\mathbf{S}_{j,p}$ and $\mathbf{M}_{j,p}$ must become dependent on an additional iteration number $p = 1, 2, \ldots m$.

Having this in mind, consider the exemplary case where the layers have an asymmetric tilt. A new parameter θ_p can be introduced: $M_{j,p} = (-1)^j \cos(xq_x + p\theta_p d_z/m)$, to control the new phase term that is responsible for displacing the phase grating along the x-direction for every sublayer step m in the z direction. To simulate the structure using these modifications it would take $2N \times m$ iterations[3]. Asymmetric filtering would be observed for $\theta_p \neq 0$.

---

[1]Note that there are different definitions of the s-coefficient. It depends on what is considered to be the scattering element. Either it is the unit cell (2 layers - single longitudinal period) or half of unit-cell (1 layer - half of one longitudinal period). I prefer to use a single layer approach here. $\sim 2 \times s$ should be used if results need to compared with [24], where a scattering matrix method was applied as in [37]. There s was defined for a pair of longitudinal layers (one unit cell).

[2]It is a heuristic assumption, meaning that it is observed to work empirically. That this intuitive assumption is justified can be seen from the BPM derivation in [36]

[3]I note that good convergence for this model is reached for $3 < m$.

Definition of the complex amplitude of the initial incident beam
$\mathbf{A}_{j=0}(\mathbf{x}, \mathbf{y}; z = 0) \Rightarrow \mathbf{A}_{j=0}$

Definition of PhC geometry (e.g. by half-unit cells length vector)
$\vec{d}_{z/2} = (d_1, d_2, \cdots, d_N)$

Iterate the layer index

$j := j + 1$

Application of scattering operator

$$\mathbf{S} \otimes \mathbf{A}_{j-1}(\mathbf{x}, y; z) = \exp(is(-1)^j \cos(2\pi \mathbf{x}/d_x)) \odot \mathbf{A}_{j-1}(\mathbf{x}, y; z)$$

Discrete Fourier transform

$$\mathbf{A}'_{j-1}(\mathbf{k}_x, \mathbf{k}_y, z) = \mathcal{F}\{\mathbf{S} \odot \mathbf{A}_{j-1}\}$$

Homogenous space propagation

$$\mathbf{A}'_j(\mathbf{k}_x, \mathbf{k}_y, z + d_j) = \mathbf{P} \odot \mathbf{A}'_{j-1} = \exp\left(id_j\sqrt{k^2 - k_x^2 - k_y^2}/2\right) \odot \mathbf{A}'_{j-1}(\mathbf{k}_x, \mathbf{k}_y, z)$$

Inverse discrete Fourier transform

$$\mathbf{A}_{j+1}(\mathbf{x}, \mathbf{y}; z + d_j) = \mathcal{F}^{-1}\{\mathbf{A}'_{j+1}(\mathbf{k}_x, \mathbf{k}_y, z + d_j)\}$$

no

Is $j = 2N$?

yes

Transmitted field
$\mathbf{A}_{2N} \Rightarrow \mathbf{A}_{j=2N}(\mathbf{x}, \mathbf{y}; z = \text{sum}_{j=1}^{2N} d_j)$

Figure 1.3: A flow chart showing how to implement eq. 1.4 for simulating a PhC characterized by N periods, s-coefficient, a transverse lattice constant d_x and geometry vector $\vec{d}_{z/2}$. $\mathbf{A}, \mathbf{S}, \mathbf{P}, \mathbf{x}, \mathbf{y}, \mathbf{k}_x, \mathbf{k}_y$ are, numerically speaking, arrays and $\odot$ elementwise multiplication. This together with the implementation examples given in [38] is enough for the reader to replicate the numeric results presented in this dissertation.

In summary, this is enough information for the reader to build a sufficient numerical model for both 2D and 3D Laue PhC filters. In addition, for more complicated structures, the model can be easily adapted. For example, if the PhC is 3D, then the BPM can be applied with taking into account the extra y-dimension. If polarization considered is transverse electric, then typical smaller values of s must be used. If the structure is axisymmetric then the Quasi-Discrete Hankel transform [39] can be used to gain calculation speed at the cost of information about the $k_\perp = 0$ component intensity value as was done

in [33] and Thesis paper **A1**.

If the refractive index becomes significant enough $\Delta n \geq 10^{-2}$, this method will fail to predict precise transmission properties of the Laue PhC filter due to significant reflections. At that point, to estimate angular transmission spectra either the (computationally costly) FDTD method should be used [40] or Rigorous coupled wave analysis as in Thesis paper **A5**.

Alternative nomenclature

For the paraxial approximation, the filtering angle α obeys the simple relation (which follows from the resonance conditions of modulation- and light wavevectors):

$$\sin(\alpha) = q_\perp \frac{1}{2k_0} (Q - 1) = \frac{\lambda}{2d_\perp} (Q - 1) \qquad (1.5)$$

Here, a dimensionless parameter Q is defined as

$$Q = 2 \frac{d_\perp^2}{\lambda d_\parallel}. \qquad (1.6)$$

The reader might wonder why such an additional definition is necessary. The first reason is that it is more simple then eq. 1.2 and easy to apply. The second is that an analogy with the Talbot effect (grating self-imaging effect) [41] exists. Assuming that $\lambda \ll d_\perp$, the Talbot length for which a diffraction grating evenly illuminated by a monochromatic wave will generate an image of itself in the near-field is $z_T = 2d_\perp^2/\lambda$ [42][4]. Therefore the physical meaning of 1.6 is the ratio of the longitudinal period with the Talbot distance $Q = z_T/d_\parallel$. Taking the Talbot effect into account has already proven to be beneficial in producing advanced multi-layered phase elements [43].

1.2.2. Bragg regime filters

As for the Bragg regime PhCs, they will be considered in the geometry shown in Fig. 1.1(f). Basically, it is a modulated substrate with alternating conformal layers with high n_h and low n_l refractive index values. Typically such structures are considered as high diffraction efficiency dielectric reflection gratings [44, 45, 46]. The principle most often applied for extreme-ultraviolet-spectroscopy [47, 48]. However, here, such structures are considered in a context of as spatially selective devices in transmission for the optical regime.

In reference to Thesis paper **A6** the typical periods are on the scale of $d_x \approx 1.67$ µm and $d_z \approx \lambda/2$ with layer thickness of $l = d_z/2$. Refractive index contrast is $\Delta n = n_\mathrm{high} - n_\mathrm{low} \approx 0.12$. The preferred method of visualizing the filtering effect is the angular *vs* wavelength intensity transmission map for the

---

[4]Also images of varying periodicity will be created at, notably, $1/4z_T$, $2/4z_T$, $3/4z_T$

zero-order component. The Bragg PhC filter is expected to be characterized by a more complicated band-structure than that of the Laue filters (see Thesis paper **A3** Supplementary information Fig. S3) as higher order stop-bands of significant importance.

Approximating these positions of said bands is relatively easy using a more convenient expression than 1.2. If the incident wave is characterized with a wave-vector $\mathbf{k}_0 = (k_0 \sin(\theta), k_0 \cos(\theta))$ and the lattice with $\mathbf{q}_{n,m} = (m_x q_x, m_z q_z)$ and same conservation laws hold as defined in 1.1, then stop-bands should appear at:

$$|\mathbf{k}|_{m,n} = \frac{m_x^2 q_x^2 + m_z^2 q_z^2}{2m_z^2 q_z^2 \cos\theta - 2m_x^2 q_x^2 \sin\theta}, m_x \in \mathbb{Z}, m_z \in \mathbb{N}. \tag{1.7}$$

m_x and m_z correspond to the transverse and longitudinal harmonics of the lattice.

For quantitative analysis, the preferred method is FDTD [40], when calibrated with observable angular transmission spectra from the experiment.

2.   PhC spatial filters by medium and fabrication method

In this chapter, I review three types of PhCs for spatial filtering that have been experimentally tested in a single pass regime. The Laue type PhC spatial filter was explored in a 2D and axisymmetric (3D) geometry and the Bragg type PhC spatial filter based on conformal thin-film dielectric coatings (2D).

2.1.   Gaussian beam based DLW of PhCs

The experimental considerations here presented are associated with Thesis papers **A1**, **A2**, **A3**, **A4**.

2.1.1.   Motivation

As explained in subsection 1.2.1 the main parameter used the characterize PhC Laue filters is the scattering efficiency coefficient s. Although the s-coefficient is useful in determining the behavior of the PhC filter, its dependence on parameters important for the PhC DLW processes has never been explored before. These parameters include the DLW speed, peak intensity, pulse repetition rate, *etc.*. Little was known about the optimization of PhC based filter fabrication conditions in general. Therefore, this section is devoted to the experimental study of the Laue spatial filter performance, in other words, the behaviors of the s-coefficient, depending on DLW conditions.

2.1.2.   Experimental methodology

DLW setup and mechanism

The DLW setup is already discussed repeatedly in detailed in numerous external sources. In short, it is comprised out of a laser beam source, focusing means, such as high NA lens producing a focused Gaussian beam, sample scanning means, such as translation stages and/or a galvanometric scanner, and some additional control means for the polarization, beam diameter *etc.*: fig. 2.1. It

would be extremely redundant to go into detail here as the same setup was used and fully described in [49, 50]. The important thing is the DLW parameters that determine the physical modification mechanism in the bulk of the transparent dielectric materials used as the substrates for PhC formation.

A pulsed laser source producing 300 fs duration pulses with a central wavelength of $\lambda_0 = 1030$ nm was used[1]. The beam was delivered into the substrate using high numerical aperture (NA) >0.9 microscope objectives resulting in TW/cm^2 peak intensities. At such high intensities, dielectric breakdown occurred inside the material resulting in a multitude of effects, of which the relevant result is the change of refractive index. Scanning speed v and laser pulse repetition frequency f are parameters that vary between the thesis papers and are disclosed in the following subsections below.
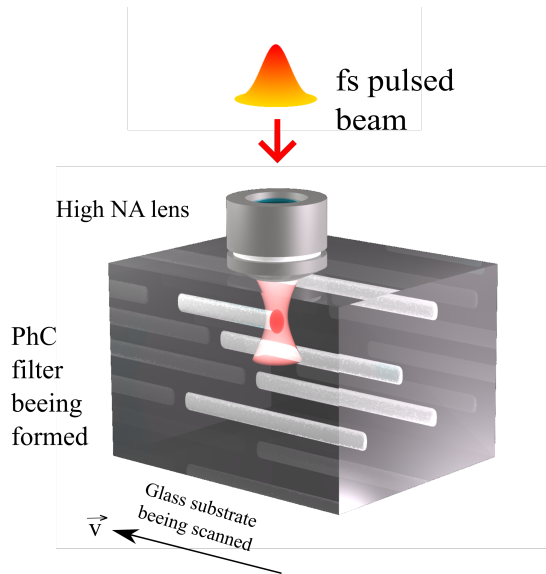
Figure 2.1: The core concept of a DLW setup used to produce localized modification inside the bulk of a transparent material.

Materials

Two of these materials chosen for the Gaussian beam based DLW experiments were soda-lime glass (SLG) and Foturan[2] photosensitive glass.

Soda-lime glass is produced when pure silica is combined with sodium or calcium ions in the form of Na_2O and CaO additives. This drastically reduces the melting point, easing manufacturing, at the same time increasing the density and refractive index compared to pure silica. However, as a trade-off this

---

[1]Photon energy is $E_p \approx 1.2$ eV
[2]This is a trade-name.

T.p.	NA	v, mm/s	f, kHz	$E_{imp.}$, nJ	I_{peak}, TW/cm^2	Mat.	λ, nm	s
A1	0.95	0.8	1	600	342	SLG	633	0.075
A2	1.4	1.25, 2.5, 10	25, 50, 100	80-320	69-276	SLG	633	0.03-0.055
A3	0.95	0.8	1	432	246	SLG	1064	0.025
A4	1.25	0.25	10	100	42	Fot.	633	0.065

Table 2.1: Experimental parameters by Thesis papers. Parameters provided have been adjusted for the transmission of the DLW system.

reduces chemical durability, electrical resistivity, increasing the thermal expansion coefficients *etc.*[51]. 3D micro-resonators [52], waveguides [53, 54], Bragg gratings [55] have been demonstrated in this material. The soda-lime glass samples used here were standard microscope slides (Carl Roth, ISO 8037-1, $n_{ref} = 1.52$). The reported make up of the material is 69 % SiO$_2$ 1 % B$_2$O$_3$ 3 % K$_2$O 4 % AI$_2$O$_3$ 13 % Na$_2$O 2 % BaO 5 % CaO 3 % MgO [56].

The second material used was Foturan ($n_{ref} \approx 1.51$). It belongs to the lithium aluminosilicate glass family and doped with a trace amount of silver and cerium oxides. Its approximate composition is reported in [57]. It is important to note that its photosensitive, ceramization or wet etching properties were of no interest here. It was used due to an empirically established relative high degree of refractive index change resulting in a high *s* value, while being structured point-by-point using a focused pulsed fs beam (without post-heat treatment) [31, 58, 59].

All relevant parameters for both materials and achieved *s* values are outlined in Table. 2.1.

Summary of the refractive index modification principles

Having listed the processing parameters and mention a couple of materials used, I make a note of some insights into the physical processes that occur during the DLW structuring.

The materials important in this thesis are multi-component glasses. They are soda-lime glass, Foturan glass (subsection 2.1.2) and N-BK7 (subsection 2.2.2). They compare to the most studied material in terms of their optical properties: fused-silica glass [60, 61, 62] that has an electronic direct band-gap energy in the range of $7.52 \leq E_g \leq 9.6$ eV [63, 64, 65] by all having lower band-gap values: soda-lime glass ∼3 eV [66], Foturan[3] ∼3.6 eV [67, 68, 69, 70],

---

[3]In actuality, the excitation process is complicated as the excitation of electrons occurs from the valence to a defect band separated by 3.6 eV and then from the defect band to the defect band to the conduction band. The valence and conduction bands are separated by ∼8 eV (see references).

N-BK7 ~4.28 eV [71, 72].

Limiting the discussion[4] to what is relevant for the listed materials at disclosed experimental conditions, the most important factors are that the DLW pulsed beam pulse duration was 200-300 fs, the dielectric materials are amorphous and transparent for the wavelength used (can only be modified through a nonlinear process). The bulk material modification mechanism is based on free-electron plasma generation, subsequent energy transfer processes to the lattice (glass matrix) subsystem [74] and thermal-elastic relaxation processes [75, 76, 77, 78].

According to the Keldysh parameter formalism and current understanding [79, 80, 81] during the radiation-matter interaction multi-photon absorption is the dominant mechanism generating free electrons excited from the valence band to the conduction band followed by to a lesser extent contributing linear absorption and avalanche ionization (impact ionization) that occurs at the end of the femtosecond pulse interaction[5]. This occurs at a localized zone, where the laser beam intensity is above the laser damage threshold for the particular material, and more precisely at the focus of the DLW system.

As the energy is accumulated in the electron subsystem on the time scales comparable to that of the femtosecond pulse duration, the lattice (here, more precisely, the glass matrix) system remains "cold" (unaffected by the radiation). After some time, the generated free electrons through self-trapping[6] [84] and the electron-phonon interaction (occurring at a time scale of 1-10 ps) [74] transfer the accumulated energy to the lattice (matrix) subsystem. The thermal diffusion is slow enough for large amounts of heat to be accumulated locally [85], resulting in cleaving and restructuring of covalent bonds - color center formation, remelting - reforming cyclic connections and ion migration, inducing mechanical stress around the modified zones [86, 78]. Ultimately, the local density changes result in observable localized refractive index changes that, if spatially distributed correctly, comprise the Laue type PhC.

Characterization methods

The structures were characterized firstly by a single pass focused beam approach. The transmitted beam was projected in on a CCD matrix placed the far-field at a known distance. The intensity values were read-out for a relevant matrix row/column or averaged multiple rows or columns and assigned to the equivalent angular value. The PhC function was analyzed by comparing the incident beam angular spectra with the one transmitted by the PhC. The probe beam was always linearly polarized in such a way that the electric field vector

---

[4]For a more detailed outlook, I recommend seeing ref. [73] for an excellent introduction concerning glass modification.

[5]Usually, free-electron plasma is induced.

[6]This occurs, for example, for soda-lime glass over a decay time of 100 ps [82] or for BK-7 over 5 ns [83].

E oscillated in parallel with the PhC features (observed as linear features of the induced refractive index change zones). In analogy to diffraction grating theory, it should be considered P-polarization (TE waves).

For the observation of the structural changes inside the glass, two methods were used. Glass substrates containing the formed PhC were diced and polished. Firstly, an inspection was performed using an optical microscope to observe possible wave-guiding (positive refractive change sites) [87, 77]. This method had a limited resolution, therefore, using the second method, samples were wet-etched in a concentrated alkaline aqueous solution (high concentration potassium hydroxide) [88] to produce a nanoscale indentation observable under a scanning electron microscope (SEM) [89].
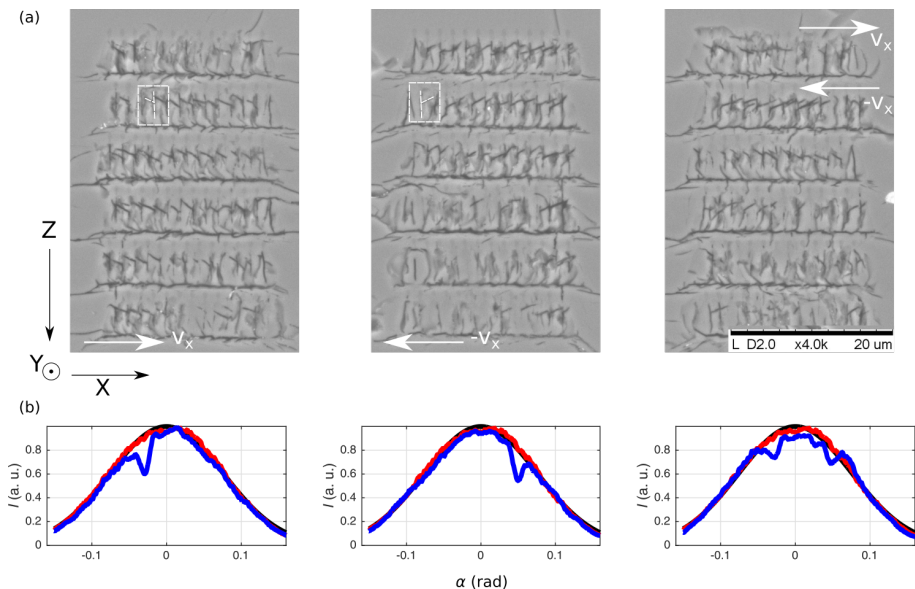
Figure 2.2: PhC transmitted far-field intensity plots and SEM images of the cleaved and wet-etched samples with up-scaled PhCs. The scanning speed was 1500 mm/s, and the polarization plane was oriented along the X-direction. An asymmetric "Y"-letter shaped structure appears depending on the scanning direction for each individual layer. [90]

2.1.3. Summary of main results

During this study, a number of interesting nuances have been discovered about PhC filter formation inside the bulk of soda-lime glass. They can be outlined as follows. There exists an optimal pulse energy/peak intensity value for three tested pulse repetition rates f that optimize the s-coefficient. For particular geometries and DLW parameters used asymmetric filtering was observed. Such asymmetric filtering is explained by an asymmetric internal structure.

In T.p. **A2** Fig. 5 it is shown that the refractive index modulation depth is increasing with increasing pulse energy up to a maximum value. At some point, a decrease is observed if the pulse energy is increased further. This happens due to the fact that not only the modulation depth increases, but also the geometrical parameters change [91, 87]. The particular way this manifests in terms of scattering efficiency is *via* the size of DLW modified zones (voxels) that increase in size until they reach optimal dimensions, and with further increased exposure become large enough to overlap transversally (along the transverse lattice vector q_x), thus reducing the index modulation depth of the periodic structure and causing the decrease of the s-coefficient value for higher pulse energy/peak intensity values.

This is also corroborated by what is known from other experiments, where at similar parameters during the DLW procedure a negative-positive refractive index changes structures are formed. A reduced refractive index rarefied core [77] that is surrounded by a shell and/or at least two separate densified positive refractive index structures [87, 92] tends to form. Overlapping positive refractive index shells should maximize the s-coefficient, while overlapping the negative refractive index core with the neighboring negative refractive index change shell would reduce it.

Also, during the experiments weakly asymmetric filtering spatial spectra patterns, wherein the angular filtering bands at $|\alpha_+| = |\alpha_-|$ differed, were observed. Mainly it featured empirically different transmission coefficients $T(\alpha) \neq T(-\alpha)$ or, in other words, scattering efficiencies $s_+ \neq s_-$. This was especially true, when deviating from the $E_{\max s}$ and $I_{\max s}$ parameter values. Such behavior was unexpected and was further explored by varying the DLW beam polarization angle and beam writing direction to isolate possible unusual interaction mechanisms. After choosing different fabrication parameters and geometries with different d_x values, cases, where the effect is significantly pronounced, were found.

A BPM model[7] that presumes a tilted internal layer structure has been developed. It successfully explained the asymmetric scattering efficiency in relation to the layer-by-layer scanning direction, wherein asymmetry is reduced as the scanning directions is varied instead of fixed for all layers.

2.2. Bessel beam based DLW PhCs

In this section, I describe what is presented in thesis paper **A7** and was to produce the structures in thesis paper **A8**.

---

[7]See subsection 1.2.1.

2.2.1. Motivation

In practice, the fabricated PhC filters, especially those written by femtosecond pulses inside inorganic material substrates using the direct laser writing techniques, have a problem of the limited functionality for spatial filtering. Firstly, the rough estimations show [12], that the filtering depth scales as $\Delta n \times l/\lambda$, where Δn is the refraction index contrast (which in glasses is of the order of $(10^{-3} - 10^{-2})$, l is the length of the written photonic crystal, λ is the wavelength. This means that for efficient filtering, with 100% intensity attenuation at the filtering angle α, can be achieved for >100 µm length PhCs. Moreover, the angular width of the angular filtering band is proportional to Δn, which is the fractions of degree for such low-index-contrast PhCs. For relevant applications, the filtering bandwidth of several degrees is required (for instance the main technological challenge in edge-emitting lasers is to reduce the slow-axis divergence from ~ 5 degrees down to 1-2 degrees). In principle, the width of the filtering band (ϕ) is not a real problem, since it can be solved by using chirped photonic crystals [24] (T.p. **A1**), *i.e.*, by sweeping of the geometrical parameters along the length of the photonic structure, which sweeps central filtering angle α in the angular transmission spectrum. Such sweep could cover greater angular ranges, see fig. 2.3(a) for the illustration. However, this eventually would result in the need for longer crystals.

Thumb rule [12] says that the 100% filtering of the angular range relates with the length of the filtering crystal: $L = \lambda \Delta \phi / \Delta n$. For example, if Δn is small, of an order of 10^{-2} and if the desired angular range of filtering is $\Delta \phi \approx 0.1$ rad., then one will need a crystal with the length of the order of 1 mm. Typically, the fabrication of such filters is done by direct laser writing using Gaussian beams, when tightly focused femtosecond laser beam induces local modification of refractive index in glass or other transparent materials [93, 94, 95]. The convenient transverse periodicity of the PhCs is in the range of 1-2 µm, meaning, that a relatively high numerical aperture (NA) focusing optics has to be used (NA > 0.8). This is not convenient for the required minimum length of the PhC (> 1 mm). The existing variety of focusing optics forces one to make a choice between high NA, but short working distance, optics, and long working distance, but low NA optics. In addition, the deeper must the focal plane be arranged in the substrate, the more the DLW beam is affected by spherical aberrations. In practice, spherical aberrations and available working distances limit the practical length of PhCs to a maximum of 0.3 - 0.5 mm.

To forgo this problem, let us consider that for some applications filtering along only one direction is sufficient. For example, such filtering is especially suitable for broad edge-emitting semiconductor lasers, where only the slow-axis filtering is required [96, 97]). In such case, the PhCs having 2D modulated

geometry are needed.
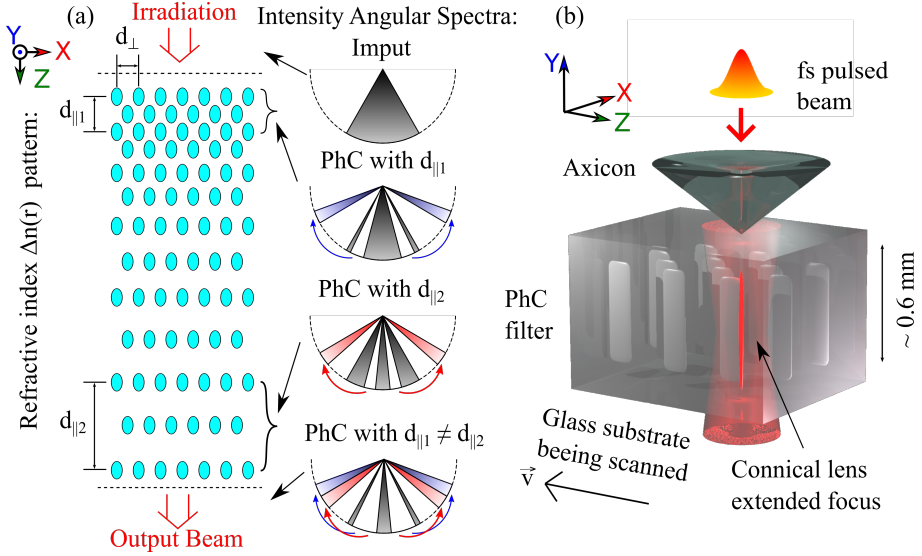
Figure 2.3: The illustration of spatial filtering using chirped PhCs (a); The PhC is fabricated by delivering a Bessel beam vertically (the filtering will follow along the vertical direction, Z) (b).

The idea presented here is to use the Bessel beams [98] for the fabrication of large scale 2D PhC spatial filters. Bessel beams can be generated by refractive, reflective or diffractive axicons and are characterized by a long and narrow high aspect ratio high-intensity ($|\mathbf{E}|^2$) zone. This property is used for machining transparent materials [99, 100, 101], *e.g.* for the fabrication of phase elements [102, 103]. Due to very long and narrow modifications, the fabrication can be performed in a "horizontal geometry", see Fig. 2.3(b). Then the maximum length of the filtering structure is no longer a problem and in principle is limited only by the mechanical travel range of the fabrication stages. Although the vertical direction is still limited, it is at least 10 times longer, when compared to the Gaussian beam strategy.

2.2.2. Experimental methodology
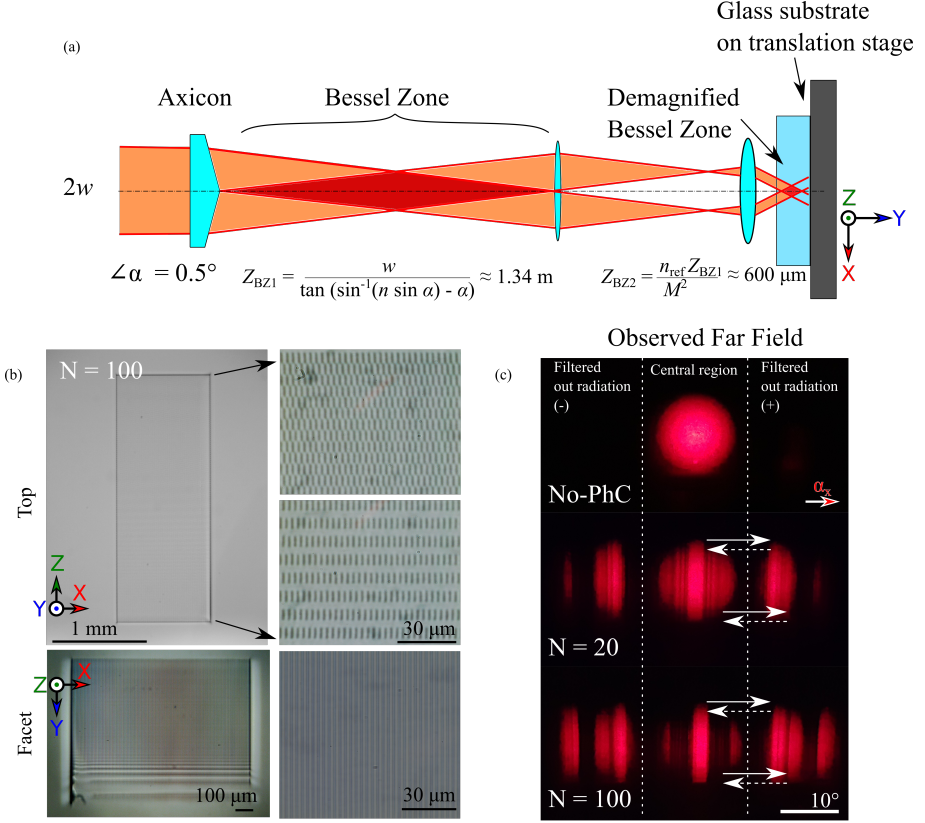
Figure 2.4: Schematic representation of the fabrication arrangement (a), transmission microscope-image of sample (b), and the 2D light far-field transmission image for a focused He-Ne beam, showing the central beam region, from which radiation must be scattered out from the filtering range (c). Arrows indicate resonant scattering that can occur outward and also inward to the central region.

The experimental DLW setup used here is shown in Fig. 2.4. It consisted of a UVFS axicon with a half angle of $\angle\alpha = 0.5°$ (apex angle 179°). It was illuminated using a collimated pulsed beam with a center wavelength $\lambda = 1030$ nm, with a pulse repetition rate of 25 kHz and a pulse duration of approximately 200 fs. Beam diameter was around $2w = 5.25$ mm (at $1/e^2$ intensity value). The demagnifying telescope was arranged from two lenses with the focal lengths of 500 and 9 mm, having a (de)magnification value of M 55.6. Pulse energy delivered to the sample corresponded to 8 µJ.

A polished N-BK7 ($n \approx 1.51$) 4 mm thick rectangular substrate was placed on a translation stage and irradiated with the demagnified beam producing

an initial refractive index change modification of around 600 μm. The sample was scanned at $v = 2500$ µm/s in consecutive linear motion to produce the patterns shown in Fig. 2.4(b). The usable aperture of such PhCs is 0.6x1 mm^2 and can be extended in the horizontal (filtering) direction without limitation. Note, that no spatial filters were used to compensate the limited axicon tip quality and therefore defects are visible ant bottom of the facet view. For such exposure conditions, it is probable that positive refractive index changes are induced [104, 105] as no scattering losses were observed in these structures as shown in the results section.

Non-chirped and chirped structures of various of different longitudinal period numbers were fabricated. The minimal transverse period achievable was $d_x = 3$ µm. The corresponding longitudinal period was chosen by using the geometry parameter $Q = 2d_\perp^2/(\lambda d_\parallel)$, since it is convenient for approximating the central filtering angle in an intuitive way: $\sin(\alpha_c) = \lambda(Q-1)/2d_\perp$. Note that the wavelength here is considered as in the dielectric substrate: $\lambda = \lambda_{\text{vac}} n_{\text{BK7}}$. For the non-chirped structures, Q was chosen to be $Q = 1.2$, 1.6, 2.0. For chirped structures $Q_1 = 1.2$, $Q_2 = 2.0$, where the $d_\parallel$ values were varied linearly between the corresponding values. The values depended on the probe wavelength λ.

Two wavelengths were used: He-Ne (633 nm) and infrared 970 nm. For chirped samples designed for $l_{\text{HeNe}} = 633$ nm the longitudinal period was varied such as 21.47 $\leq d_\parallel \leq 35.78$ µm and for $\lambda_{\text{IR}} = 970$ nm accordingly $14.01 \leq d_\parallel \leq$ 23.35 µm. After fabrication, the PhC samples were inspected with an optical transmission microscope (Fig. 2.4(b)) and then probed them with focused Gaussian profile laser beam. Angular filtering bands were observed as shown in Fig. 2.4(c). To record the transmitted intensity pattern, the transmitted beam was directly projected on a CCD camera matrix placed in the far-field.

2.2.3. Summary of main results
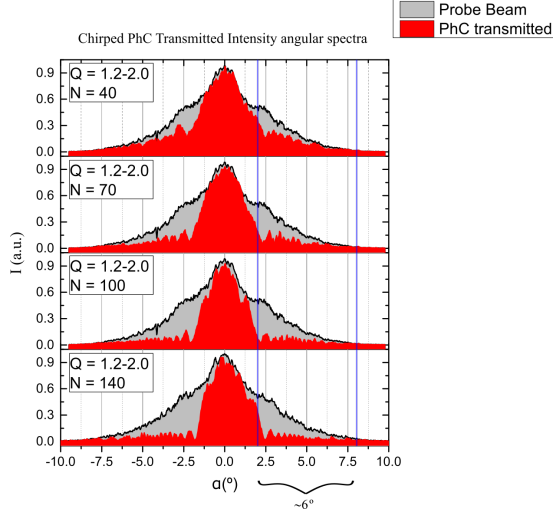
Figure 2.5: Angular intensity spectra for PhC designed for an operating wavelength of $\lambda = 970$ nm. The empirically measured filtering band corresponds to $2.21° \leq |\alpha| \leq 8.05°$

In this way, the new, convenient method for writing the relatively long photonic crystal spatial filters was proposed. Such PhC can be efficiently applied for 1D spatial filtering, for instance in broad-area semiconductor lasers, where the slow-axis filtering is highly desired.

This technique, however, optimally works for 2D photonic crystals, providing 1D spatial filtering. Such filters are ideal to be incorporated into edge-emitting laser diodes, where the divergence of the laser beam along the slow axis is a real problem. Typically, the divergences in the slow axis reach 3 to 10 degrees [96]. The Bessel DLW technique, as can be seen from the summary in Fig. 2.5, provides a sufficient angular filtering range.

Advanced chirping schemes could be applied to make use of a large number of periods to either extend the filtering range or tune the angular transmission spectrum shape T.p. **A5** [12]. Making a stitched structure as in [102] could increase the usable aperture by a factor of 2-5 times. The integration of such advanced PhC filters into the edge-emitting semiconductor lasers is discussed in T.p **A8**.

2.3. Conformal Thin-films filters

In the presented study an experimental demonstration of the signatures of angular filtering in the Bragg configuration is provided for the first time. PhCs

were fabricated on micro-textured substrates using physical vapour deposition method. The results experimentally prove the concept of 2D Bragg spatial filtering, but they do not lead to the ideal filtering performance yet, wherein the filtered plane wave components are 100% attenuated.

Results are presented in detail in Thesis paper **A6**.

2.3.1. Motivation

The PhC filters so far were designed and fabricated to work in Laue diffraction regime where the waves diffract predominantly in a forward direction as schematically illustrated in Fig. 1.1(a,b). In general, the Laue regime occurs for $d_z > \lambda/2$. In this case, no full photonic band gap exists. As the wave propagates through the PhC in the Laue regime, the periodic revivals called Rabi oscillations start to occur between the zero- and first- diffracted orders (fig. 1.2 (a)). For this reason, the length of the structure must be selected precisely to get efficient filtering. The advantage of the Laue regime is that the lattice periods are well achievable by optical fabrication techniques in organic/inorganic materials [106, 107, 108], as the PhC periods along the optical axis d_z are in the range of tens of microns, and along the transverse directions $d_{x,y}$ - of several microns.

The spatial filtering is also possible in the so-called Bragg regime (1.1 (c,d)). Here the length of the structure is less critical, as the Rabi oscillations between filtered and unfiltered modes do not appear. Instead exponential decay of the filtered modes occurs (Fig. 1.2). In the Bragg regime (most typically $d_z \approx \lambda/2$), the optical fabrication techniques can be hardly implemented. Holographic methods, despite promising experiments [109, 110], require ultraviolet sources and complicated optical designs. Therefore, their use for the PhC fabrication is very restricted, especially when the two-dimensional (2D)/three-dimensional (3D) volume gratings are required. Here, the physical vapor deposition method can be considered as a promising alternative solution for the fabrication of such spatially filtering photonic structures in Bragg regimes. The thin-film deposition methods have been demonstrated to be able to control the thickness and optical parameters at high accuracy [111]. Additionally, evaporation techniques, equipped with glancing angle deposition method, showed promising results in forming microstructures on structured substrates [112].

Such deposition methods are preferable not only because they enable to use the Bragg regime PhCs. It should be understood that Laue type PhCs can be fabricated using the same technique. However, the method described in section is considerably slower in terms of throughput. The reader can understand the difference by considering the situation as the problem of "serial" *vs.* "parallel". Direct laser writing point-by-point is considered a "serial" process, where producing PhCs with the parameters listed in table 2.1 takes hours for

usable apertures to be of few $\approx mm$ in scale. Ironically, the glass substrates used before or after the fabrication should be AR or HR coated. In contrast, physical vapor deposition is a "parallel" process, and even considering a hypothetical situation where it could take a day to complete a single deposition session, the amount of resulting usable aperture would be unmatched (roughly consider the probable case where multiple PhCs can be produced on multiple, lets say one inch diameter, substrates loaded in the deposition chamber). Therefore the latter method is very attractive for applications beyond the scope of prototypes.[8]

2.3.2. Methodology

Numerical

The commercial FDTD software was used for the light-matter interaction analysis in the designed structure [40, 114]. Due to the periodicity of the structure in the X-direction, time domain calculations were conducted via the supercell approach by assigning periodic boundary conditions in the X-direction. Here, the FDTD method solves Maxwell's equations by infinitely repeating the defined periodical supercell in the X-direction[9]. To observe the angular filtering property, the proposed structure is illuminated with P-polarized plane wave source at a variable angle and the corresponding zero-order transmission is calculated in the range of the wavelengths between 450 nm and 850 nm.

Experimental

The fabrication of the designed structure involved three main steps. First, a PDMS mold of a commercially available diffraction grating (with a pitch of $d_x = 1.67$ µm) was made [112]. Second, a base grating was stamped on soda-lime glass slides using a UV curable hybrid polymer (OrmoComp [119], $n_{ref} = 1.52$) as the material for the replica. Finally, the multilayer coatings were deposited on the base grating, by alternating high and low refractive index thin films.

An electron beam based physical vapour deposition [120] system equipped with glancing angle deposition (GLAD) technology was used in all evaporation processes. GLAD method allows modulating the porosity of the thin films by changing the angle between the substrate normal and evaporation flux. In such

---

[8]I must note that improvements to the DLW techniques are ongoing and are summarized elsewhere, for example in [108, 113], including the considerations for Bessel beams in section 2.2. Nonetheless, at this moment for mass-producing the PhCs with the geometry considered no better alternatives exist.

[9]I note that a very exciting alternative way of solving the same problem (numerically) is using the so called C-method [115] and, more precisely, its variations for multi-layer gratings [116, 117, 118]. The benefit here would the rapid rate of calculations, however, a more robust understanding of eigenvalue of problems and quantum mechanics formalism is needed to apply it correctly.
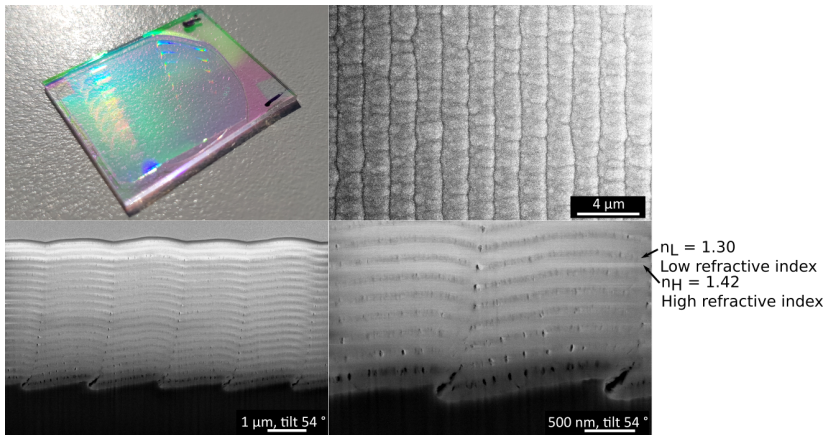
Figure 2.6: Fabricated all silica Photonic crystal. Cross-sections are represented in SEM micrographs made after focused ion beam milling.

a way the refractive index of individual layers is controlled easily and with high precision [121, 122, 123, 124, 125, 126]. During the coating process, the substrates were rotated at a constant speed to ensure the conformal evaporation. High and low refractive indexes were $n_H = 1.42$ and $n_L = 1.30$ respectively. Structures with $N_L = 33$ and $N_L = 39$ layers were deposited starting with the higher refractive index material. The physical thickness of each layer was equal to 120 nm (value for $d_z/2$ or half of the longitudinal period). The coating processes were started at room temperature, in high vacuum of and a trace amount of oxygen gas (for oxidizing of evaporated material).

Surface morphology of the grated substrate was measured by an atomic force microscope (AFM). Height distribution measurements of 20×20 µm^2 surface areas were performed in tapping mode and in ambient conditions. A commercial silicon probe with a tip diameter of < 10 nm was used. The inner structure of the samples was characterized using an SEM after an ion beam milling procedure (see Fig. 2.6).

The spectroscopic measurements (collimated beam) with spectrometer having a rotating sample holder. Linearly polarized light was used for two perpendicular polarizations: S and P, where S polarization is perpendicular to the grating lines on the substrate. The 0-order intensity transmission was measured in VIS range from -40° to 40° angles of incidence.

For characterization, the $N_L = 39$ layer structure was tested by probing with a divergent beam to make sure that the filtering effect can be observed not only for plane waves but also for beams with curved wavefronts. A Gaussian beam with a wavelength of $\lambda = 532$ nm was focused onto the structure using a 2.5 cm focal length cylindrical lens. The beam was characterized by a full divergence angle of 6°. The transmittance was measured using sample that was mounted

on a rotating conical mount. The mount angle was set to 21° to simulate an effective wavelength of $\lambda_{\text{eff}} = 570$ nm for which the most interesting effect was expected. The transmitted (filtered) beam was projected directly on the matrix of a CCD camera placed at the far-field (fig. 2.7). The angle between the mean plane of the PhC and the detector was changed from -40° to 40° by steps of 1°, and the total spatial transmittance spectrum has been averaged for overlapping angular positions.
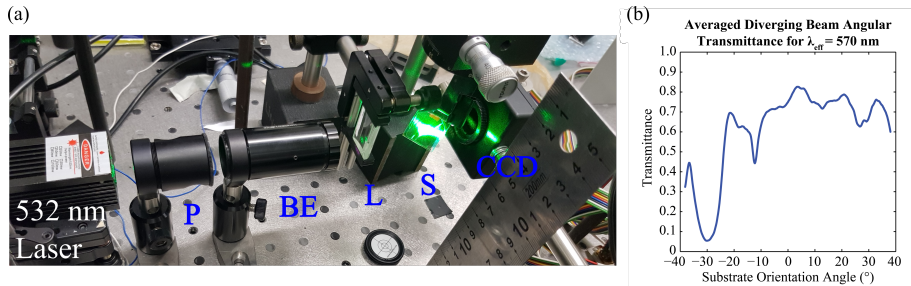
Figure 2.7: (a) Angular transmission spectra measurement setup. Comprised of: a laser source, P-polarized, BE- beam expander, L - cylindrical lens, S-sample mounted in a rotating holder, and CCD camera. (b) measured angular intensity spectra as transmitted by the PhC. The intended filtering bands are located at around ± 10 deg.

2.3.3. Summary of results

Here, the signatures of spatial filtering in the Bragg regime, based on periodic photonic microstructures fabricated by physical vapour deposition, were demonstrated. Attenuation for the selected angular components occurs *via* the geometry determined stop-gaps. Further developments need to be made for such structures to be of practical use, however, the principle of angular filtering has been convincingly demonstrated. The main reason for the relatively weak filtering performance used structures is the relatively large transverse periods d_x. As evidenced by eq. 4.6, the filtering parabolas for each Bragg component cross at small angles; therefore, the narrow low-angle-pass transmission peaks could not be obtained.

3. Optimization, advanced design.

In this chapter, I present the results concerning the modulation of the longitudinal period d_z as a function of either layer or period (unit cell) in the optical axis direction.

The results provided in this chapter are based on Paper **A1**, **A4** and **A5**. The discussion is starts with achievements for more basic 3D axisymmetric structures and is followed by results for 2D structures, in both cases arranged to function in the Laue regime.

3.1. Axisymmetric 3D PhCs with chirp

3.1.1. Motivation

The axisymmetric Photonic crystal spatial filters that were demonstrated in [25] could be interesting, when considered for active systems. I propose that such filters be used inside lasers to provide a selection mechanism for the transverse cavity modes, where diffraction losses needed to produce a high-quality output beam are too small due to the short cavity length, *e.g.* microchip lasers [127], VCSELs [128]. It would be ideal to have a low-angle pass band adjusted to favor the fundamental mode (TEM00), which is, usually, the most centered and of the narrowest angular spectrum. The increased loss for higher-order transverse modes should increase their lasing threshold, but since the angular filtering band is finite and optical pumping power fcan always be increased for some higher-order modes, generation will occur nonetheless. The reader is invited to consult T.p. **A3** or fig. 4.2(g) for practical proof, wherein maximum achievable laser beam brightness [97] is limited by aforementioned phenomena.

To use the PhC for spatial filtering in an advanced way, the angular filtering ranges must be expanded beyond what was available. Therefore, here it is demonstrated that a longitudinal chirp (the variation of the longitudinal period along the structure) in axisymmetric photonic structures can be used as an alternative method to increase the angular width ϕ of the filtering band. The
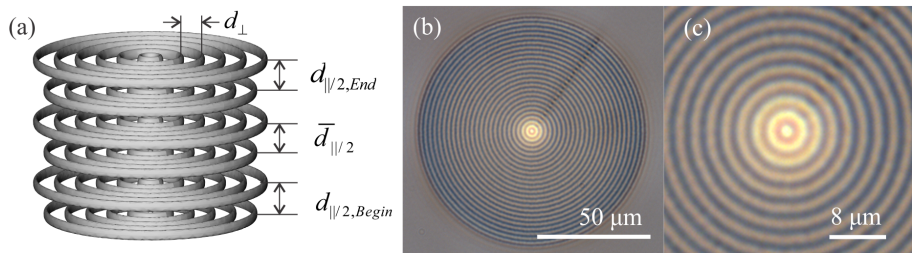
Figure 3.1: Crystal geometry and samples. (a) A 3D schematic representation of the axisymmetric photonic structure. (b) The optical microscope image (top view) and (c) the magnified image of the fabricated structure.

use of longitudinal chirp to enhance the filtering range in 2D structures was proposed in [24]. Such chirping for axisymmetric structures is explored here. In particular, the filtering band angle width is explored by measuring the FWHM (full width at half maximum) of the dominant normalized filtering line found in the angular "deflection" spectrum: $((I_0(\alpha) - I(\alpha)))/(I_0(\alpha)) = \Delta I(\alpha)/(I_0(\alpha))$. Additionally, numerical calculations show that the chirped structures have a potential to enlarge filtering angular ranges, either by using longer structures (greater N values), or by using larger amplitudes of refractive index modulation.

3.1.2. Methodology

The rings in each layers of the axisymmetric structure extend up to 100 µm in diameter and have a 2 µm separation between the rings. In every second layer the structure of the rings is reciprocal, *i.e.*, the radii with refractive index maxima correspond to radii with index minima in the next layer. Two layers comprise a one crystal period. The longitudinal period was chosen to vary around $d_\parallel = 13.4$ µm, in accordance with expression 1.6. Such longitudinal period corresponds to central filtering angle of 68 mrad. These parameters are selected for a viable comparison with results from [25].

For chirped crystals the longitudinal distance between the individual layers $d_{\parallel/2} = d_{\parallel/2}$ is linearly incremented by Δd for every new layer: is $d_{\parallel/2} = d_{\parallel/2,\text{begin}} + j \cdot \Delta d$, where j counts the layers j $= 1..2N$, where $2N$ is the number of layers and (double of the number of periods). The dimensionless chirp parameter is defined as $C = \Delta d_{\parallel/2}/\overline{d_{\parallel/2}}$, where $\overline{d_{\parallel/2}} = (d_{\parallel/2,\text{begin}} + d_{\parallel/2,\text{end}})/2$ is the average distance between layers. The chirp parameter C was varied from sample to sample.

The numeric analysis was of the structure was using the procedure defined by eq. 1.4 and the Quasi-Discrete Hankel transform BPM algorithm [39].

As for the fabrication parameters, they are indicated in table 2.1. Characterization was the same as described in subsection 2.1.2 and is shown here in
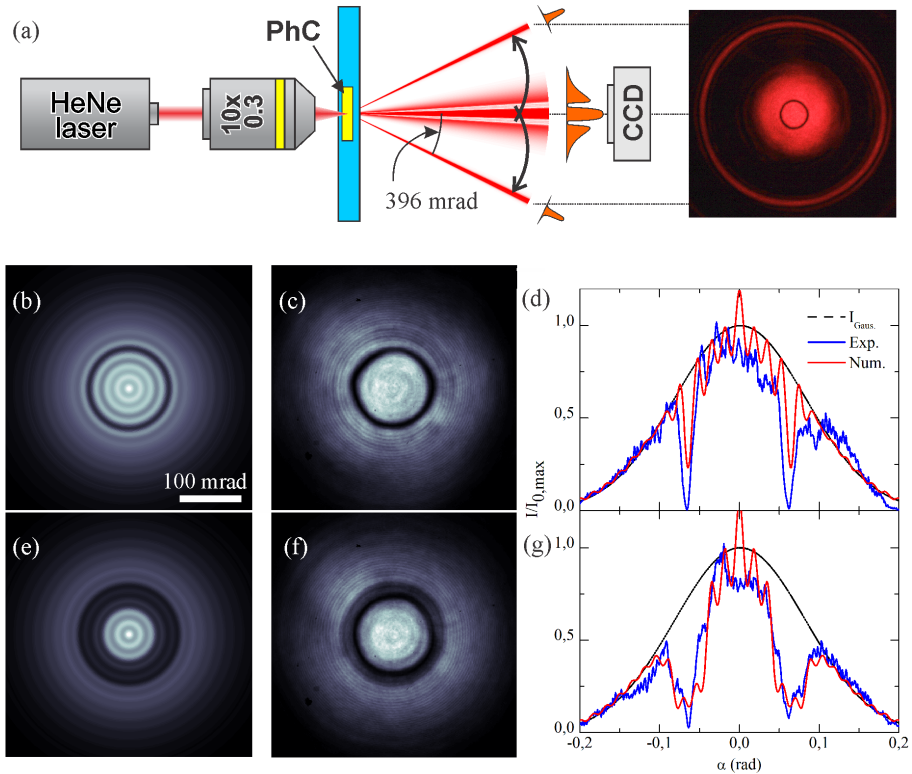
Figure 3.2: (a) Scheme of the experimental measurements: the HeNe laser beam is focused into PhC, a part of the angular components are deflected to the diffraction maxima and the rest passes through. A CCD camera is positioned to record the far-field images of the central part of the beam. A corresponding digitally enhanced optical image of the projected output beam is shown on the right. A numerically calculated (b) and experimentally measured (c) 2D angular intensity spectra of a beam after passing through the sample with $N = 14$ periods without chirp ($C = 0\%$) is demonstrated including the crosssections (d) of the intensity distributions from the central parts of the calculated and measured spectra. (e) Numerically calculated angular spectrum of a chirped structure with the same number of periods ($C = 1\%$), (f) a corresponding experimental spectrum, with the vertical crosssections shown in (g).

fig. 3.2(a). No noticeable change in far-field images behind the structure was observed under different angles of polarization of the incident beam.

3.1.3. Summary of main results

The numerical and experimental results are summarized in fig. 3.2(b-g). Chirping allows increasing the filtering angle width from 17 until 43 mrad, as found by measuring the FWHM (full width at half maximum) of the dominant normalized filtering line. This an increase by a factor of ≈ 2. This is not a par-

ticularly extreme result. It is still limited by the maximum length of the PhC structure possible to produce in glass using the Gaussian beam DLW method. However, this enforced the idea that the intuition developed for 2D structures is reasonably transferable to 3D axisymmetric structures. More importantly, the axisymmetric structures have the disadvantage of not having the property of translational invariance, however, as opposed to 2D structures [24], their transverse lattice constant can also be chirped. With one degree of freedom explored, the research could continue for the second one with the added benefit of exploring the supercollimation effect further [33].

3.2. Inverse design of 2D PhC Laue spatial filters

This section presents the summary for thesis paper **A4** and initial basis for **A5**.

Photonic Crystal Spatial Filters, apart from stand-alone spatial filtering function, can also suppress multi-transverse-mode operation in laser resonators, increasing their beam spatial quality and its brightness. Here it is shown that such Photonic Crystals can be designed by solving the inverse problem: for a given spatial filtering profile, the architecture of the Photonic Filter can be systematically designed by a local search algorithm. Optimized Photonic Crystal Filters were fabricated in a photosensitive glass. Experiments have shown that such Filters provide a more pronounced filtering effect for total and partial transmissivity conditions.

3.2.1. Motivation

The Laue configuration does not lead to the conventional angular bandgaps, as the diffracted wave components propagate in the same direction as the incident beam. The diffracted wave components, therefore, in the course of propagation, couple back into the incident beam, resulting in Rabi-like oscillations between the near-axis- and diffracted wave components. This results not in complete angular bandgaps, but in quasi-bandgaps. The filtering angles can be calculated following the wave Talbot-resonance conditions: specifically that the angular component with $\mathbf{k} = (k_x, k_z)$ and $k^2 = k_x^2 + k_z^2 = \omega^2/c^2$, subjected to the diffraction on wavevector $\mathbf{q} = (q_x, q_y)$, results in a scattered wave $\mathbf{k}_1 = \mathbf{k} + \mathbf{q}$ which is also resonant: $k_1^2 = \omega^2/c^2$. In the paraxial approximation this results in a simple expression:

$$\sin(\alpha) = (Q-1) \cdot q_x/(2k_0) = (Q-1) \cdot \lambda/(2d_x) \,, \tag{3.1}$$
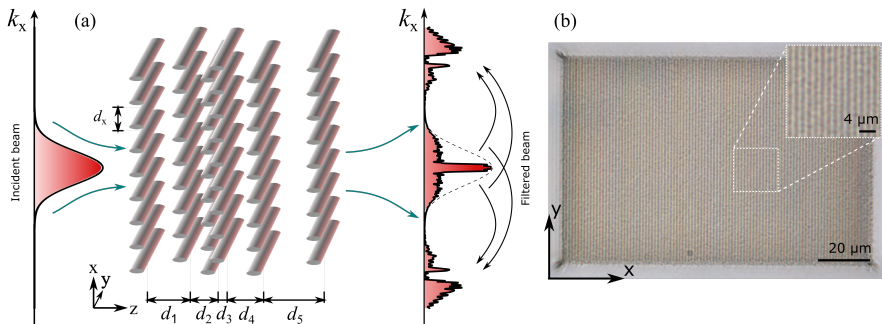
Figure 3.3: The PhC spatial filtering concept. (a) shows the side-view of the incident beam propagation through the aperiodic optimized PhC, where the planes of modified refractive index plane structures are placed at different positions $d_1, d_2 \ldots d_n$. (b) the optical microscopy image of the PhC embedded in glass (top-view).

where the dimensionless coefficient $Q = 2d_\mathrm{x}^2/(\lambda d_\mathrm{z})$ is a PhC geometry parameter.

The Rabi-oscillatory character of Laue diffraction imposes the limitation on the length of the PhC: the optimum length is approximately: $L = 2 \cdot \lambda/\Delta n_\mathrm{ref}$, and the angular width of the line is limited to $\Delta\phi = \sqrt{3} \cdot \Delta n_\mathrm{ref} \cdot d_\mathrm{x}/(2\lambda)$ (see T.p. **A4** supplement material), where Δn_ref is refraction index contrast. Also the filtering line is of bell-profile for $z < L$, but an oscillatory or even disordered for $z > L$. For many applications one needs broader/narrower angular ranges of filtering, also frequently the filtering line should have a particular shape, for instance a rectangular.

One of the possible solutions to broaden the angular quasi-bandgap is to use the chirped PhCs. As the filtering angle depends on the periods of the structure, it is in principle possible to design a structure where the period smoothly varies along the PhC, and respectively the filtering line adiabatically sweeps through the required angular range. This allows to increase the angular range of spatial filtering [129], however, the shape of the filtering line is hardly controllable.

A principally different scenario of engineering the angular quasi-bandgaps in PhCs is proposed: instead of attempting to systematically calculate the chirped structure, an optimization algorithm is used to design the PhC according to the required spatial filtering characteristics. In the simplest case such characteristics can be the width and depth of the dips in the angular transmission curve, while in a more sophisticated case one can define an exact shape of the angular transmission function. Different applications have different requirements for the spatial filtering line: for instance the intracavity PhC filters in high finesse resonators [130] do not require 100% filtering (zero transmission), but rather shallow and broad dips in the transmission function.

The angular transmission function of the PhCs is engineered on demand. The rest of the section is devoted to the calculation, fabrication, and measurement of such PhC filter with required characteristics. In concluding part, it is also shown that such an approach can be used to generate a quite sophisticated angular transmission spectra.

3.2.2. Methodology

Numerical

The PhCs have been designed using a numerical optimization based on steepest descent algorithm. The interlayer distances (in longitudinal direction) of the structure were subjected to variation. In order to maintain the transverse translational invariance, the transverse period constant was kept constant and equal to $d_x = 1.2$ µm. Interlayer distance (half-unit cell distances) vector is defined $\mathbf{d} = (d_1, d_2, d_3, \ldots, d_{(n-1)}, d_n)$ is defined as a set of longitudinal (in the propagation direction) layer spacings. A fitness function $F(\mathbf{d})$ has been introduced that defines how well the spatial transmittance spectrum $T(\alpha, \mathbf{d})$ corresponds to a target ("ideal") spatial transmission spectrum. The target transmission spectrum in most cases was defined to be equal to 1 in a central angular band $|\alpha| < |\alpha_1|$, and was restricted to exceed a predefined value T_{max} in an angular range (band) $\alpha_1 \leqslant |\alpha| \leqslant \alpha_2$. Thus the fitness function is:

$$F^{-1}(\mathbf{d}) \triangleq \int_{-\delta_2}^{+\delta_2} \left(T(\delta, \mathbf{d}) - T_t(\delta) \right)^2 \cdot G(\delta)$$
$$\cdot H\left[T(\delta, \mathbf{d}) - T_t(\delta) \right] \, \mathrm{d}\delta \,. \tag{3.2}$$

In order to deal with a dimensionless fitness function, a normalized wave-vector projection value $\delta = k_x/k_0 = k_x\lambda/2\pi = \arcsin\alpha$ is used. In addition, to ensure that the more relevant angular components lead to a larger impact when a weight function that corresponds to the probe beam angular intensity profile (for convenience a Gaussian is chosen as the most generic: $G(\delta) = \exp(-\delta^2/\delta_0^2)$) is employed.

The range of values that d_i can assumed is limited to d_{min}, d_{max}. The lower bound, specifically $d_{min} = 2.4$ µm is empirically determined by the limits of fabrication (the resolution). The upper bound $d_{max} = 10.9$ µm is set somewhat arbitrarily limiting the maximum possible dimensions of the PhC. The optimization problem was solved for the most part using the steepest descent numerical (gradient) method, which for T.p. **A5** was substituted by the genetic algorithm. The optimization starts from a predefined initial vector $\mathbf{d_0}$ and at each iteration the angular transmission profile for a given $\mathbf{d}$ is computed by the BPM (see 1.4) approach and compared to the target transmittance function $T_t(\delta)$ and the $\mathbf{d} = \mathbf{d} + \Delta$ value is updated to a presumably more optimal value.

Consider two relevant cases: 100% low angle pass filtering $T_{\max} = 0\%$. The other case is $T_{\max} = 50\%$, where keep in mind that for many applications, *e.g.* laser resonators not necessarily 100% filtering is needed. For this reason in eq. (3.2) the integral argument features a step (Heaviside – H) function. Note that not only the bounds can be selected in multiple ways, but also the optimization method itself.

The basic BPM method cannot bet used to estimate reflections from the structure, however, physically they are expected. Some results were validated using the RCWA method [131, 132, 133]. Excellent agreement is observed for low index contrast $\Delta n_0 = 0.004$, and slightly larger deviations for $\Delta n_0 = 0.02$, which is prohibitive due to large resonant backscattering. Altogether, extensive simulations with the RCWA solver reveal that the BPM yields reasonable results for lateral periods $d_x \gtrsim 2$ µm (i.e., larger than approximately twice the wavelength), longitudinal periods d_z corresponding to $Q \in [0.4, 1.6]$ [1], refractive index contrast of the order of $\Delta n \sim 0.01$, and not more than some ten longitudinal periods. In that case, the RCWA also predicts a tolerable intensity in the backscattered[2] field below the 1%-level.

The above considerations indicate that broader angular transmission gaps, which are potentially useful for spatial filtering, are obtained either for larger index contrast or increased number of longitudinal layers. However, in case of strictly periodic PhCs, this comes at the cost of increased resonant Laue-Rabi energy return. In the following, it is shown that PhCs with variable longitudinal periods avoid this detrimental side effect.

Experimental

Fabrication of PhCs was performed by a point-by-point modification of refractive index using a tightly focused femtosecond laser beam using a DLW setup, described more in detail in [24]. The DLW method is widely used for inscription of various micro-optical and photonic components in glass, such as waveguides [107], Bragg gratings [134], also a variety of other structures and materials [135]. The PhCs were fabricated in Foturan glass $n_{\text{ref}} = 1.52$ (a lithium-aluminum-silicate based photoetchable glass). This material is frequently used for etching of micro-fluidic channels or tailoring light transmission by controlling the volume of laser/light exposed volume [136, 137]. For the current experiments, no annealing step was applied, as it decreases the filtering function of the fabricated PhCs, due to diffusion of laser affected regions

---

[1]The reader should note that this results is declared for $\lambda_0 = 975$ nm in accordance to the context of T.p. **A5**. If there should arise the need to consider other wavelengths. The results should hold in accordance to frequency/geometry scaling principles $\lambda_1/\lambda_2 \sim d_2/d_1$, however, at least empirically the scattering efficiency coefficient s is still wavelength dependent, therefore this claim is limited to the applicability of the model, but not about the automatic scalability of the results.

[2]Backscattering means that in the angular intensity reflection spectrum of the PhC significant peaks appear that are neat the projected filtering angles.
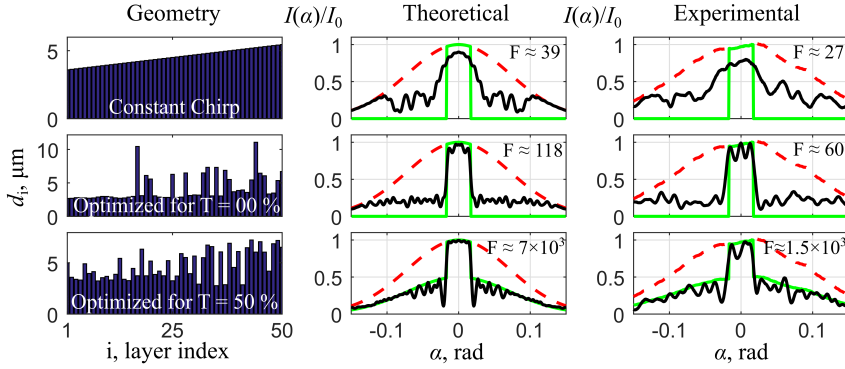
Figure 3.4: Numerical and experimental results compared. Cases are shown for constant chirp and optimized for both $T_{\max} = 50\%$ and 0%. Numerically derived angular intensity spectra and experimentally derived spectra are shown.

and scattering by nanocrystallites. However, higher refractive index change is still achieved in non-post-treated Foturan glass compared to the soda-lime or borosilicate glass, and lower scattering is observed compared to the fused silica, where the scattering is very pronounced due to formation of nanogratings [138].

For fabrication parameters are given in table 2.1. For characterization of the filtering performance samples were probed by a linearly polarized continuous 633 nm wavelength He-Ne laser beam focused into the structure using a 0.3 NA objective. Angular divergence was 180 mrad (≈ 10 degrees). To quantify observed the spatial filtering the beam was observed in the far field profiles by CCD camera positioned at ≈ 10 mm distance behind the PhC.

3.2.3. Summary of main results

The experimental measurement results are summarized in Fig. 3.4 and Fig. 3.5. Fig. 3.4 shows the transmission characteristics of the designed structure, compared with the transmission by a chirped structure. The fitness F as defined for the $T_{\max} = 0\%$ case is the worst for constant chirp, where the chirping interval is tuned to the filtering range from 17 mrad to 150 mrad. Qualitative agreement is apparent and an improvement of performance for optimized cases is observed. The imperfections of fabrication of the PhC structure result in lower F values compared to the numerically calculated cases. Also, the minimum interlayer distances are at the limit of the fabrication resolution, which is another source of the discrepancy. Nevertheless, for the 100% case ($T_{\max} = 0\%$) the merit value increased by factor of $F_{\mathrm{Opt.,T=0}}/F_{\mathrm{Chirp.,T=0}} \approx 2$ times compared to the chirped case (see Fig. 3.5(a)). Furthermore, for the $T_{\max} = 50\%$ filtering case the increase of performance from the chirped to optimized case is even larger $F_{\mathrm{Opt.,T=0.5}}/F_{\mathrm{Chirp.,T=0.5}} \approx 3$. To quantify the discrepancies ran-
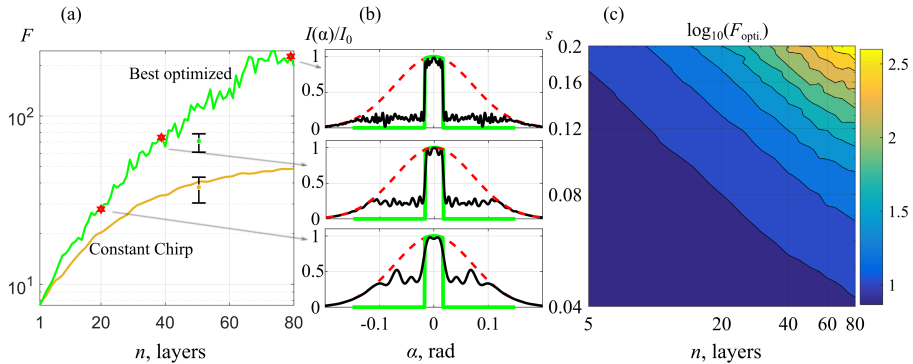
Figure 3.5: (a) Optimized geometry fitness values vs. the initial chirped and periodic PhC cases, where (b) shows numeric intensity profiles expected for selected cases. (c) fitness value dependence on the s parameter and number of layers n is shown (computations were limited to maximum 400 iterations per point).

dom perturbations were added to the optimal solutions, similarly as in [139] (see T.p. **A4** Note 4 in Supporting Information). By taking only the error for layer displacements into account, the amount of displacement needed to produce drastic changes for observable F would be of two magnitudes larger than for band-gap based structures.

Due to the fabrication restrictions, the number of periods in the fabricated structure was limited to $n = 50$ layers, which however can be increased by using more advanced fabrication techniques. Therefore numerical optimization of angular PhC filtering was performed, with parameters beyond those fabrication restrictions in Foturan glass (which come out to be a more suitable glass compared to soda-lime glass used in our previous works [24, 130]). For Foturan, the single-layer scattering coefficient is: $s \approx 0.065$. In addition, calculations were made for longer crystals compared to those that could be fabricated with Gaussian beam fs-DLW method[3]. Fig. 3.5 gives a quantitative summary of filtering efficiency dependence on the PhC length. The optimized values are calculated starting from the chirped case where the interlayer distances are distributed between the values of 3.585 to 5.71 µm. As the PhC length increases a steeper central pass boundary is achieved. In addition, different optimized solutions are always present for different initial chirp configurations. Note that these solutions are non-trivial such as in Fig. 3.4 and often feature non-smooth distribution of interlayer distances. If the scattering efficiency parameter s and number of layers n could be increased further, then even higher fitness values would be possible (Fig. 3.5(c)).

---

[3]however, now such structures could be made according to T.p. **A7**

4.   Applications

4.1.   Photonic Crystal Microchip Laser

The information and results provided in this section are based on Paper **A3**.

4.1.1.   Motivation

The microchip lasers (and generally other micro- and millimeter size lasers such as edge-emitting or vertically-emitting semiconductor lasers) usually suffer from a low beam quality, especially in high power operation regimes. There have been proposed several techniques to improve the beam quality of microchip lasers, *e.g.* by using optical injection [140], external feedback [141], external gratings [142, 143], external beam manipulation techniques [144] and others, however, this results in a loss of the main advantage - the compactness and simplicity of the laser design.

In order to obtain high beam quality in microchip lasers, usually the emission area is confined in transverse space, localizing the fields by a defect[145] or by using a relatively narrow pump area. The restriction of the pump area and pump intensity enables a single-transverse mode emission, however, strongly reduces the emitted power (P_{out}). The increase of the pump power (either by increasing pump area or the pump intensity) results in multi-transverse mode emission, and therefore in a drastic reduction of the beam quality. The power of emitted radiation still increases with the increase of the pump power, however, the brightness ($B = P_{\text{out}}/A\Omega$, where A is the surface area of the beam cross-section, Ω is the solid angle of divergence) of the radiation, saturates and does not increase.

The idea, is elaborated theoretically and proved experimentally here, is that the specially designed intracavity Laue type Photonic Crystals (PhC) can solve the beam quality problem for high pump power decreasing the beam quality factor M^2. The spatial filtering by PhCs is based on the angular band-gaps PhCs [9, 10] and angular quasi-bandgaps PhCs [11, 12], and does not require the access to the far-field domain of resonating field like in conventional filtering techniques by confocal lens arrangement. The PhC spatial filters can provide

efficient filtering in extremely short propagation distances (typically around 200 µm) [24]. The arrangement, therefore, comprises an efficient, compact laser source, which is named the microchip photonic crystal laser, able to emit powerful beams of good spatial quality (single transverse mode beams), and of high brightness (fig. 4.1).
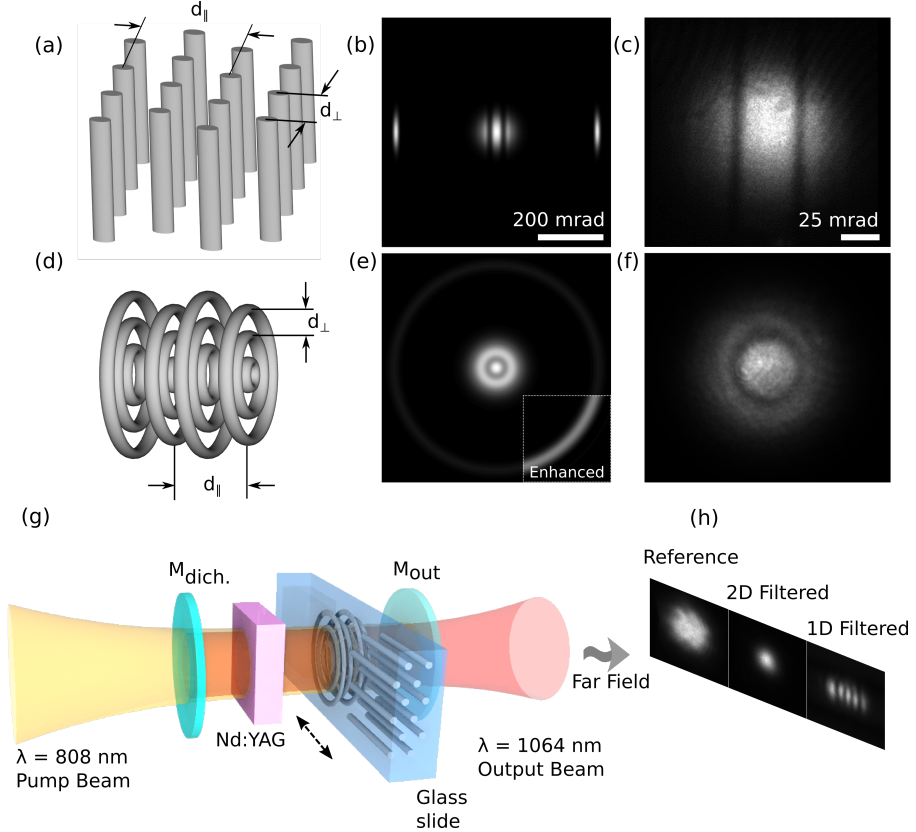
Figure 4.1: (a) Spatial PhC filter, consisting of periodic structure of parallel rods, results in one-dimensional filtering, as shown in single-pass angular far-field distribution, numerically (b) and experimentally (c). Respectively, PhCs of circular geometry (d) causes axisymmetric filtering (e,f). The (g) schematically shows the microchip laser structure, with inserted intracavity PhC filters (1D, axisymmetric and no filter), and (h) shows the experimentally measured far-field profiles in corresponding cases.

4.1.2. Methodology

Numerical tests

Numerical simulations of the microchip laser were performed to justify the experimental observations, and also to show the potential of a photonic crystal

microchip laser with- and without the intracavity spatial filtering. Simulations are based on numerical integration of the Maxwell-Bloch Equation (MBE) system:

$$\frac{\partial E}{\partial t} = \left[-\left(1 + i \cdot \omega_0\right) + ia\nabla_\perp^2 + iV\left(r_\perp\right) + F\left(\nabla_\perp\right)\right] E + P \qquad (4.1a)$$

$$\frac{\partial P}{\partial t} = -\gamma_\perp (P - ED) \qquad (4.1b)$$

$$\frac{\partial D}{\partial t} = -\gamma_\parallel \left(D - D_0\left(r_\perp\right) + \frac{EP^* + E^*P}{2}\right), \qquad (4.1c)$$

where the envelope of the beam $E(r_\perp, t)$, the field polarization $P(r_\perp, t)$, and the population inversion $D(r_\perp, t)$ are defined in two-dimensional transverse space, and evolving in time. $D_0(r)$ is the normalized pump profiled. Time is normalized to photon life time $\tau = Lf/c$, L being the full (round-trip) length of the resonator, and f is the cavity fines (in experiment $\tau \approx 0.1$ ns). Diffraction coefficient $a = L\lambda f/2\pi$ scales the transverse space (in experiment $a \approx 2 \times 10^3$ µm$^2\omega_0$ is the resonance detuning from the gain line center, $\gamma_\perp$ is the polarization relaxation rate, which is typically of order of 10, and $\gamma_\parallel$ is the inversion decay rate, typically of order of 10^{-6} (both normalized to photon relaxation rate). $V(r_\perp)$ is the confining potential in transverse space. Thermal lensing as accounted for as a refraction index profile following the pump profile $V(r_\perp) = a \cdot D_0(r_\perp)$. The filtering function of intracavity PhC is introduced phenomenologically by the operator providing the far-field transmission profile, and matching the experimentally measured angular transmission dependencies of PhC filters.

Microchip laser setup

For the experiment a Nd:YAG based microchip laser has been assembled. It was characterized by a cavity length 5 mm, and maximum emission power 900 mW (in multi-transverse mode regime). To ensure single transverse mode emission, the width of the pump beam was restricted (typically to 80 µm, depending on pump power). The use of broader pump area increases the Fresnel number, and results in multi-mode emission if no special means are taken. PhC filters inside the cavity are used, in order to maintain a high beam quality while increasing the pump area and pump intensity.

For that purpose PhC filters of two different symmetries were fabricated: the axisymmetric filter [25] to achieve the main goal, *i.e.*, the single-transverse mode emission; and also a one-dimensional (1D) spatial filter [24], filtering in one transverse direction. The latter allows to convincingly demonstrate the appearance of a beneficial filtering effect, *i.e.*, to have simultaneously a laser

with- and without filtering in different directions in transverse space under identical conditions (the same pump power and the same losses for both field quadratures). PhCs were fabricated using Gaussian beam point-by-point direct laser writing technique, see the 2.1.2. The ratio between the longitudinal and transverse periods of the index modulation in the photonic crystal structure provides the angular position of the filtering range. For instance, the high angle pass filtering (removal of the axial mode) is obtained for $Q = 2d_x^2/(\lambda d_z) = 1$. In order to obtain the low-angle pass filtering (transparent for the axial mode and opaque for small angle of-axis modes), which is the purpose here, the geometry parameter Q slightly deviates from unity.

4.1.3. Summary of main results

The PhC filters were first tested in stand-alone configuration (see the experimentally measured transmission), and then positioned inside the cavity of microchip laser[1]. The experimental outcome is shown in Fig. 4.2(h). The axisymmetric spatial filter in the cavity of microchip laser causes the narrowing of the far-field radiation (decrease of angular spread of the beam) and formation of single-transverse-mode beam. For comparison, 1D filter results in the decrease of the angular divergence along the filtering direction only (vertical direction in Fig. 4.1(g)) whereas the beam in unaffected (horizontal) direction remains largely diverging (containing higher-order transverse modes).

Fig. 4.2 summarizes the quantitative experimental results. Without the PhC filter the increasing pump power results in the increase of the emission power and of the divergence of the output beam, whereas the brightness of the radiation remains approximately constant. With the PhC filter in microcavity the divergence of the beam remains independent on the pump power (up to a particular pump level), and the brightness constantly increases with the pump. Note that the emission power in the presence of the PhC spatial filter just slightly decreases compared to the case without spatial filtering; also, the pump threshold power[2] increases from 0.453 W to 0.464 W. The increase of brightness due to intracavity photonic crystal is 2.8 (maximum brightness) — 3.1 times (at equal pumping) in this particular experimental measurement. Behind a particular threshold for the pump power the spatial filtering is no more sufficient, and the beam quality as well as brightness starts decreasing. Maximal power of single transverse mode beam was 88 mW without filtering and 335 mW with the PhC filter (area with divergence <9 mrad). It depends on the efficiency of the spatial filtering (the width and the depth of filtered out

---

[1]It would be interesting to compare the results of the PhC filter with a conventional filter, however for a microchip laser the typical pinhole filter is not possible to test as the cavity length is minimal. However, o model cavity has been assembled with a slit-filter for comparison for a semiconductor external cavity laser and is discussed in section 4.2

[2]The values were estimated from the first data points fig. 4.2(c).

area in angular domain). Speaking in numbers, the spatial quality factor of the beam from the PhC microchip laser remained $M^2 = 1.2$, for the emission power up to 300 mW, whereas the spatial quality factor of the beam from the laser without spatial filtering increased until $M^2 = 2.5$ for the same output power.
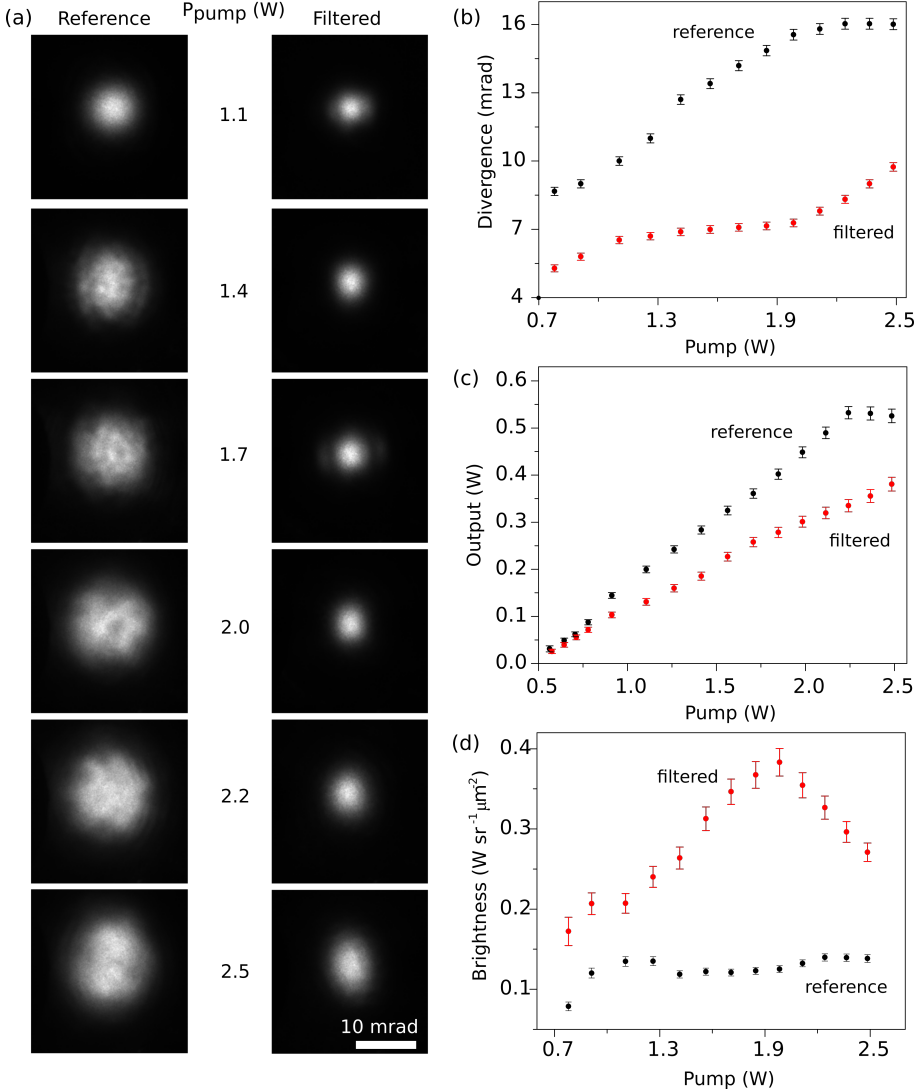
Figure 4.2: (a) Experimentally measured far-field distributions from the microchip laser without a PhC spatial filter (first column), and with (second column) axisymmetric intracavity spatial filter ($Q = 1.18$, $N = 20$). The width of the pump beam was 200 μm. Presence of the axisymmetric filter results in TEM00 mode of emitted radiation. (b), (c), (d) shows the beam divergence, output power, and brightness dependencies on the pump power respectively.

Concluding, a substantial improvement of the spatial quality of the beam emitted by microchip laser due to the spatial filtering functionality of intracavity photonic crystals is shown. Specifically, the power of single transverse mode emission was increased from 90 mW without intracavity PhC, to 340 mW with intracavity PhC, *i.e.*, almost 4 times. The brightness of the emitted radiation has been increased approximately by a factor of 3.
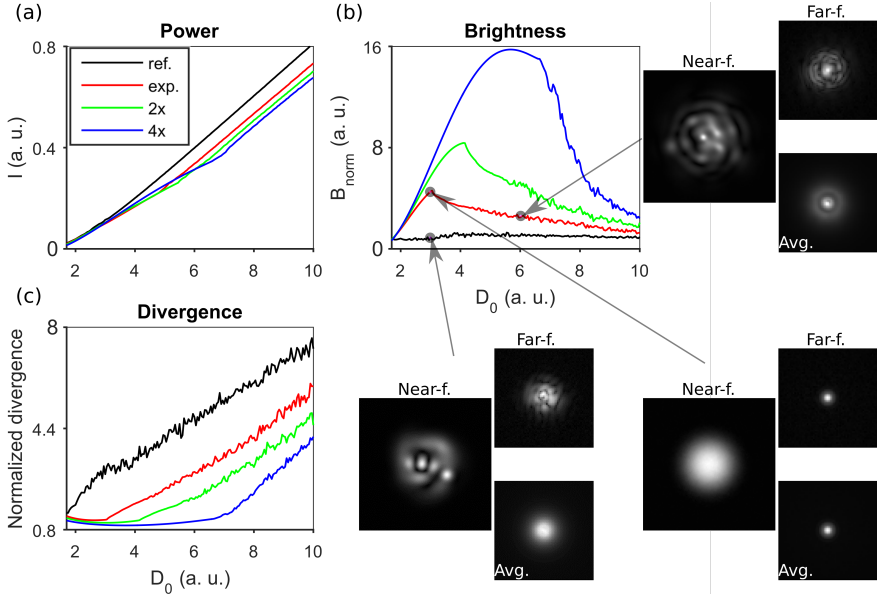
Figure 4.3: Summary of numerical simulations of photonic crystal microchip laser: (a) shows the emission power, (b) the brightness and (c) the angular divergence of the emitted beam, depending on the pump power, for three realizations of spatial filters. The black line depicts the reference case (no filter), the red line corresponds to the filter with transmission profile corresponding to the experimental situation (Fig. 4.2), and the green and blue lines correspond to the filters with 2 and 4 times increased filtering performance (correspondingly increased width of the filtering area). The near- and far-field beam profiles as well as averaged far-field profiles are shown on insets: the near field window size is 2×2 mm^2, and far field windows size is 40×40 mrad.

The performance can be strongly improved by advancing the angular transmission characteristics of the spatial filters. The angular filtering range is limited by the material characteristics of the filter (the amplitude of refraction index modulation, and the length of the PhC (the number of longitudinal periods). The performance of photonic crystal microchip laser is thus restricted by technological limitation (aberrations of femtosecond laser writing arrangement, available materials) of the PhC filters. With the future advance of microfabrication technologies and with new materials providing the larger refraction index modulation, the performance of the PhC microchip laser can be significantly

improved. Technically, the idea can be brought to perfection by fabricating the PhC directly on the microchip active media using DLW techniques, resulting in a completely monolithic device [146]. The present work demonstrates the principle of intracavity spatial filtering by PhCs, and thus constitutes a new class of laser - the photonic crystal microchip laser. The numerical simulations show huge potential of the photonic crystal microchip laser improved using advanced technologies. In particular, numerics show that the concept is applicable for pulsed microchip lasers too.

Finally, the proposed idea could be applied to the other types of micro-lasers, like semiconductor edge-emitting lasers, and vertical cavity semiconductor lasers, the VCSEL (in fact the VCSELS would convert into VECSELS, the Vertical External Cavity Semiconductor Lasers, when one incorporates at approximately 200 µm length PhC filter inside the cavity).

4.2. Photonic Crystal Spatial Filtering in Broad Aperture Diode laser

4.2.1. Motivation

Broad Aperture Semiconductor (BAS) lasers usually lack good spatial quality of the emitted beams, especially in the high power emission regimes. This, among others, imposes limitations for tight focusing or coupling of its radiation into the single-mode optical fibers. The strong beam divergence in the vertical direction (fast axis) does not represent a problem since the single-transverse-mode-character of the radiation in this direction allows perfect collimation of the beam. Collimation in the slow axis direction instead is quite problematic due to the intrinsic multi-transverse-mode emission. Other micro-laser types, such as microchip lasers, or Vertical Cavity Surface Emission Lasers (VCSELs), show similar poor-beam quality characteristics, for the same reason — the lack of intra-cavity spatial filtering in such lasers. Conventional lasers (*e.g.* solid-state lasers) usually use the intra-cavity spatial filters, typically using a confocal arrangement of lenses with a diaphragm placed in the confocal plane [147, 148]. This configuration allows direct access to the far-field, where the diaphragm acts as a "low-pass" spatial filter blocking the high angular components. This type of spatial filter has been demonstrated in an external resonator of diode laser array for improving the beam quality [149]. However, such a filtering design is very inconvenient or even impossible for intra-cavity use in micro-lasers: microchip, semiconductor lasers, or VCSELs. The length of such resonators is in the millimeter range (in VCSELs case even in micrometer range) and provide no space for direct access to the far-field. For the case of high power diode lasers, usually configured in an array of multiple emitters, the use of bulky
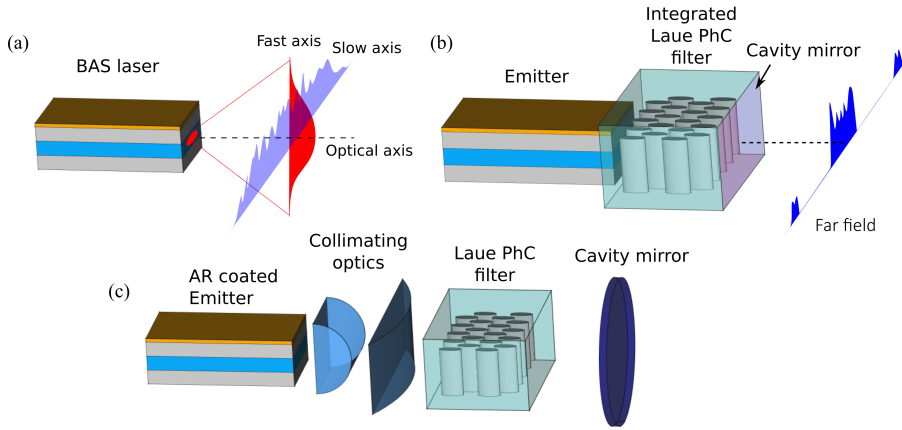
Figure 4.4: (a) The illustration of the typical beam structure emitted by a regular BAS lasers (with partial reflective output facet mirror) in high power arrangements. (b) The idea of spatial filtering by PhCs. The higher order modes are diffracted by the PhC, and the lower order TEM modes propagate unaffected as shown in a schematic far-field profile. (c) The PhC placed inside external resonator, which simulates the situation of intracavity spatial filtering.

lenses is not possible.

The quality of the BAS laser beams at low powers can be improved by several methods, for instance, (i) confining the radiation transversally by inscribing a waveguide structure in the semiconductor material. This microstructure fabrication, however, severely restricts the amplification area, and thus the emission power; (ii) by restricting the amplification/emission area through the use of apertures in VCSELs or (iii) by accurate gain guiding in microchip lasers. None of these methods are useful to solve the problem of beam quality in the high-emission-power regimes. For the BAS lasers, some other techniques have been proposed, like the use of tapered geometries, evanescent spatial filtering, and external cavity [150, 151, 152]. However, these methods have a limitation in terms of power achievable and the size of the device.

A promising idea to solve the beam quality problems of the microlasers in the high emission power regime is the use of intra-cavity Photonic Crystal (PhC) spatial filters integrated into the laser cavity. The idea is based on the Laue type PhCs discussed in subsection 1.2.1, where a selective deflection of the angular components of the light propagating through a 2-D photonic structure that are resonant with the transverse and longitudinal periodicities of the photonic structure diffract efficiently and are deflected from the zero-diffraction order of the incident beam. The use of such PhC spatial filtering [25] was already used to clean the spatial structure of a laser beam for a microchip laser as discussed in T.p. **A3** and section 4.1.

The goal here is the design of efficient intra-cavity PhC acting as a spatial filter in BAS lasers. The possible monolithic implementation scheme is illustrated in Fig. 4.4(b), showing how the PhC structure could be integrated directly between the active medium and the laser output cavity mirror. Such integration is, however, very challenging technologically.

To test the spatial filtering effect of the PhC more simply, an extended-cavity configuration was designed to mimic the action of the more compact cavity. By adding an antireflective coating at the output facet of the semiconductor element, lasing is prevented from the semiconductor emitter alone. Collimation optics and an external output cavity mirror provide the necessary feedback to achieve the laser action in this extended-cavity configuration, which allows placing the PhCs inside the laser cavity to test their filtering capabilities, as schematically depicted in fig. 4.4.

The effect of the PhC filtering for BAS has been numerically studied for BAS in external cavity configuration T.p. **A5**. Here, successful proof of the physical implementation of the intracavity spatial filtering by PhCs in BAS lasers is reported. Compact PhC filters of sub-millimeter length were fabricated, and their spatial filtering properties demonstrated to affect the emission of the BAS laser. The intracavity use of such filters allows a significant improvement of the beam spatial quality and increase in brightness of the emitted radiation in high power regimes. These results open the way for a promising future goal, *i.e.*, the technological implementation of a compact (monolithic) intracavity designed system for spatial filtering. This task is beyond the current scope.

4.2.2. Experimental

To prove the thesis that PhCs interact with the laser beam radiation as intended (observed brightness B increase) have been tested for:

- the BAS laser without any spatial filter;

- the BAS laser with an intracavity slit spatial filter arranged for the slow-axis;

- the BAS laser with an non-chirped PhC filter;

- the BAS laser with a chirped PhC filter.

The laser and characterization

For the experiment, a BAS laser was arranged, as shown in Fig. 4.5. The lasing wavelength was around 970 nm. The emitter (an InGaAs double heterojunction type device) was of a 400-µm transverse width and 1500-µm length active area, had an AR coating on the output facet. During the experiment, the emitter
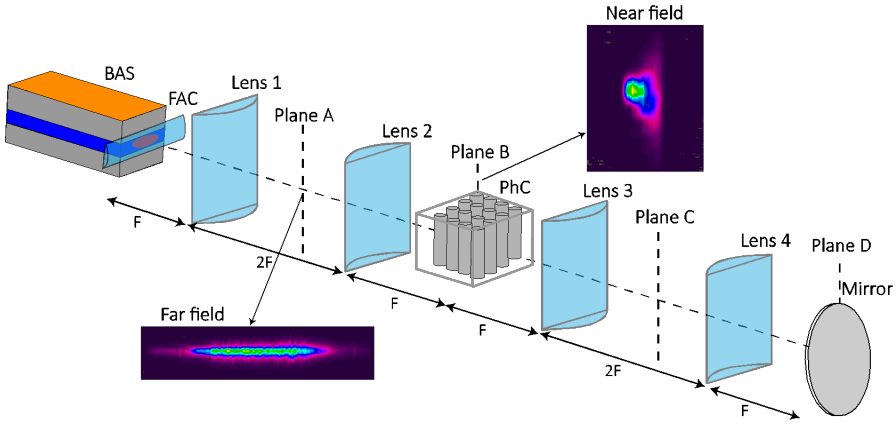
Figure 4.5: Experimental setup of spatial filtering in external cavity configuration. BAS: broad area semiconductor, FAC: fast axis collimator. Lens 1-4 with a focal length of 50.8 mm. The far-field planes are marked as (plane A) and (plane C). The near-field planes (images of the BAS output facets are marked as B and D). The reflectivity mirror is 4%.

was driven by a 3A current[3] at a repetition rate of 50 Hz and 25 % duty cycle. A 4% reflectivity mirror[4] was used as the outcoupling mirror. The cavity was arranged with cylindrical lenses acting separately in the slow and fast axis. The fast axis emission was collimated by using a cylindrical lens (FAC) of a very short focal length of 590 µm, with a numerical aperture (NA) of 0.8. For the slow axis direction, a double 4-f system was used in order to obtain two conjugated planes of the output facet of the active medium. The PhC could be inserted in the first conjugated plane, with 1:1 magnification. The second 4-f system provides a second near-field plane (marked as D), where the output cavity mirror was placed and carefully aligned to obtain lasing action. All lenses were AR coated. Spatial filtering means were placed at the center of the 4f system.

The beam profile at the output of the laser was recorded by imaging the external cavity mirror plane into a CCD camera with proper magnification. The near-field profile recorded by this means has dimensions of 450 micrometer x1.4 mm. The effect of the PhC filtering was observed experimentally by looking at the far-field distribution of the emitted radiation. The recording of the far-field pattern was conducted placing an external lens out of the cavity and imaging the rear focal plane into the CCD.

The spatial quality of the beam is quantified by the measurement of the beam quality factor given by $M^2 \approx BPP_{\text{Observed Beam}}/BPP_{\text{difr. lim. beam}}$.

---

[3]The lasing threshold was at 1.3 A.

[4]The reflectivity of this external mirror is limited to 4% to avoid the possible damage of the emitter facets [153].

Where BPP refers to beam parameter product and is given by $BPP = Beam\ waist \times Divergence\ Angle$. While the Brightness, B is defined as $B = P_{\text{opt}}/\lambda^2 M_{\text{slow}}^2 M_{\text{fast}}^2$ [154]. Where P_{opt} is the average optical power, M_{slow}^2 and M_{fast}^2 are the beam quality factors along slow and fast axis respectively and is the central wavelength.

The M^2 factor was calculated by recording the profile of the beam as a function of propagation distance after being focused using an ancillary external lens of 100 mm focal length. The beam diameter recorded independently in the fast and slow axis, was determined using the D4σ method [16]. From the diameter versus distance plot, the minimum spot size and divergence angle can be measured to determine M^2. The initial M^2 factor measured without any filtering means was $M_{\text{slow}}^2 = 47$ and[5] $M_{\text{fast}}^2 = 3.3$. These values are consistent with reported values in similar systems [155].

The slit and PhC filters

A variable aperture slit (aperture) filter was used as an etalon to gauge how much improvement can be expected compared to the Laue PhC filters. The slit was arranged in the far-field planes of the cavity. Laue type PhC spatial filters were arranged in near field planes of the cavity. The PhC filters had to be made for this experiment.

The PhCs were fabricated in N-BK7 ($n_{\text{ref}} \approx 1.52$) glass substrates with a broadband antireflective coatings on both facets. Two versions of PhC filters were fabricated: one inscribed by using a Gaussian beam DLW approach, and another with Bessel beam (fig. 4.6). Both fabricated structures were characterized by the transverse lattice constant d_{x} and the longitudinal lattice constant d_{z}. The Bessel beam DLW made PhC was chirped, therefore its was characterized by a longitudinal period d_{z1} for the first period in the PhC, and d_{z2} for the end period, with d_{z} values changing linearly along with the structure.

The Gaussian-beam fabricated (non-chirped) structure was characterized by $d_{\text{x}} = 2$ µm, $\lambda = 970$ nm and $Q = 0.9$ with an aperture of 2x2 mm^2 and number of longitudinal periods $N_{\text{L}} = 10$. The Bessel-beam fabricated structure had a different transverse period $d_x = 3$ µm value and was chirped in the propagation direction with a linear increment of $d_{z,i}$ in the range $1.15 \leq Q \leq 1.27$ with $N_{\text{L}} = 80$ and an aperture of 2.85 x 2.3 mm^2. An example is demonstrated in Fig 4.6(c) as it was made from 5 identical segments stacked along the intended fast-axis direction (stitched vertically similarly as in [102]).

For more details about the fabrication procedures and exposure parameters see [24] and T.p. **A3** for Gaussian, T.p. **A7** and section 2.2.2 for Bessel beam. Due to the limited length of PhCs, the Gaussian beam fabrication strategy

---

[5]The larger value of M^2 in the fast axis could be due to a small misalignment of the FAC lens.
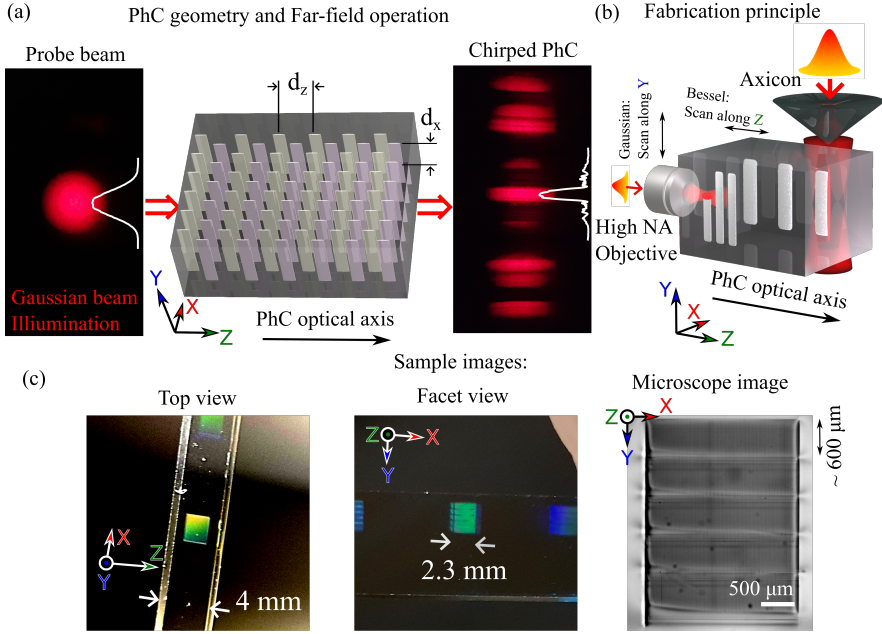
Figure 4.6: The illustration of the PhC showing how refractive index modified structures are arranged inside the glass substrate and expected effected on the far-field intensity spectra of the beam (a), the illustration of the PhC fabrication using femtosecond pulsed Bessel beam (b), and photographs and microscope image of the Bessel made structures after fabrication (c). Images of the far-field beam intensity patterns that demonstrate the principle of angular filtering with non-chirped and chirped geometry PhCs and resulting in either narrow or wide angular filtering bands, corresponding large angle filtered out radiation bands.

allowed the filtering range of 1 degree, which turned out to be not wide enough for BAS lasers (5-10 degrees preferred).

4.3. Summary of results

The result of spatial filtering for conventional confocal filtering, PhC (Gaussian beam) and PhC (Bessel beam) compared with the situation without filtering is summarized in fig. 4.7. Although the best performance was obtained for the confocal filtering case, it is convincingly shown that the action of the improved PhCs filters tends towards the achievement of these optimal values. The threshold current is only slightly increased compared to the case, where no filter is used and the output power is also reduced.

Spatial filtering of a broad-area semiconductor laser using a PhC in external cavity configuration, which mimics the internal cavity configuration, has been demonstrated. The main result was a reduction of M^2 and the brightness enhancement of the emitted radiation. Comparison with the conventional
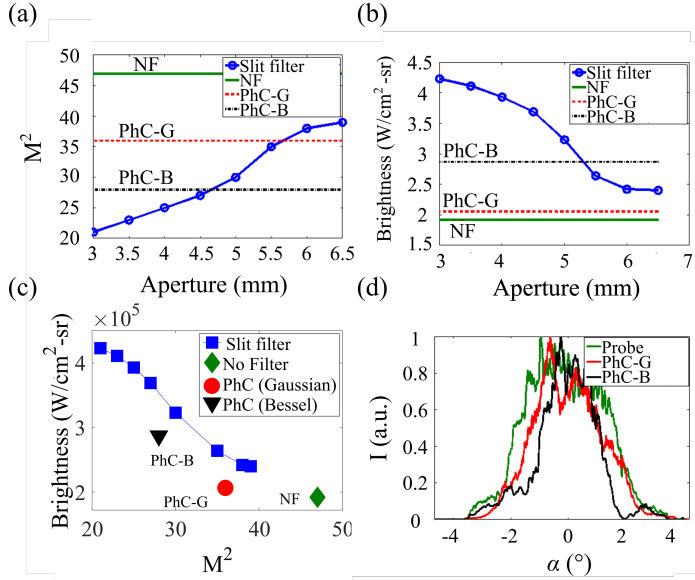
Figure 4.7: (a) M^2 reduction by action of spatial filtering with conventional filter (blue line) compared with PhC fabricated by Gaussian (PhC-G) and Bessel beam (PhC-B) and No filter (NF). (b) Shows the brightness as a function of aperture. (c) Brightness versus M^2. (d) Far-field intensity profiles for cases without PhC (green) and with PhC, Gaussian beam fabricated (red) and Bessel beam (black).

confocal filtering technique shows that using PhCs filtering one can achieve results approaching the same values of spatial beam quality improvement. The added advantage of the use of PhCs filtering comparing with the conventional technique is that it offers the possibility of integration of the PhC into the BAS leading to a serious breakthrough in regimes of high power emission. Here such integration is not demonstrated due to technological limitations; however, it shows the potential for such integration by proving the physical principle.

Conclusions

The conclusions from these three parts of the dissertation work are drawn and presented as follows:

1. Laue type 2D PhC filtering function has been explored depending on the DLW in soda-lime procedure. This was done to increase the scattering (s-)coefficient, which is a phenomenological value indicating the phase modulation aggregated for a wavefront passing through a layer comprising the PhC. Incidentally, with varied exposure conditions, it was discovered that the structures, in contrast to earlier research, can feature an asymmetric spatial (angular) intensity transmittance function. This asymmetry is explained by exploring the actual structure of the PhC and introducing a tilted sub-layered PC BPM model. Experimental and numerical studies show layers comprising PhCs feature a tilted feature internal structure, which becomes apparent as the Gaussian beam fs-DLW method is used to decrease the periods (lattice constants) of the PhC. This is a new degree of freedom that can be used to control the properties of the PhC.

2. The Laue type 2D PhCs for spatial filtering featured a limitation for a particular geometrical parameter - their length or maximum longitudinal period number. As the single method used for producing such structures was the Gaussian beam fs-DLW in glass approach, the major limitation was the maximum spherical-aberration free working distances extendable not more than 300 µm for high-NA objective lenses used. A paradigm shift was needed, and a Bessel-beam DLW approach was hypothesized as a solution to this problem. A DLW system was assembled and successfully used to produce structures reaching a period $N = 160$ over 3 mm. Using the new method functional PhC filters have been demonstrated ranging for two design wavelengths (633, 970 nm) with filtering (angular) bands up to 4 and 6 deg, thus proving the feasibility of the new approach.

3. The Bragg type 2D PhCs for spatial filtering was proposed as an alternative to the Laue type filters. The structures are characterized by a higher refractive index contrast and sub-wavelength feature size in at least one dimension. The hypothesis here is that if modulated surface

templates (relief gratings) could be combined with thin conformal alternating dielectric constant (refractive index) layers, then the resulting structure would feature photonic stop-gaps. This was tested by analytically calculating the photonic band-structure, using the FDTD technique to numerically calculate the angular intensity transmission spectra and through fabricating the modulated surface substrates followed by physical vapor. Stop-bands have been observed for collimated and focused beams. The consequence of the idea is that new thin photonic spatial filter devices become possible are shown to be achievable, which could be applied at least into some surfaces of functioning devices.

4. The axisymmetric Laue type 3D PhCs that are proposed for microlasers to generate near diffraction limited beams had been shown to have filtering (angular) bands limited to only 17 mrad (0.3 deg). Laue-Rabi oscillatory relation of the filtering band shape and the PhC length did not allow for practically considering such PhCs to be placed inside a laser cavity, therefore more degrees of freedom needed to be explored. It is proposed to employ chirping of the longitudinal period length to tune angular filtering range for larger values. The hypothesis was tested empirically and numerically and proved to be true, consequently increasing the angular filtering range by a factor of two. This justifies the search for new materials, fabrication techniques, and even modulation techniques for even more advanced structures, suitable to be applied in micro-lasers.

5. Confirming the applicability of the linear chirping to the Laue type 2D (and 3D) PhCs for spatial filtering allowed for the next logical step: non-linear chirping. The hypothesis here was that using the established BPM method combined with optimization techniques new PhCs geometries could be found, that could be tailored to specific low-angle pass spatial filtering requirements. Such geometries have been found and even realized by Gaussian beam based fs-DLW in glass. Structures with filtering range up to 150 mrad (~ 2.6 deg) have been realized. Furthermore, numerical solutions to abstract (arbitrary) angular transmittance functions have been found. This includes solutions that optimize the beam brightness of an external cavity broad-area semiconductor laser. The possibility of tuning the angular transmittance function of PhCs has been proven true, without detriment to the advantages of translational invariance and (theoretically) unlimited aperture.

6. A Laue type axisymmetric PhC for spatial filtering has been experimentally tested inside the cavity of a laser CW Nd:YAG microchip laser. The presence of the PhC decreased the beam M^2 parameter (improving the beam quality) and increased the laser beam brightness B. The observed beam brightness increase was of a factor of 3. As the PhC filters are

designed to some extent work as a low pass angular filter, the higher-order transverse cavity modes are suppressed. The laser output beam divergence is decreased.

7. Finally, a Bessel beam based DLW made Laue type chirped 2D PhC spatial filter has been experimentally tested inside the cavity an external cavity of a semiconductor edge-emitting broad-area single emitter laser. The presence of the PhC decreased the beam M^2 quality parameter and increased the laser beam brightness B by a factor of 1.5. This empirically shows that the PhC spatial filtering mechanism is applicable even to low quality factor cavities.

SANTRAUKA

Naudojami trumpiniai

1D	vieno matavimo, vienmatis
2D	dviejų matavimų, dvimatis
3D	trijų matavimų, trimatis
FDJT	fotoninių draustinių juostų tarpas
FDTD	(iš angl. k.) baigtinių skirtumų laiko plotmės (metodas)
FK	fotoninis kristalas
fs	femtosekundinis
HeNe	helio neono (lazeris)
KFDJT	kampinis fotoninių draustinių juostų tarpas
Nd:IAG	neodimio jonais legiruotas itrio aliuminio granatas
PPPM	pilnas plotis pusė maksimumo
PSM	pluošto sklidimo metodas
TLR	tiesioginis lazerinis rašymas

Disertacijos tikslas

Naudojantis skaitmeniniais modeliavimo metodais ir mikrogamybos technologijomis, pagaminti ir ištirti fotoninių kristalų filtrus, kurių savybės būtų gerai suprastos ir jie būtų tinkami taikyti lazerių rezonatorių viduje.

Darbo naujumas ir svarba

1. Išvystytas naujas FK gamybos būdas, kuris yra paremtas Besselio pluošto pritaikymu TLR metu. Šis būdas leidžia gaminti ilgesnius FK nei anksčiau.

2. Eksperimentiniu būdu parodyta, kad Brego režimo fotoniniai kristalai pasižymi erdvinio filtravimo efektu, kuris stebimas matomajame diapazone.

3. Parodytas ašisimetrinės geometrijos fotoninis kristalas su išilginio periodo ilgio linijiniu moduliavimu. Įrodyta, kad tolimojo lauko filtravimo kampo intervalas gali būti padidintas du kartus.

4. Eksperimentiniu būdu įrodyta, kad nelinijinis, kitaip nei linijinis išilginių periodo ilgių moduliavimas (čirpavimas), pagerina dviejų dimensijų Laue režimo fotoninių kristalų pralaidumo profilį erdvinio šviesos filtravimo reiškiniui.

5. Pademonstruotas mikrolustinis lazeris su ašisimetriniu fotoninio kristalo erdviniu filtru rezonatoriaus viduje. Lazerio pluošto skaistis dėl erdvinio filtravimo padidėjo tris kartus.

6. Įrodyta, kad kraštu spinduliuojančio emiterio išorinio rezonatoriaus puslaidininkinis lazeris su fotoninio kristalo filtru rezonatoriaus viduje pasižymi didesniu pluošto skaisčiu.

Ginamieji teiginiai

1. 2D FK erdviniam filtravimui Laue režime gali būti realizuojami naudojant Besselio pluošto pritaikymu grįstą fs-TLR būdą, pašalinant eksperimentinius apribojimus FK išilginių periodų skaičiui ir padidinant pademonstruotų kampinio filtravimo juostų pločius bent iki $\sim$4° matomojoje srityje ir 6° infraraudonojoje srityje.

2. 2D fotoniniai kristalai, veikiantys Brego režimu, kurie sudaryti iš konforminių dielektrinių plonasluoksnių dangų ant periodiškai moduliuotos 1D reljefinės gardelės, rodo erdvinio filtravimo užuomazgas matomųjų bangos ilgių intervale, kurios pagrįstos daliniais draustiniais fotoninių juostų tarpais.

3. 3D ašisimetriniai fotoniniai kristalai erdviniam filtravimui, veikiantys Laue režime matomųjų bangos ilgių intervale ($\lambda = 633$ nm), gali būti pagaminti Gauso pluošto TLR būdu taip, kad pasižymėtų tokiu tiesiniu išilginio periodo ilgių čirpu, dėl kurio centrinis filtravimo kampas tolydžiai kinta išilgai viso darinio ir leidžia stebėti filtruojamųjų kampų intervalo padidėjimą nuo 17 iki 43 mrad.

4. 2D fotoniniai kristalai, veikiantys Laue režime ir skirti erdviniam filtravimui, gaminami naudojant TLR metodą, turi netrivialias išilginio periodo ilgio (tarpsluoksnių atstumų) čirpo variacijas, kurios gali būti randamos panaudojant skaitmeninius gradientinio arba genetinio algoritmo būdus taip, kad atitiktų pasirinktas kampinio intensyvumo pralaidumo funkcijas.

5. 3D ašisimetriniai fotoninių kristalų erdviniai filtrai, veikiantys Laue režime, gali padidinti išilgai diodu kaupinamo nuolatinės veikos Nd:IAG ($\lambda = 1064$ nm) lazerio pluošto skaistį bent 3 kartus, tolimojo lauko domene įnešdami taip moduliuotą kampinį intensyvumo pralaidumo profilį, kad būtų slopinamos aukštesniųjų eilių skersinės rezontoriaus modos.

6. Išorinio rezonatoriaus kraštu spinduliuojančio vieno emiterio puslaidininkinio IR lazerio ($\lambda = 970$ nm) skleidžiamo pluošto skaistis gali būti padidintas bent 1,5 karto, naudojant Laue režime veikiantį 2D fotoninio kristalo erdvinį filtrą, patalpintą rezonatoriaus viduje, tolimojo lauko domene įnešantį tokį kampinių nuostolių profilį lėtosios ašies plokštumoje, kuris slopina aukštesniųjų eilių skersines rezonatoriaus modas.

Trumpas principų aptarimas

Norėdamas skaitytojui padėti geriau suprasti fizinį tokio filtro veikimo mechanizmą, aš apibūdinsiu dviejų tipų filtrų terminus ir principus: Laue ir Brego. Čia vartojama terminologia buvo pasiūlyta [12]. Kryptimi atrankūs dariniai, turintys išilginius periodų ilgius, didesnius nei bangos ilgis λ, priskiriami „Laue" režimui. Čia naudojamas terminas analogijoje su Rentgeno spinduliuotės difrakcija kristalinėse medžiagose (Laue difrakcija [28]), tačiau pritaikyta optiniam kontekstui [29]. Panašiai aš apibrėžiu Brego režimą. Optikoje esant $\lambda \geq d_z/2$ vyksta reiškiniai analogiški Rentgeno spindulių difrakcijai kristalinėse medžiagose, kur atsiranda stiprūs atspindžiai tam tikrais kampais nuo kristalinės gardelės. Tai iš esmės atitinka minėtus atvejus: pirma - Laue režimas - kvazidraustiniai fotoninės juostos tarpai ir, antra, Brego režimas - draustiniai fotoninės juostos tarpai. Abiem atvejais tiek sklaida, tiek atspindžiai yra konstruktyvios ir destruktyvios interferencijos rezultatai.

Šiame darbe yra aktualios dvi gardelių sistemos (bent jau 2D atveju). Laue FK atveju – centruotoji stačiakampė (ortorombinė), o Brego FK užtenka vertinti stačiakampę. Abiem geometrijom toliau pateikti pasvarstymai galioja vienodai. Gardeles apibūdina atvirkštiniai gardelių vektoriai k-erdvėje (arba atvirkštinėje erdvėje): $\mathbf{q} = (q_\perp, q_\parallel)$. Minėti vektoriai čia turi ir alternatyvius žymėjimus, pvz., $q_\parallel \equiv q_x \equiv q_y \equiv q_r$ ir $q_\parallel \equiv q_z$ (palei optinę ašį), priklausomai nuo konteksto. Gardelės vektorių ortogonalios dedamosios yra susietos su gardelių konstantomis kaip $q_\perp = 2\pi m_\perp/d_\perp$ ir $q_\parallel = 2\pi m_\parallel/d_\parallel$. Vertės m yra tokios, kad $m_\perp \in \mathbb{Z}, m_\parallel \in \mathbb{N}$. Rezonansinė sklaida įvyksta kai plokščioji elektromagnetinė banga, apibūdinama banginiu vektoriumi $\mathbf{k}_1$ su bangos skaičiumi $\|\mathbf{k}\| = 2\pi n_0/\lambda_{\mathrm{ore}}$, FK gardelės išsklaidoma į $\mathbf{k}_2$, tenkinant impulso ir energijos tvermės dėsnius (elastinė sklaida).

Atsižvelgiant tik į pirmosios eilės sklaidą $m_\perp, m_\parallel = 1$ filtravimo kampas α

ir difrakcijos kampas β lūžio rodiklio n_0 aplinkoje turės vertes:

$$\alpha_{filtr.} = \arcsin(k_{\perp 1}n_0/k). \tag{4.2a}$$

$$\beta_{difr} = \arcsin(k_{\perp 2}n_0/k). \tag{4.2b}$$

Paraksialiniu atveju Laue FK filtravimo kampas gali būti apibrėžiamas:

$$\sin(\alpha) = q_\perp \frac{1}{2k_0}(Q-1) = \frac{\lambda}{2d_\perp}(Q-1), \tag{4.3}$$

kur Q yra bedimensinis geometrijos koeficientas ir apibrėžiamas kaip:

$$Q = 2\frac{d_\perp^2}{\lambda d_\parallel}. \tag{4.4}$$

Laue FK filtrų parametrai ir skaitmeninis modelis

Laue FK, kurie buvo formuojami tiesioginio lazerinio rašymo (TLR) stiklo tūryje būdu, pasižymi mikrometrų eilės gardelės konstantomis ir tolydžiai kintančio lūžio rodiklio pokyčiais, dėl to juos sunku charakterizuoti tokais tradiciniais metodais, kaip fazinio kontrasto mikroskopija. Sprendimas pagrįstas vadinamuoju s koeficientu, kuris yra fenomenologinė konstanta ir leidžia apibūdinti periodinius darinius, nežinant jų specifinių savybių (pvz., lūžio rodiklio moduliacijos gylio $\Delta n_{\max}$, lūžio rodiklio pokyčio profilio, modifikuotų sričių dydžio arba, tiksliau, modifikacijų išilginis dydžio Δl). s- koeficientas gali būti suprantamas kaip vieno kristalinio išilginio periodo kompleksinės amplitudės sklaidos koeficientas, išreikštas (žr. disertacijos straipsnį **A2** priedus A ir B arba disertacijos darbo **A4** komentarą nr. 1 papildomoje informacijoje):

$$s = \pi^{3/2}\Delta n_{max}\Delta l/2\lambda_0, \tag{4.5}$$

ir kaip buvo nurodyta [24], gali būti naudojamas kaip įrankis, skirtas nustatyti tinkamiausiai kristalų geometrijai, naudojamiems TLR lazerinio apdorojimo parametrams. Pavyzdžiui, atsižvelgiant į FK gamybos sąlygas, jeigu yra žinoma s vertė, o tam tikra taikomoji programa reikalauja 100% intensyvumo išfiltravimo išilgai iš anksto nustatyto filtravimo kampo α, tai FK išilginių periodų (arba primityvių narvelių išilgine kryptimi) skaičius N turi tenkinti sąlygą $s \times N \approx 1.5$. Be to, galima nustatyti apytikslį filtravimo juostos plotį, kuris atitinka santykį $w \approx 50\sqrt{s}$ mrad.

Norint skaitmeniškai ištirti Laue filtrų savybes gali būti naudojami keli metodai. Šviesos sklidimo metodas (PSM) yra pageidautinas pasirinkimas [35, 36]. Jis naudojamas, kai difrakcinis sklidimas homogeniška erdve gali būti vertinamas atskirai nuo sklaidos begalo plona fazine gardele, nagrinėjant spinduliuotės sąveiką su vienu FK sluoksniu. Tai reikalauja mažų skaičiavimo išteklių, yra paprasta ir jo naudojimas pateisinamas tol, kol lūžio rodiklio mo-

duliavimo gylis mažas $\Delta n < 10^{-2}$ (atspindžiai gali būti ignoruojami) ir išilginis periodo ilgis yra didesnis nei numatytasis spinduliuotės bangos ilgis taip, kad $7.2 \leq n_0 d_z/\lambda$, kaip aprašyta disertacijos straipsnio **A2** priede A.

Brego FK filtrų parametrai ir skaitmeninis modelis

Brego režimo FK, tiriami šiame darbe, atitinka harmoninės reljefinės gardelės formą, kuri padengta konforminėmis plonasluoksnėmis dangomis. Sluoksniai pasižymi aukštu n_h ir žemu n_l lūžio rodikliu. Paprastai tokie dariniai yra naudojami kaip didelio difrakcijos efektyvumo dielektrinės atspindindžio gardelės [44, 45, 46]. Jie taip pat taikomi ekstremalių ultravioletinių spindulių spektroskopijoje [47, 48]. Tačiau čia tokios struktūros vertinamos kaip kryptiškai atrankūs dariniai optiniuose bangos ilgiuose pralaidumo režime.

Remiantis disertacijos darbu **A6**, nagrinėjamų FK skersiniai periodai yra $d_x \approx 1.67$ µm ir $d_z \approx \lambda/2$, kur sluoksnio storis yra $l = d_z/2$. Lūžio rodiklio kontrastas $\Delta n = n_{high} - n_{low} \approx 0.12$. Pasirinktas filtrų veikimo vizualizavimo būdas – nulinės eilės praėjusio intensyvumo nuo kampo ir bangos ilgio žemėlapis. Tikimasi, kad juose bus sudėtingesnės fotoninių juostų struktūros nei Laue filtrams (žr. Disertacijos dokumento **A3** papildoma informaciją S3 pav.).

Šių juostų padėtis nustatyti gana paprasta, naudojant patogesnę išraišką nei 1.2. Jei krentančioji plokščia banga pasižymi bangos vektoriumi $\mathbf{k}_0 = (k_0 \sin(\theta), k_0 \cos(\theta))$, o FK atvirkštinės gardelės vektoriumi $\mathbf{q}_{n,m} = (m_x q_x, m_z q_z)$, tai taikant energijos ir impulso tvermės dėsnius 1.1 filtravimo juostų padėtys pralaidumo žemėlapiuose randamos pagal:

$$|\mathbf{k}|_{m,n} = \frac{m_x^2 q_x^2 + m_z^2 q_z^2}{2m_z^2 q_z^2 \cos\theta - 2m_x^2 q_x^2 \sin\theta}, m_x \in \mathbb{Z}, m_z \in \mathbb{N}. \tag{4.6}$$

m_x and m_z atitinka skersinį ir išilginį atvirkštinės gardelės vektoriaus kartotinius (harmonikas).

Kokybinei analizei kaip tinkamiausias metodas buvo pasirinktas baigtinių skirtumų laiko plotmės skaičiavimo metodas (angl. akronimas FDTD) [40], kur modelis kalibruojamas su eksperimentiniais duomenimis.

FK erdviniai filtrai pagal terpę ir gamybos būdus

Šiame skyriuje apžvelgiu tris FK tipus, kurie buvo eksperimentiškai išbandyti vieno praėjimo režimu.

FK TLR panaudojant Gauso pluoštą

Čia aptariami reiškiniai ir FK savybės svarbios disertacijos straipsnių **A1**, **A2**, **A3**, **A4** kontekste.

Kaip paaiškinta ankstesniuose skyriuose, pagrindinis parametras, naudojamas apibūdinti FK Laue filtrus, yra sklaidos efektyvumo koeficientas s. Nors s-koeficientas yra naudingas nustatant FK filtro veikimą, reikėtų pabrėžti, kad niekada nebuvo ištirta jo priklausomybė nuo bet kokių TLR parametrų, pvz., TLR greičio, smailinio intensyvumo (energijos srauto tankio), impulso pasikartojimo dažnio ir t.t. Apskritai, gamybos sąlygų optimizavimas mažai tirtas. Todėl šis skyrius skirtas eksperimentiniam FK erdvinio filtro efektyvumo tyrimui, priklausomai nuo TLR sąlygų.

TLR eksperimentinė sistema išsamiai aptariama daugelyje atviros prieigos šaltinių. Trumpai tariant, jis susideda iš impulsinės lazerinės spinduliuotės šaltinio, mėginio skenavimo priemonių, lazerinio pluošto fokusavimo priemonių, tokių kaip aukštos skaitinės apertūros (NA) objektyvai Gauso pluoštui fokusuoti ir kai kurios papildomos priemonės, skirtos poliarizacijai, rašymui naudojamo lazerinio pluošto skersmeniui valdyti ir t.t. Naudota TLR sistema išsamiai aprašyta [49, 50]. Svarbūs TLR parametrai: 300 fs trukmės impulsai, kurių centrinis bangos ilgis yra $\lambda_0 = 1030$ nm. Pluoštas buvo fokusuojamas į mėginį didelės skaitinės apertūros objektiniais lęšiais NA$> 0{,}9$, gaunant didelius smailinius intensyvumus TW/cm^2. Esant tokiems dideliems intensyvumams medžiagos viduje, mėginiuose buvo sukeliamas lokalus lūžio rodiklio pokytis. Mėginio skenavimo greičio v ir lazerio impulso pasikartojimo dažnio f parametrai buvo keičiami.

Charakterizavimo tikslais mėginiai buvo peršviečiami žinomo kampinio spektro fokusuotais lazerio pluoštais. CCD kamera registruojamas praėjusio pluošto intensyvumo spektras, įvertinamas kampinis pralaidumas.

Mėginiai, kurie pasižymėjimo asimetriniu veikimu, buvo pjaunami, poliruojami, apžiūrimi optiniu mikroskopu pralaidumo režime, vėliau ėsdinami koncentruotame vandeniniame kalio hidroksido tirpale ir apžiūrimi skenuojančiu elektronų mikroskopu.

Tyrimo metu buvo naudojami skirtingi stiklai: Foturan [57], N-BK7 ir detaliausiai tirtas natrio-kalcio silikatinis stiklas [56].

Tendencija aprašyta disertacijos straipsnyje **A2**, kur lyginama s koeficiento priklausomybė nuo ekspozicijos sąlygų, leidžia teigti, kad stikle gaminamų FK darinių lūžio rodiklio moduliacijos gylis didėja, didėjant impulso energijai. Tačiau keičiasi ne tik moduliacijos gylis, bet ir geometriniai parametrai. Čia daroma prielaida, kad kai lūžio rodiklio modifikuotų zonų dydis tampa per didelis, jos pradeda persidengti, tokiu būdu sumažindamos darinio lūžio rodiklio moduliacijos gylį ir kartu s-koeficiento reikšmę didesnėms impulsų energijos / didžiausioms intensyvumo vertėms.

Stebimi silpnai asimetriniai filtravimo erdviniai spektrai, ypač kai nukrypsta nuo $E_{\max s}$ ir $I_{\max s}$ reikšmių. Toks elgesys buvo netikėtas ir toliau tiriamas keičiant TLR spindulio poliarizacijos kampą ir rašymo kryptį tam, kad būtų galima išskirti neįprastus sąveikos mechanizmus. Parinkus skirtingus gamybos

ir geometrinius parametrus, bei skirtingas d_x reikšmes, buvo aptikti atvejai, kai efektas yra išreikštas. Efektą galima paaiškinti pakrypusių sluoksnių sandara atliekant PSM skaičiavimus.

FK TLR panaudojant Beselio pluoštą

Čia pateikiamas disertacijos straipsnio **A7** aptarimas, kurio pagrindu buvo gaminami mėginiai disertacijos straipsnio **A8** tyrimams.

Kai kuriems taikymams pakanka erdvinio filtravimo viena kryptimi. Pavyzdžiui, jis ypač tinka platiems kraštu spinduliuojantiems puslaidininkiniams lazeriams, kur reikalingas tik lėtos ašies filtravimas [96, 97]). Tokiu atveju reikalingi 2D FK.

Čia pateikta idėja naudojant Besselio pluoštus [98] gaminti didelės apertūros 2D FK erdvinius filtrus. Besselio pluoštai gali būti sukurti panaudojant refrakcinius, atspindinčius arba difrakcinius aksikonus ir yra charakterizuojami ilga ir plona aukšto intensyvumo ($|\mathbf{E}|^2$) zona (kartais vadinama Besselio zona). Ši zona išnaudojama skaidrioms medžiagoms apdirbti [99, 100, 101], pvz. fazių elementų gamybai [102, 103]. Dėl šių labai ilgų ir siaurų modifikacijų, FK gamyba gali būti atliekama „horizontalioje geometrijoje". Tada FK ilgis nebėra ribojamas, kitaip nei FK gaminamiems Gauso pluošto TLR būdu. Apribota tik apertūra išilgai vertikaliosios krypties, bet ji yra mažiausiai 10 kartų ilgesnė, palyginti su gaunama naudojant Gauso spindulių TLR strategiją.

Eksperimentinę TLR sistemą sudarė UVFS aksikonas, kurio pusinis kampas $\angle\alpha = 0{,}5°$ (viršūnės kampas 179°). Jis buvo apšviestas naudojant kolimuotą impulsinį pluoštą, kurio centrinis bangos ilgis $\lambda = 1030$ nm, impulsų pasikartojimo dažnis - 25 kHz ir impulso trukmė apie 200 fs. Pluošto skersinis diametras buvo maždaug $2w = 5{,}25$ mm (esant $1/e^2$ intensyvumo vertei). Mažinantis teleskopas buvo įrengtas iš dviejų lęšių, kurių židinio nuotoliai buvo 500 ir 9 mm, o gaunama mažinimo vertė $M \sim$ 55,6. Mėginį pasiekiančių impulsų energija atitiko 8 µJ.

Poliruotas N-BK7 ($n \approx 1{,}51$) 4 mm storio stačiakampis padėklas buvo skenuojamas 9 mm lęšio židinio plokštumoje. Indukuoto lūžio rodiklio zonų ilgis buvo apie 600 μm. Mėginys buvo skenuotas $v = 2500$ µm / s nuosekliais linijiniais judesiais. Tokių FK apertūra buvo 0,6x1 mm^2.

Pagaminti nečirpuotos ir čirpuotos išilginės geometrijos FK. Minimalus pasiekiamas skersinis periodas buvo $d_x = 3$ µm. Atitinkamas išilginis periodas buvo pasirinktas naudojant geometrijos parametrą $Q = 2d_\perp^2/(\lambda d_\parallel)$, nes patogu suderinti centrinį filtravimo kampą intuityviu būdu: $\sin(\alpha_c) = \lambda(Q-1)/2d_\perp$. Atkreiptinas dėmesys į tai, kad bangos ilgis nustatomas toks, koks yra stiklo padėkle: $\lambda = \lambda_{\mathrm{vac}} n_{\mathrm{BK7}}$. Nečirpuotiems FK Q buvo pasirinktas taip, kad $Q = 1{,}2$, $1{,}6$, $2{,}0$. Čirpuotiems taip, kad $Q_1 = 1.2$, $Q_2 = 2.0$, kur $d_\parallel$ vertės buvo keičiamos tiesiškai tarp atitinkamų verčių minimlios ir maksimalios vertės.

Vertės priklausė nuo zondo bangos ilgio λ (633 ir 970 nm).

Tokiu būdu buvo pasiūlytas naujas, patogus būdas gaminti santykinai ilgus fotoninių kristalų erdvinius filtrus. Toks FK gali būti efektyviai taikomas 1D erdviniam filtravimui, pavyzdžiui, plataus krašto puslaidininkiniuose lazeriuose, kur filtravimas lėtosios ašies plokštumoje yra labai pageidautinas. Stebėti filtravimo kampinių juostų intervalai siekė 4 ir 6 laipsnius.

Konforminių plonasluoksnių dangų filtrai

Kampinio (ar erdvinio) filtravimo fotoniniais kristalais idėja yra pagrįsta selektyvia šviesos difrakcija, kai šviesa sklinda dvigubai periodiškais dariniais. Tokiais dariniais sklindančios šviesos pluošto kampinio spektro komponentai, kurie rezonuoja su skersiniais ir išilginiais darinio periodais, efektyviai išsklaidomi ir pašalinami iš nulinės difrakcijos eilės perduodamos šviesos. Kita vertus, nesikeičia kampinių komponentų, kurie yra ne rezonansai, sklidimo kryptis. Todėl kampinis / erdvinis filtravimas gali vykti kai FK geometrija tinkamai parinkta. Ši idėja jau buvo įrodyta kaip naudinga alternatyva tradiciniams erdvinio filtravimo metodams ir pademonstruota keliuose atvejuose, pvz., mikrolustiniuose lazeriuose [130].

Anksčiau erdvinis filtravimas parodytas vadinamajoje Laue konfigūracijoje, kurioje išilginis periodas yra gerokai didesnis nei bangos ilgis. Čia pateikiamas pirmasis eksperimentinis Brego (sub-bangos ilgio) tipo FK kampinis filtras, kuriame išilginis periodas yra maždaug pusė bangos ilgio. Erdviškai filtruojantis fotoninis darinys yra pagamintas naudojant fizinį garų nusodinimo metodą, konkrečiai – nusodinimo kampu metodą, kuris leidžia lengvai ir labai tiksliai keisti atskirų sluoksnių lūžio rodiklį [123]. Pageidautinos geometrijos yra parinktos pagal galutinių skirtumų laiko srities (FDTD) skaičiavimus. Pagrindinis rezultatas, kaip aprašyta žemiau, vis dar toli nuo „švaraus" kampinio filtravimo, tačiau jau parodo šio reiškinio pirmines apraiškas.

Šviesos perdavimas per FK taip pat buvo modeliuojamas FDTD metodais. Modeliavimas rodo, kad dariniai turi potencialą būti technologiškai pritaikomi: filtravimo (pralaidumo mažais kampais atveju) kampas gali būti valdomas ir sumažintas iki technologiškai svarbių verčių. Taip pat filtravimo gylis (pralaidumas filtravimo kampuose) gali būti sumažintas iki nulio, padidinant sluoksnių skaičių ir skersinį FK periodą. Tokie Brego FK erdviniai filtrai, dėka pasirinkto gamybos būdo, gali būti gaminami dideliais kiekiais, lyginant su TLR būdu gaminamais Laue FK ir todėl būti pirmieji industriškai pritaikomi erdviniai filtrai komercinėse mikrolazerių sistemose.

Optimizacija ir pažengusios geometrijos

Šiame skyriuje pateikiu rezultatus, susijusius su išilginio periodo d_z moduliavimu priklausomai nuo sluoksnio arba periodo (vienetinio narvelio) numerio, ieškant netrivialių moduliavimo būdų.

Pateikti rezultatai yra pagrįsti disertacijos straipsniais **A1**, **A4** ir **A5**. Diskusija prasideda pasiekimais, susijusiais su pagrindiniais pasiekimais 3D ašisimetriniams dariniams, o po to seka 2D darinių rezultatai, abiem atvejais skirtais veikti Laue režime.

Ašisimetriniai čirpuoti FK

Norint naudoti ašisimetrinius FK erdviniam filtravimui, kampinis filtravimo diapazonas turi būti išplėstas pranokstant anksčiau pasiektas vertes. Todėl čia parodoma, kad išilginis čirpas (išilginio periodo kitimas optinės ašies kryptimi) ašisimetriniuose fotoniniuose dariniuose gali būti naudojamas kaip alternatyvus būdas padidinti filtravimo kampinį plotą. Šaltinyje [24] pasiūlyta naudoti išilginį čirpą tam, kad būtų padidintas 2D struktūrų filtravimo diapazonas. Čia ištirta, kiek galima padidinti ašisimetrinių FK filtravimo intervalą, taikant tokį čirpavimą.

Konkrečiai, ištirtas filtravimo juostos kampo plotis, matuojant pagrindinių filtravimo linijų išfiltruotos spinduliuotės kampinius pločius PPPM (pilnas plotis pusė maksimumo) intensyvumo lygyje: $((I_0(\alpha) - I(\alpha)))/(I_0(\alpha)) = \Delta I(\alpha)/(I_0(\alpha))$. Be to, skaitmeniniai skaičiavimai rodo, kad čirpuoti FK gali padidinti filtravimo kampinius diapazonus, naudojant ilgesnius darinius (didesnius N), arba didesnes lūžio rodiklio moduliacijos amplitudes.

Skaitiniai ir eksperimentiniai rezultatai apibendrinti 3.2(b-g) pav. Čirpavimas leidžia padidinti filtravimo kampo plotį nuo 17 iki 40 mrad, kaip nustatyta, matuojant dominuojančio normalizuoto filtravimo linijos PPPM (pilnas plotis pusę maksimalaus). Padidėjimas siekia ≈ 2. Tai nėra itin ekstremalus rezultatas. Jį vis dar riboja maksimalus FK darinio ilgis, kurį galima pagaminti stikle naudojant Gauso pluošto TLR metodą. Tačiau tai suteikia vilties, kad intuicija, sukurta 2D FK filtrams, gali būti pagrįstai taikomas 3D ašisimetriniams dariniams. Dar svarbiau yra tai, kad ašisimetriniai dariniai neturi skersinio poslinkio invariacijos, tačiau, priešingai nei 2D FK, jų skersinė gardelės konstanta gali būti čirpuota. Išnagrinėjus vieną laisvės laipsnį, antrasis tyrimas galėtų būti tęsiamas, papildomai nagrinėjant superkolimacijos efektą [33].

Atvirkštinis 2D FK Laue erdvinių filtrų dizainas

Jau buvo įrodyta, kad fotoniniai kristalai, pagaminti skaidrių dielektrinių terpių tūryje, rodo žemo erdvinio dažnio (kampinio) pralaidaus filtro funkcionalumą.

Šie FK filtrai yra pagaminti neorganiniuose stikluose, naudojant femtosekundinį lazerio rašymo procesą. Labiausiai perspektyvus tokių filtrų aspektas yra jų tiesioginis integravimas į lazerinių mikrorezonatorių ertmes. Didžiausias galimas pluošto kokybės pagerinimo lygis priklauso nuo FK kampinio filtravimo diapazono. Todėl labai svarbu optimizuoti filtravimo FK struktūrą, kad būtų gautas optimalus filtravimas. Iš tiesų įrodyta, kad linijiniu būdu čirpuoti FK padidina filtravimo efektyvumą, tačiau jų geometrija gali būti dar labiau optimizuota. Čia parodoma, kad gradientinis ir genetinis optimizavimo algoritmai (kartu su euristiniu PSM modeliu) gali pasiūlyti dar geresnes geometrijas, vengiant brangių globaliųjų optimizavimo metodų.

Imant čirpuotą FK kaip pradinį paieškos tašką, pasiekiami optimalūs sprendimai skirtingiems FK ilgiams. Demonstruojamas sprendimų įgyvendinamumas, pagaminant optimizuotus FK Foturan stikle. Filtrai su 2D kintamos gardelės konfigūracija, pasižymėjo skersiniais ir išilginiais periodais: $d_x = 1{,}2$ ir mažiausiai $\min d_z = 4{,}8$ µm, 633 nm veikimo bangos ilgiui. Parodoma, kad žemo erdvinio dažnio paralaidumo (iki 34 mrad) konfigūracijai filtravimo diapazoną galima pagerinti kelis kartus, pasiekiant 150 mrad filtravimo juostų pločius.

Taikymai

Fotoninio kristalo mikrolustinis lazeris

Šiame skyriuje pateikta informacija ir rezultatai yra pagrįsti disertacijos straipsniu **A3**.

Mikrolustiniai lazeriai (ir bendrai visi mikrolazeriai, tokie kaip diodiniai lazeriai ar vertikaliojo rezonatoriaus puslaidininkiniai lazeriai) yra itin kompaktiški ir efektyvūs koherentinės spinduliuotės šaltiniai, bet paprastai turi vieną ryškų trūkumą – mažą spinduliuojamo pluošto erdvinę kokybę. Tik mažos galios režimuose (nedidelio kaupinimo ploto) mikrolustiniai lazeriai pasižymi didele erdvine kokybe, t.y. vienos skersinės modos režimu. Kiekvienas bandymas padidinti emisijos galią, didinant kaupinimo galingumą arba didinant kaupinimo plotą, lemia pluošto erdvinės kokybės pablogėjimą.

Čia siūlomas Laue FK erdvinio filtro panaudojimas mikrolustinio lazerio rezonatoriuje tam, kad būtų pagerinta lazerio pluošto kokybė ir padidintas jos skaistis. Patalpinus ašisimetrinį FK mikrolustinio lazerio rezonatoriuje, eksperimentiškai stebėtas pluošto skaisčio padidėjimas maždaug 3 kartus. Tai aiškinama aukštesnės eilės skersinių modų slopinimu.

Erdvinis filtravimas fotoniniu kristalu didelio ploto diodiniame lazeryje

Didelio ploto (krašu spinduliuojantys) puslaidininkiniai (BAS) lazeriai paprastai pasižymi prasta pluošto kokybe, ypač esant didelės galios režimui. Greitosios ašies plokštumoje lazerio aktyvioji zona yra mikrometrų eilės. Išilgai šios krypties generuojasi tik fundamentalioji skersinė moda, pluoštas difrakciškai ribotas. Išilgai lėtosios ašies, kur aktyviosios terpės matmenys siekia kelis šimtus mikrometrų, veikimo metu, susižadina keletas skersinių modų, dėl ko pluošto kokybė būna prastesnė ir pluošto skaistis ribotas.

FK yra formuojamas skaidrioje terpėje, sukuriant periodiškai moduliuotą lūžio rodiklio pasiskirstymą. Du skirtingi FK buvo pagaminti naudojant Gauso pluošto TLR ir Beselio pluošto TLR. Šie filtrai veikia sukeldami nuostolius didesnio kampinio pasiskirstymo skersinėms rezonatoriaus modoms.

Tokie filtrai panaudoti BAS lazeryje. Čia buvo naudojamas BAS, į kurio konstrukciją įėjo emiteris, kurio plotis yra 400 µm, o ilgis - 1,5 mm. Rezonatoriaus išvadinis veidrodis pasižymėjo 4% atspindžio koeficientu. Papildomai rezonatoriuje buvo išstatyti 4 cilindriniai lęšiai konfokalinėje konfigūracijoje. BAS lazeryje buvo 2 vietos, kur buvo talpinamas plyšinis konfokalinis filtras (tolimajame lauke) ir FK (artimajame). Lyginamas filtravimo efektyvumas abiejų filtrų atvejais.

Buvo stebimi lazerio pluošto M^2 ir nežymus išėjimo galios sumažėjimas, kai rezonatoriuje buvo išstatomas FK. Stebėtas skaisčio padidėjimas sudarė apie 1,5 karto.

Išvados

Pastarųjų trijų disertacijos dalių išvados pateikiamos taip:

1. Buvo ištirtas Laue tipo 2D FK filtro veikimas, priklausomai nuo TLR natrio-kalcio silikatiniame stikle procedūros. Tai buvo padaryta siekiant padidinti sklaidos s-koeficientą, kuris yra fenomenologinis dydis, nurodantis fazės moduliaciją, atsirandančią bangos frontui sklindant per vieną FK sluoksnį. Esant įvairioms ekspozicijos sąlygoms, buvo nustatyta, kad dariniai, lyginant su ankstesniais moksliniais darbais, gali pasižymėti asimetrine erdvinio (kampinio) intensyvumo pralaidumo funkcija. Ši asimetrija paaiškinta ištyrus tikrąją FK sandarą ir sukūrus pakreiptojo daugiasluoksnio FK PSM modelį. Eksperimentiniai ir skaitmeniniai tyrimai rodo, kad sluoksniai, kurie sudaro FK, pasižymi pakreipta vidine sandara, kuri išryškėja, kai Gauso pluošto fs-TLR metodu formuojamų FK periodų ilgiai (gardelės konstantos) ženkliai sumažinamos. Atrastas naujas laisvės laipsnis, kuris gali būti išnaudotas derinant FK savybes.

2. Laue tipo 2D FK erdviniam filtravimui pasižymėjo tam tikro geometrinio parametro – jų ilgio arba didžiausio išilginio periodų skaičiaus – apribojimu. Kadangi vienintelis metodas, naudojamas tokiems dariniams gaminti, buvo Gauso pluošto fs-TLR stikle būdas, tai svarbiausias ribojantis veiksnys buvo maksimalus sferinių aberacijų neturintis darbinis atstumas, siekiantis ne daugiau kaip 300 µm kai naudojami didelės skaitinės apertūros NA objektiniai lęšiai. Šiam apribojimui įveikti buvo būtinas paradigmos pokytis, todėl parinktas Besselio pluoštu paremtas TLR metodas. Surinkta TLR sistema, sėkmingai panaudota gaminant darinius, kurių išilginių periodų skaičius siekė $N = 160$ (per 3 mm ilgį). Naudojant metodą, buvo pademonstruoti funkcionalūs FK filtrai dviems bangų ilgiams (633, 970 nm) su filtravimo (kampinėmis) juostomis siekiančiomis 4° ir 6° pločius, taip įrodant naujo būdo pritaikomumą.

3. Brego tipo 2D FK erdviniai filtrai buvo pasiūlyti kaip alternatyva Laue tipo filtrams. Šiems dariniams būdingas didesnis lūžio rodiklio kontrastas ir mažensi nei bangos ilgis charakteringi elementų matmenys. Čia iškelta hipotezė, kad jei moduliuoto paviršiaus šablonai (reljefinės gardelės) galėtų būti sukombinuoti su plonasluoksnėmis konforminėmis periodiškai kintančio lūžio rodiklio dielektrinėmis plėvelėmis, tada gaunamajam dariniui būtų galima stebėti dalinius draustinius fotoninės juostos tarpus. Ši hipotezė buvo patikrinta išnagrinėjus tokias FK darinių savybes: analitiškai apskaičiavus draustinių fotoninės juostos tarpų padėtis, skaitmeniškai apskaičiavus kampinius intensyvumo pralaidumo spektrus (FDTD) ir pagaminus šabloninius padėklus, ant kurių fiziniu garų nusodinimo būdu buvo suformuotos dangos. Apšvietus pagamintus FK kolimuotu ir fokusuotu pluoštu buvo stebimi daliniai draustiniai fotoninnės juostos tarpai. Tikimasi tokio FK idėją būtų galima integruoti kuriant naujus plonus fotoninius erdvinių filtrų įtaisus, kuriuos galima būtų integruoti į egzistuojančių prietaisų paviršius.

4. Ašisimetrinių Laue tipo 3D FK pritaikymas mikrolazeriuose buvo apribotas, dėl jų siaurų kampinio filtravimo juostų iki 17 mrad (0,3°) pločio. Laue-Rabi tipo svyravimų santykis tarp filtravimo juostos formos ir FK ilgio neleido sukurti FK tinkamų taikyti lazerio rezonatoriuje, todėl atsirado poreikis ištirti daugiau galimų laisvės laipsnių. Čia pasiūlytas išilginio periodo ilgio čirpo pritaikymas tam, kad būtų išplėstas kampinis filtravimo diapazonas. Hipotezė buvo patikrinta empiriškai ir skaitiniu būdu, ir patvirtinta: stebėtas kampinio filtravimo diapazonas padidėjo dvigubai. Tai pateisina naujų medžiagų, gamybos ir netgi geometrijos moduliavimo metodų, skirtų dar pranašesniems FK, kurie būtų tinkami naudoti mikrolazeriuose, paiešką.

5. Patvirtinus, kad tiesinis išilginio periodo čirpavimas pritaikomas Laue

2D (ir 3D) FK erdviniam filtravimui, tolimesnis etapas buvo netiesinio čirpavimo tyrimas. Iškelta hipotezė, kad naudojant pasiteisinusį PSM metodą kartu su optimizavimo metodais galima rasti naujas FK geometrijas, kurios galėtų būti priderinamos mažais kampais pralaidžiam erdviniam filtravimui. Tokias geometrijas pavyko rasti ir įgyvendinti pagaminus jas Gauso pluošto fs-TLR būdu stiklo tūryje. Gauti dariniai, kurių filtravimo diapazonas yra iki 150 mrad ($\sim 2{,}6°$). Be to, rasti sprendiniai, atitinkantys laisvai pasirinktas kampinio intensyvumo pralaidumo FK funkcijas. Tai apima sprendinius, kurie optimizuoja išorinio rezonatoriaus puslaidininkinio kraštu emituojančio lazerio pluošto šviesį. Įrodyta galimybė derinti FK kampinio intensyvumo pralaidumo funkciją, nepažeidžiant poslinkio invariantiškumo ir (teoriškai) neribotos apertūros pranašumų.

6. Laue tipo ašisimetrinis FK skirtas erdviniam filtravimui buvo eksperimentiškai išbandytas nuolatinės veikos Nd:IAG mikrolustinio lazerio rezonatoriuje. Taikant FK sumažėjo pluošto M^2 parametras (pagerėjo pluošto kokybė) ir padidėjo lazerio pluošto skaistis B. Pluošto skaistis padidėjo 3 kartus. Tai aiškinama tuo, kad FK filtrai pralaidūs mažu kampu, todėl aukštesnės eilės skersinės rezonatoriaus modos slopinamos. Sumažėja lazerio pluošto skėsties kampas.

7. Besselio pluošto TLR pagrindu pagamintas Laue tipo 2D FK erdvinis filtras buvo eksperimentiškai išbandytas išorinio rezonatoriaus puslaidininkio kraštu spinduliuojančio didelio ploto vieno emiterio lazerio rezonatoriuje. FK pritaikymas rezonatoriuje sumažino pluošto M^2 kokybės parametrą ir padidino lazerio pluošto skaistį B 1,5 karto. Tai empiriškai parodo, kad FK erdvinio filtravimo mechanizmas yra pritaikomas net žemos kokybės faktoriaus rezonatorių viduje.

Curriculum vitae

Name:	Darius
Surname:	Gailevičius
Date of birth:	1990-01-06
Place of birth:	Alytus, Lithuania
E-mail:	darius(d0t)gailevicius(e+a)@gmail(d0t)com;
	darius(d0t)gailevicius(e+a)ff(d0t)vu(d0t)lt

Education:

1997-2009	"Alytaus Putinų" secondary school. (Currently "Alytaus Putinų gimnazija")
2009-2013	Vilnius University, Faculty of Physics, *Bachelor's degree.*
2013-2015	Vilnius University, Faculty of Physics, *Master's degree.*
2015-2019	Vilnius University, Faculty of Physics, Laser Research Center, *Ph.D. studies.*

Work experience:

2012-2013	Freelance technical writer.
2014-2015	UAB "IAM Consultants" CEO.
2014-Current	Researcher, Junior Researcher at Vilnius University, Laser research center.
2018-Current	Researcher at UAB "Femtika".

Trumpos žinios apie autorių

Vardas: Darius
Pavardė: Gailevičius
Gimimo data: 1990-01-06
Gimimo vieta: Alytus, Lietuva
E-paštas: darius(d0t)gailevicius(e+a)@gmail(d0t)com;
                  darius(d0t)gailevicius(e+a)ff(d0t)vu(d0t)lt

Išsilavinimas:

1997-2009   Alytaus Putinų vidurinė mokykla.
                  (Dabar Alytaus Putinų gimnazija)
2009-2013   Vilniaus universitetas, Fizikos fakultetas,
                  Bakalauro laipsnis.
2013-2015   Vilniaus universitetas, Fizikos fakultetas,
                  Magistro laipsnis.
2015-2019   Vilniaus universitetas, Fizikos fakultetas,
                  Lazerinių tyrimų centras, *Doktorantūra.*

Profesinė veikla:

2012-2013   Laisvai samdomas techninis rašytojas.
2014-2015   UAB „IAM Consultants" Direktorius.
2014-Dabar   Tyrėjas, Jaunesnysis mokslo darbuotojas,
                  Vilniaus universitetas, Lazerinių tyrimų centras.
2018-Dabar   Tyrėjas, UAB "Femtika".

Copies of included publications

Some published manuscripts are included only in the print version. Singular copies of manuscripts that are not published in open access sources are available *via* corresponding journal websites or can be provided in compliance to copyright rules/laws *per* request by the corresponding authors or by D.G. using the contacts listed in the CV pages above.

A1

CHIRPED AXISYMMETRIC PHOTONIC MICROSTRUCTURES FOR SPATIAL FILTERING

D. Gailevicius, V. Purlys, L. Maigyte, M. Peckus, and K. Staliunas

PAGE LEFT INTENTIONALLY
BLANK

A2

FEMTOSECOND DIRECT LASER WRITING OF PHOTONIC SPATIAL FILTERS IN SODA-LIME GLASS

D. Gailevičius, V. Purlys, L. Maigytė, E. Gaižauskas, M. Peckus, R. Gadonas, and K. Staliūnas

FEMTOSECOND DIRECT LASER WRITING OF PHOTONIC SPATIAL FILTERS IN SODA–LIME GLASS

D. Gailevičius [a], V. Purlys [a], L. Maigytė [b], E. Gaižauskas [a], M. Peckus [a], R. Gadonas [a],

and K. Staliūnas [b, c]

[a] *Laser Research Center, Department of Quantum Electronics, Vilnius University,*
Saulėtekio 10, LT-10223 Vilnius, Lithuania
[b] *Departament de Fisica i Enginyeria Nuclear, Universitat Politecnica de Catalunya, Spain*
[c] *Institucio Catalana de Recerca i Estudis Avancats (ICREA)*
E-mail: darius.gailevicius@ff.vu.lt

An experimental study of the efficiency of recently predicted photonic crystal (PhC) based spatial filtering is provided. Photonic structures are fabricated using a direct laser writing technique employing point-by-point modification by tightly focused femtosecond pulses in soda–lime glass. Such PhCs are characterized by using an *s*-coefficient – a parameter defining PhC filter efficiency. We explore the dependences of filtering efficiency on different laser writing conditions, such as irradiation peak intensity and the polarization of laser beam. In addition, we show that the PhCs can also exhibit even asymmetric shapes of voxels under particular conditions.

Keywords: photonic crystal, spatial filtering, femtosecond fabrication, glass

PACS: 42.60.-v, 42.79.Ci, 81.16.-c, 81.05.-t

1. Introduction

Spatial (or angular) filtering is frequently used to improve the spatial quality of light beams by removing the undesired angular or far-field components of the radiation. A conventional design for spatial filtering comprises a confocal system of lenses with a diaphragm of appropriate diameter positioned in the confocal plane, blocking the undesired angular components of the spatial spectrum [1]. Such a configuration extends over at least two focal lengths of both lenses and is of a relatively large size – it could hardly be used in micro- or nano-scale photonic devices. Other, more sophisticated arrangements for spatial filtering based on liquid-crystal cells [2], utilization of thin film interfaces [3], anisotropic media [4], metallic grids [5], possibly including monolithically integrated passive beam shaping elements [6], etc. have not resulted in widespread technological applications. Recently, an alternative approach to spatial filtering has been suggested, which is based on propagation of light beams through photonic crystals (PhCs) – materials with a periodic modulation of the refractive index on a wavelength scale [7–10]. PhC based spatial filters are

potentially advantageous due to their relatively small size as compared to the conventional spatial filters, that could enable the integration of such filters into micro-optical devices or micro-laser resonators.

The well-known property of PhCs is the appearance of photonic band gaps, i. e. forbidden frequency ranges at which light waves cannot propagate [11]. Thus, the PhCs can provide frequency (chromatic) filtering, eliminating (reflecting) specific frequency components from the incident radiation. Similar to the chromatic band gaps, angular band gaps can also appear in PhCs, which can be engineered in such a way that for a given frequency only on- and around-axis waves are allowed to propagate. Angular filtering has been shown in two- and three-dimensional (2D and 3D) PhCs in the microwave and infrared regime [7–10]. The most simple mechanisms of spatial filtering by PhCs are based on angular band gaps, which appear if a condition related to a longitudinal modulation period, $d_\parallel < \lambda$, is met. However, despite the enormous progress in micro- and nano-structure fabrication technologies, the latter condition is still difficult to fulfill in the visible and near-infrared ranges. Perhaps, this is the reason why the spatial filtering by angular band gaps has never been experimentally

demonstrated in optics. We note the recent demonstration of spatial filtering in acoustics by the so-called sonic crystals [12, 13], where the fabrication of structures on a millimeter scale is less challenging.
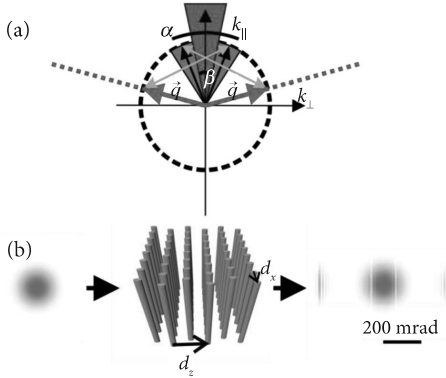
Fig. 1. Illustration of spatial filtering in a 2D PhC: (a) is the mechanism of resonant wave scattering in a gapless configuration, (b) is the schematic of the experimental arrangement. Filtering occurs when the waves in the dark triangle zones get into the resonant scattering condition with modulation wave vectors $\vec{q} = (q_x, q_z)$. Dashed lines show the direction of filtered out angular components. The spatial spectrum (far field) of the initial beam, consisting of the central (regular) part, and of the wings (the part to be removed), is shown by red and grey triangles.

As an alternative to the spatial filtering based on the angular band gaps, a mechanism of PhC based spatial filtering was proposed with the PhCs arranged in a gapless configuration [14]. In the latter case, a deflection of the angular components of radiation in the forward direction is observed (see Fig. 1(a)). The gapless spatial filtering can be obtained for substantially larger longitudinal periods of modulation $d_\| > \lambda$ (we will use d_z to denote the thickness of one layer, two layers comprise one period $d_\| = 2d_z$); hence, current fabrication techniques can be applied more easily. Such kind of filtering has been recently demonstrated experimentally in different 3D configurations using PhCs with a square symmetry in transverse space [15, 16], as well as photonic structures with axisymmetric rings [17, 18]. The gapless filtering has been recently proposed also to clean atomic ensembles on Bose–Einstein condensates [19].

Another advantage of the proposed spatial filtering alternative is the required relatively low refractive index modulation (of the order of 10^{-2}), that is around two orders lower compared to [7–10]. Such a low index modulation suggests the possibility of inscription of such PhCs into the bulk of transparent materials, such as glass, by using femtosecond direct laser write techniques. Glass is an excellent alternative to other media, such as photoresists used in 3D laser lithography, that are more prone to issues with shrinkage, noise sensitivity and also destructive optical breakdown [20, 21]. However, this technique typically allows refractive index modulation, that is on the lower side ($\approx 10^{-3}$) of the required index modulation, therefore a careful choice of processing parameters must be made in order to maximize it.

Due to the fact that relatively small transversal periods (of the order of 1 and 2 μm for 2D and 3D axisymmetric PhCs, respectively) were used in the multilayer structures, formation of successive layers can modify the previous one and induce tension in the area of further successive layer fabrication. This makes it difficult to characterize such structures using conventional methods, such as phase contrast microscopy. The solution uses a characterization method based on the so-called s-coefficient, that is a phenomenological constant and allows the characterization of periodic structures without knowing its specific details (such as the amplitude Δn_{max} of refractive index modulation, the profile of refractive index change, the size of the modified regions or, more particularly, the longitudinal size of the modifications Δl). The s-coefficient can be interpreted as the scattering coefficient of one crystalline longitudinal period of the structure and expressed by (see Appendix A and B for detailed derivation)

$$s = \pi^{3/2} \Delta n_{max} \Delta l / \lambda_0, \qquad (1)$$

and as it was shown in [16], can be used as a tool for determining the most appropriate crystal geometry for available laser processing parameters for a given application. For example, if we consider that for a given set of PhC fabrication we know the value of s, and a particular application requires 100% intensity depletion along a predefined filtering angle α for an arbitrary input beam, then to determine the number of PhC periods N needed to achieve the best result we can use the condition $s \cdot N \approx 1.5$ (see Fig. 2). In addition, an approximate line width could be determined, which follows the relation $w \approx 50\sqrt{s}$ mrad. Similarly, controlling s might also be beneficial for other applications, e. g. axisymmetric super-collimation [22] or flat lensing [23]. A more complete overview of progress made in the field of PhC filters can be found in [24].

Although the s-coefficient has been found to be useful in determining the behaviour of the PhC filter, it should be stressed that the dependence of s on any of processing parameters, such as DLW speed, peak
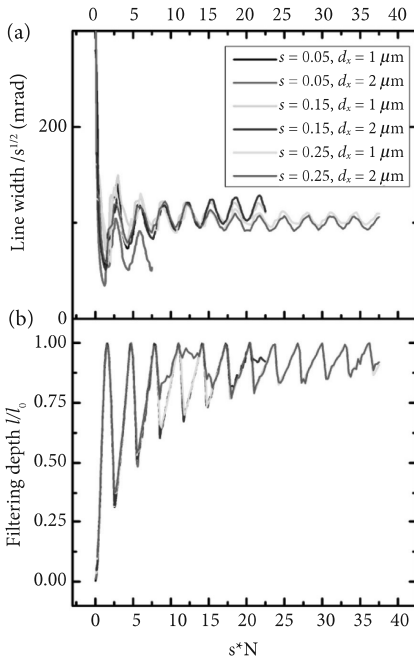
Fig. 2. (a) is the numerically calculated width and (b) is the depth of the angular filtering range, depending on the length of the structure for three different *s*-coefficient values: 0.05, 0.15, and 0.25 (for details on the numeric computation procedure see Appendix C).

intensity, pulse repetition rate, etc., has never been explored before. Little is known about optimization of PhC based filter fabrication conditions, in general. Therefore, this article is devoted to the experimental study of the PhC spatial filter efficiency depending on DLW conditions, or, in other words, the behaviours of the *s*-coefficient.

2. Materials and methods

The photonic structures were fabricated using a direct laser writing (DLW) technique employing point-by-point volumetric modification by tightly focused IR (λ = 1030 nm from a Yb:KGW laser) femtosecond laser pulses (FWHW/1.41 = 300 fs) in standard microscope soda–lime glass slides (*Carl Roth*, ISO 8037-1, n_{ref} = 1.52). This method is widely used for the inscription of various micro-optical and photonic components in glass, such as waveguides [25, 26], Bragg gratings [27], as well as vortex generators [28].

The geometry of fabricated PhCs is schematically depicted in Fig. 1(b). It is the simplest case, that allows only one-directional filtering. The geometry consists of parallel equidistant layers that are arranged to be perpendicular (in the longitudinal direction) to the optical axis of an incident beam. Each layer contains a one-dimensional periodic arrangement of parallel linear modified regions. The transverse period (lateral distance between modifications) was chosen to be d_x = 1 μm for the analysis of irradiation conditions. Every second layer is transversally shifted by half of the transverse period with respect to the previous layer. This results in *N* longitudinal periods, each having two layers. The length of longitudinal periods was selected to be $2d_z$ = 6 μm.

During formation of PhCs focusing was achieved by using a Zeiss 63 × 1.4 NA objective. PhC length was limited by the maximal working distance of the objective, i. e. ≈300 μm, that for the given geometry corresponds to the highest possible number of periods of N_{max} = 50. A lower NA <1 objective lens, as used in [16, 19], might be more suitable for generating higher length modifications Δl with a potentially higher amplitude of the refractive index modulation Δn_{max}, but results in spherical aberrations. Also, large period number PhCs are difficult to realize as mechanical stress accumulated throughout the structure can induce failures, leading to crack formation or even shattering. The process is similar to that which is used for cleaving brittle materials [30].

The fabrication algorithm and the fabrication setup are reported in detail in [15]. PhCs were inscribed layer by layer by relative translation of the focal point inside the bulk of the glass sample. The translation speed was limited to v_{max} = 5 mm/s, beyond which error free fabrication was not possible. We varied the pulse frequency *f* and pulse energy *E* during the first experiment phase, whereby *E* was established by measuring the average beam power before the objective and by taking into account the total transmittance of the objective. The number of pulses per unit length (PPUL) was fixed at 20 μm⁻¹, which allows us to compare our results to those achieved in [16]. *f* was selected to be 25, 50, 100 and 200 kHz. *E* values were set in the range of 0.01 μJ to 0.3 μJ. We calculated the peak intensity (irradiance) values as in [29], with an approximate beam waist radius ~300 nm.

For every discrete combination of such parameters we formed 100 × 100 μm² transversal size crystals having a different number of periods *N*. It should be noted that if the *s*-coefficient is below the approximate value of *s* < 0.025, in order to achieve the condition of full filtering dips defined by the relation s·*N* ≈ 1.5, a large number of longitudinal periods *N* > 60 is required,

whereby for samples of $f = 200$ kHz this condition was not met due to low filtering performance. Structures having a large number of periods, fabricated using high values of E and I, succumbed to cracking, which was expected due to the fact that soda–lime glass is prone to thermal shock and has a higher expansion rate than optical grade glasses such as fused silica. Therefore, results for some low s-coefficient structures have not been analyzed. Furthermore, producing a sufficient number of samples is difficult due to the allowed processing speeds. This can be illustrated by taking into account time needed to produce an array of PhCs for $f = 25$ kHz, with at least 12 values of E, and $N = 3, 4, 5 \ldots 50$. Such an array takes at least ~3 days to produce, whereby for $f = 1$ kHz it would take at least 71 days, therefore an experimental part of this article dealing with the relation of s to E (including I) and f has been limited to only a few frequency values acceptable for the level of the scope and scale of this study.

An interesting effect that we observed was the scattering efficiency asymmetric behaviour, that is discussed in further section. To minimize the dependence on multiple variables we employed a new single directional raster scan pattern in the DLW process of each individual layer of the PhCs. We selected 4 fixed angles of the linear polarization plane (electric field vector **E**). The plain was fixed to be parallel to the z axis and at $\gamma = 0°$ parallel to the x axis. Other positions $\gamma = 45, 90, 135°$ are defined counter-clockwise to the positive z axis. The PhCs (and line structures) used for asymmetry observation were written using the fabrication parameter values: $f = 2$ kHz, $E = 65$ nJ ($I = 56$ TW/cm^2), $\nu = 500$ μm/s (PPUL 4 μm^{-1}), $N = 20$, where a lower frequency and PPUL value were chosen to reduce thermal accumulation effects while maintaining a reasonable processing speed.

Characterization of the fabricated PhCs was carried out by illuminating the samples with a continuous 633 nm wavelength He–Ne laser beam focused into PhC samples with a 10×0.25 NA objective (see Fig. 3(b)). Focusing provided a large angular range of the radiation illuminating the PhC. To register the output, a CCD camera was placed 11 mm behind the sample in a fixed position. Only the central beam part of the radiation was recorded.

By measuring the angular intensity profile at the output of the PhC, we determined which components are filtered out. The s-coefficient was determined by calibrating numerical simulation data (derived by solving the paraxial propagation equation with a scattering matrix algorithm as in [15, 16, 24], and also by using the split-step procedure as described in Appendix C, whereby both gave equivalent results) with spatial intensity spectra behind PhCs of varying N.
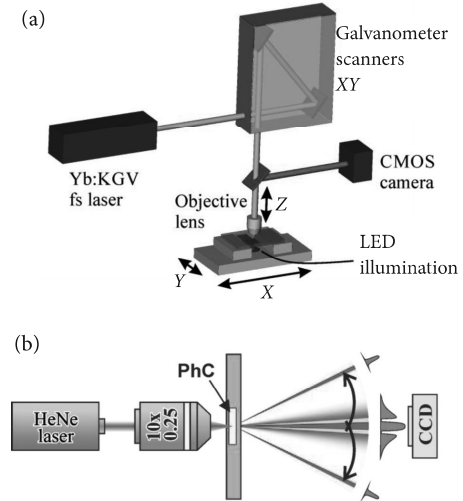
Fig. 3. Illustration of PhC fabrication (a) and characterization setup (b).

Calibration was performed while measuring the saturation value $N_{\max(s)}$ for which the filtering depth reaches the first peak as in Fig. 2(b).

For sample inspection, we additionally used an optical microscope. To perform the observations the glass samples were cut (using a manual glass cutter), optically polished perpendicularly to the inscribed lines with varied d_x (variation in the range of 0.5 to 3 μm), and then examined under an optical microscope in the transmittance regime (Fig. 4). Smaller peak intensity values were used to produce the high contrast clearly observable line structures, since with higher levels of exposure the structures overlap more strongly, and change of spatial boundaries is even more difficult to observe. We chose the described inspection routine due to several reasons, such as a large size of a sample, the complexity of a structure and a small size of the modifications, which made the use of other possible inspection methods, such as microelipsometry [31] or refractive near-field techniques [32–33] not feasible.

3. Results and discussion

3.1. Scattering efficiency measurement results

The basic results are shown in Fig. 4, in which a cross-section view of extending modified areas is shown, and further summarized in Fig. 5. s-coefficient dependence on pulse energy has maxima for different frequencies of
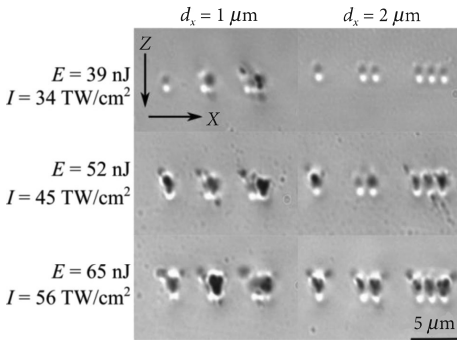
Fig. 4. Six examples of optical microscope cross-section views of mechanically cut and polished samples containing lines written in glass (with two different minimal distances between the closest neighbours). DLW order was chosen to be in the positive x direction. Beam was incident in the $+z$ direction. The pulse repetition rate was f = 2 kHz.

writing pulses. Particularly, for f = 50 kHz the highest value of s was achieved with a pulse energy of E = 260 nJ and a peak intensity value of I = 224 TW/cm².

The general trend in Fig. 5 allows claiming that the refractive index modulation depth of structures produced in glass is increasing with increasing pulse energy. However, not only the modulation depth increases with increasing pulse energy, but also the geometrical parameters change. We assume that when the size of index modified areas becomes too large (Fig. 4 shows that with increasing E the modified refractive index structure increases in size), they start to overlap (clearly observed for the d_x = 1 μm case), thus reducing the index modulation depth of the periodic structure and causing the decrease of the s-coefficient value for higher pulse energy/peak intensity values (Fig. 5).

By examining the single layer gratings, it was observed that the overlap of index modification areas occurs before reaching the critical pulse energy (resulting in the highest s, Fig. 5). This might seem like a counterintuitive result, but for parameters, such as used in our experiment, soda–lime rarefaction (decrease of density) occurs at the centre of the femtosecond pulse absorbing area and densifications at the boundaries, and when densified areas from two linear modifications overlap, then the largest modulation depth is achieved. If we take into consideration Eq. (1) and assume a continuous refractive index modulation pattern (see Appendix B), then the maximum local depth would be $\Delta n_{max} \approx 2 \cdot 10^{-3}$, which is a smaller value than that estimated in [16].

It should be noted that this overlap mechanism is not always clearly observed for different gratings at various writing conditions, as seen from Fig. 4. For low modulation depths (low values of s < 0.025) the modifications can be optically observed (e. g. E = 39 nJ), but no sufficiently functional PhCs can be produced. Therefore, a high optically observable contrast is not indicative of the observable filter performance.
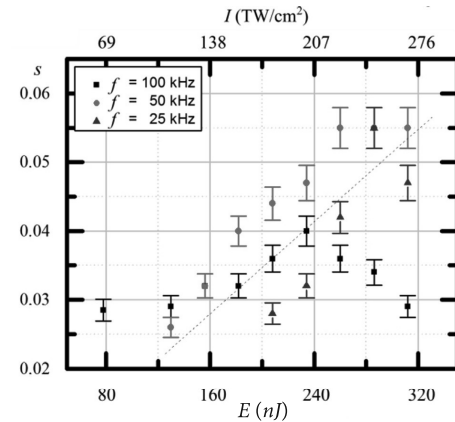
Fig. 5. Illustration of selected results. A summary of averaged s measurements as dependent on frequency and pulse energy. Dotted line shows a general trend of s increase until an observed peak or saturation ($s \lesssim 0.06$) is reached. Lower energy values for which s could not be measured (s < 0.025) are omitted.

3.2. Asymmetric voxels

Weakly asymmetric filtering spatial spectra patterns were observed in the cases of Fig. 5, especially when deviating from $E_{max(s)}$ and $I_{max(s)}$ values. Such behaviour was unexpected, and we chose to further explore the influence of the DLW beam polarization angle and beam writing direction to isolate possible unusual interaction mechanisms. After choosing different fabrication parameters and geometries containing different values of d_x, we found cases where the effect is pronounced. A selection of particular cases is shown in Fig. 6.

For the cases with d_x = 1.2 μm, where a strong transverse voxel overlap occurs, the dominant filtering lines change from one diffraction minimum to another. For another instance where d_x = 1.4 μm, the asymmetry appeared without any change, depending on different values of γ. Asymmetry that is explained by
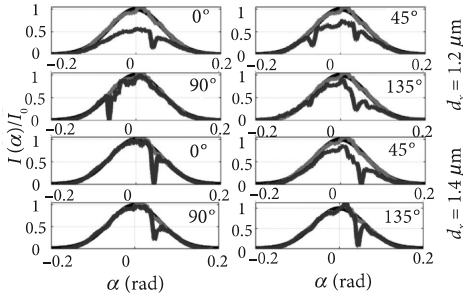
Fig. 6. Filtering patterns for different geometries and DLW beam polarization.

the far-field component diffraction from $+k_x$ to $+k_x + q_x$ becomes more efficient (less efficient for $-k_x$ to $-k_x - q_x$). This implies that in order to describe the PhC filter not one but two scattering coefficient values are needed: $s_{+q} \neq s_{-q}$ and also the refractive index modified structure is itself asymmetrical, the asymmetry depends on both the polarization and the relative scanning direction of the DLW beam.

The modified refractive index areas most probably contain an effectively tilted structure. To check the viability of such assumption, we performed numerical calculations to simulate PhCs having a harmonic type volume grating structure with different angles of a tilt. The tilted structures and resulting beam angular spectra are shown in Fig. 7. No asymmetry is observed when voxels have a zero tilt (Fig. 7(a)), yet the asymmetry starts to appear with a homogeneously increased tilt angle as seen in Fig. 7(b–c).

We expected a semi-homogeneous tilt structure, where the unidirectional raster scan was employed, but it was not always observed (e. g. the case in Fig. 6: $d_x = 1.2$ μm, $\gamma = 45°$). Also, a strong asymmetry was not always observed in the filtering patterns for the parameter sets of Fig. 5, but a possible explanation is found in Fig. 7(d). As the tilt direction is reversed for each individual PhC plain, structures of different tilt might compensate the effect. In reality, the refractive index profile might be even more complex, as can be seen from Fig. 4, where Y-shaped cracks form along the length of the PhC.

4. Conclusions

In this article, we presented a study of PhC spatial filters characterizing s-coefficient dependence of laser direct writing conditions in soda–lime glass.

We have found that for different pulse repetition rates s increases together with the irradiation intensity peak value until it reaches a peak or saturation value.
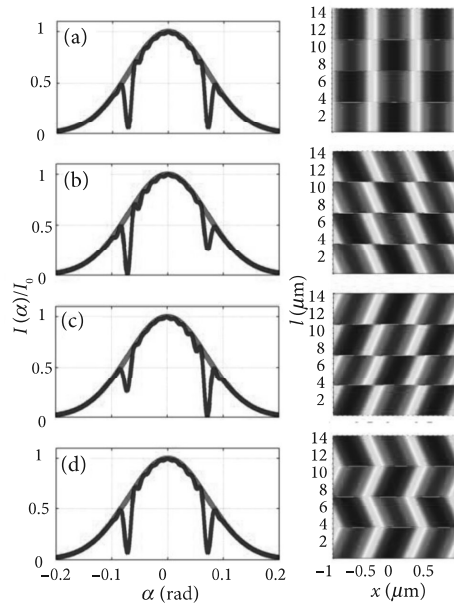
Fig. 7. Results of numerical simulations (see Appendix C). Different angular spectra (blue online) result for an input Gaussian beam (red online) for a 15 deg. tilt harmonic modulation structure model. (a) is the regular structure, (b) and (c) are opposite homogeneously tilted structures, (d) is the alternating tilt structure.

We have formulated a possible explanation, where for different fabrication conditions the redistribution of material density between successive linear writing operations plays a detrimental role in achieving the highest s-coefficient available. Under optimal writing conditions rarefaction at the centre of irradiation and densification around the rarefied centres can be beneficial in the formation of harmonic modulation of the PhCs layers, which is not seen in a conventional measurement due to increased diffraction.

Also, we have shown that scattering from different intended filtering lines in the PhC transmittance spectrum can become asymmetrical for different DLW polarizations and scanning patterns. Therefore, the behaviour of PhC filters cannot always be described in using a single value s, but needs to be characterized in terms of separate values, for example, s_{+q}, s_{-q}. As a result, writing a 2D filter with maximal symmetry requires that PhC geometry factors, the DLW direction and beam polarization should be taken into account as well.

However, little is known about the distribution of the refractive index inside the processed glass that would

help to further improve the technology and understanding of real PhCs. In light of this, more research is needed to improve the models and also the fabrication procedures for determining the best DLW conditions.

Appendix A: Mathematical model

Here we derive the scalar wave equation for the propagation of the unipolarized electric field **E**. For simplicity's sake the **E** is polarized along the "bars" of the PhC layer (y direction – TM polarization). The refractive index is expected to be in the form of

$$n(x, z) \triangleq n_0 + \Delta n(x, z), \tag{A1}$$

where $n(x, z)$ is the local value of the refractive index, n_0 is the average ambient refractive index, and $\Delta n(x, z)$ is the local deviation from n_0, expected to be $\Delta n(x, z) \ll n_0$.

For a complex wave function describing the electric field $\mathbf{E}(x, z, t) = \mathbf{E}(x, z)e^{i\omega t}$, with a complex amplitude $E(x, z) = A(x, z)e^{i\varphi(x,z)}$ and a complex envelope $A(x, z)$, the wave equation can be written down as

$$\nabla^2 \mathbf{E}(x, z, t) - \frac{1}{c^2(x,z)} \frac{\partial^2 \mathbf{E}(x,z,t)}{\partial t^2} = 0 \tag{A2}$$

with $\nabla^2 = \partial^2 / \partial x^2 + \partial^2 / \partial z^2$. $c(x, z)$ is the local speed of light expressed as $c(x, z) = c_0/n(x, z)$ and using $k_0 \triangleq \omega/c_0$ and the approximation $(n_0 + \Delta n(x, z))^2 \approx n_0^2 + 2\Delta n(x, z)n_0$, together with the slowly varying envelope approximation $\partial A(x, z)/\partial z \ll A(x, z)z$, we arrive at

$$\frac{\partial A(x,z)}{\partial z} = \frac{i}{2k} \frac{\partial^2 A(x,z)}{\partial x^2} + ik \frac{\Delta n(x,z)}{n_0} A(x,z)\cdot \tag{A3}$$

This equation is correct as long as two conditions are satisfied. First, the refractive index modulation $\Delta n(x, z)$ must be small compared to the average refractive index n_0, which in the case of this paper is lower than $\Delta n < 10^{-2}$. Second, PhC periods must be larger than the wavelength. In our case, where interlayer distances are on the average $d_z = 3 \ \mu m$ and larger, the relation is $n_0 d_z/\lambda \leq 7.2$, which is sufficient.

Appendix B: Scattering by one layer

Here we want to relate the s, that is the amplitude scattering coefficient from one layer (grating) of a PhC,

to the maximum modulation of the refraction index Δn_{max}. If the plane wave $A(x; z_0) = A_0$ illuminates the grating with the wavenumber $q = 2\pi/d_x$ (d_x is the transverse period), then the field behind the grating becomes

$$A(x, \Delta z = 2l_0) = A_0(1 + is(e^{iqx} + e^{-iqx})). \tag{B1}$$

This is valid for weakly scattering gratings $s \ll 1$, in the linear approximation with respect to s. (In the next quadratic approximation with respect to s the transmitted wave will be $A(x, \Delta z = 2l_0) = A_0(1 - s^2 + is(e^{iqx} + e^{-iqx}))$, fulfilling the energy conservation, however, for simple estimation the linear approximation is sufficient). We assume that a refractive index modulation profile follows a cosine along the transversal and Gaussian function in the longitudinal direction:

$$\Delta n(x, z) \triangleq \Delta n_{max} \cos(qx) e^{-z^2/l_0^2}, \tag{B2}$$

where l_0 is the thickness of one layer.

If we ignore the diffraction term in (A3) and perform integration of (B2), we arrive at a solution in the form of

$$\frac{A(x,z)}{A_0} = \exp\left(\frac{i\pi\Delta n_{max}(e^{iqx} + e^{-iqx})}{\lambda_0} \int_{z_0}^{z} e^{-\frac{z^2}{l_0^2}dz} \right). \tag{B3}$$

Assuming the layer thickness is less than the interlayer distance $d_z \geq 2l_0$, the Taylor series expansion of the exponent up to the first term and integration yields

$$A(x, \Delta z = 2l_0) \approx$$
$$A_0 \left(1 + i \frac{\pi^{3/2} l_0 \Delta n_{max}}{\lambda_0} e^{iqx} + \frac{\pi^{3/2} l_0 \Delta n_{max}}{\lambda_0} e^{-iqx} \right). \tag{B4}$$

Comparing (B4) to (B1) shows that s can be expressed as (1). In this way we have estimated the amplitude scattering coefficient s for symmetric phase gratings, where the wave is equally directed to the $+q$ and $-q$ components. For asymmetric gratings considered in the main part of the article the amplitude scattering coefficients are $s_{+q} \neq s_{-q}$, respectively.

Appendix C: Numerical method

To calculate the complete angular spectra for regular PhC and asymmetrical PhC structures we used a split-step method approach (a detailed implementation for the general case is found in [34]). The split-step method is used when diffractive homogenous space propagation can be evaluated separately from scattering from an infinitely thin phase grating, which, in this case, applies to one crystal layer, where the feature spatial period size is larger than the wavelength $d_x, d_z > \lambda$.

A scattering operator (matrix) is defined as $\mathbf{S}_j = \exp(i^2 s\mathbf{M}_j)$ ($\mathbf{M}_j$ can be defined as $(-1)^j \cos(qx)$, with $j = 1, 2\dots N$ counting the PhC layers), together with a propagation operator $\mathbf{P} = \exp\left(i\dfrac{d_z}{2}\sqrt{k_0^2 - k_x^2}\right)$. The resulting $\mathbf{A}_0 \to \mathbf{A}_N$ field for a PhC having N layers can be calculated by iteratively performing this operation:

$$\mathbf{A}_j = F^{-1}(\mathbf{P}F(\mathbf{S}\mathbf{A}_{j-1})). \tag{C1}$$

F and F^{-1} are the discrete Fourier and inverse Fourier transform operators.

If the structure is irregular, (C1) has to be modified to be applied not N times, but $m \cdot N$. In this case, m is the sublayer step number for a sublayer of thickness d_z/m. $\mathbf{S}_{j,p}$ and $\mathbf{M}_{j,p}$ become dependent on an additional iteration number $p = 1, 2, \dots$ m. A new parameter θ_p is introduced: $\mathbf{M}_{j,p} = (-1)^j \cos(qx + p\theta_p d_z/m)$ to control the new phase term that is responsible for displacing the phase grating along the x direction for every sublayer step m in the z direction. The scattering coefficient must also be scaled $s \to s/m$ to avoid incorrect modeling m times more efficient PhCs. In the simplest case θ_p = const, and selected according to the desired tilt value.

References

[1] A.E. Siegman, Defining, measuring, and optimizing laser beam quality, Proc. SPIE **1868**, 2–12 (1993), http://dx.doi.org/10.1117/12.150601

[2] J.I. Kato, I. Yamaguchi, and H. Tanaka, Nonlinear spatial filtering with a dye-doped liquid-crystal cell, Opt. Lett. **21**, 767 (1996), http://dx.doi.org/10.1364/OL.21.000767

[3] I. Moreno, J.J. Araiza, and M. Avendano-Alejo, Thin-film spatial filters, Opt. Lett. **30**, 914 (2005), http://dx.doi.org/10.1364/OL.30.000914

[4] D. Shurig and D.R. Smith, Spatial filtering using media with indefinite permittivity and permeability tensors, Appl. Phys. Lett. **82**, 2215 (2003), http://dx.doi.org/10.1063/1.1562344

[5] O.F. Siddiqui and G. Eleftheriades, Resonant modes in continuous metallic grids over ground and related spatial-filtering applications, J. Appl. Phys. **99**, 083102 (2006), http://dx.doi.org/10.1063/1.2189929

[6] A. Žukauskas, M. Malinauskas, and E. Brasselet, Monolithic generators of pseudo-nondiffracting optical vortex beams at the microscale, Appl. Phys. Lett. **103**, 181122 (2013), http://dx.doi.org/10.1063/1.4828662

[7] E. Colak, A.O. Cakmak, A.E. Serebryannikov, and E. Ozbay, Spatial filtering using dielectric photonic crystals at beam-type excitation, J. Appl. Phys. **108**, 113106 (2010), http://dx.doi.org/10.1063/1.3498810

[8] A.Y. Petrov and E. Ozbay, Toward photonic crystal based spatial filters with wide angle ranges of total transmission, Appl. Phys. Lett. **94**, 181101 (2009), http://dx.doi.org/10.1063/1.3127443

[9] Z. Luo, Z. Tang, Y. Xiang, H. Luo, and S. Wen, Polarization-independent low-pass spatial filters based on one-dimensional photonic crystals containing negative-index materials, Appl. Phys. B **94**, 641–646 (2009), http://dx.doi.org/10.1007/s00340-009-3376-4

[10] Z. Tang, D. Fan, S. Wen, Y. Ye, and C. Zhao, Low-pass spatial filtering using a two-dimensional self-collimating photonic crystal, Chin. Opt. Lett. **5**(S1), 211–213-3 (2007).

[11] E. Yablonovitch, Inhibited spontaneous emission in solid-state physics and electronics, Phys. Rev. Lett. **58**, 2059–2062 (1987), http://dx.doi.org/10.1103/PhysRevLett.58.2059

[12] R. Picó, V.J. Sánchez-Morcillo, I. Pérez-Arjona, and K. Staliunas, Spatial filtering of sound beams by sonic crystals, Appl. Acoust. **73**, 302–306 (2012), http://dx.doi.org/10.1016/j.apacoust.2011.09.011

[13] R. Picó, I. Pérez-Arjona, V.J. Sánchez-Morcillo, and K. Staliunas, Evidences of spatial (angular) filtering of sound beams by sonic crystals, Appl. Acoust. **74**, 945–948 (2013), http://dx.doi.org/10.1016/j.apacoust.2013.01.003

[14] K. Staliunas and V.J. Sánchez-Morcillo, Spatial filtering of light by chirped photonic crystals, Phys. Rev. A **79**(5), 053807 (2009), http://dx.doi.org/10.1103/PhysRevA.79.053807

[15] L. Maigyte, T. Gertus, M. Peckus, J. Trull, C. Cojocaru, V. Sirutkaitis, and K. Staliunas, Signatures of light-beam spatial filtering in a three-dimensional photonic crystal, Phys. Rev. A **82**(4), 043819 (2010), http://dx.doi.org/10.1103/PhysRevA.82.043819

[16] V. Purlys, L. Maigyte, D. Gailevicius, M. Peckus, M. Malinauskas, and K. Staliunas, Spatial filtering by chirped photonic crystals, Phys. Rev. A **87**, 033805 (2013), http://dx.doi.org/10.1103/PhysRevA.87.033805

[17] V. Purlys, L. Maigyte, D. Gailevicius, M. Peckus, M. Malinauskas, R. Gadonas, and K. Staliunas, Spatial filtering by axisymmetric photonic microstructures, Opt. Lett. **39**(4), 929–932 (2014), http://dx.doi.org/10.1364/OL.39.000929

[18] D. Gailevicius, V. Purlys, L. Maigyte, M. Peckus, and K. Staliunas, Chirped axisymmetric photonic microstructures for spatial filtering, J. Nanophoton. **8**(1), 084094 (2014), http://dx.doi.org/10.1117/1.JNP.8.084094

[19] K. Staliunas, Removal of excitations of Bose-Einstein condensates by space- and time-modulated potentials, Phys. Rev. A **84**, 013626 (2011), http://dx.doi.org/10.1103/PhysRevA.84.013626

[20] A. Žukauskas, G. Batavičiūtė, M. Ščiuka, T. Jukna, A. Melninkaitis, and M. Malinauskas, Characterization of photopolymers used in laser 3D micro/

nanolithography by means of laser-induced damage threshold (LIDT), Opt. Mater. **4**(8), 1601–1616 (2014), http://dx.doi.org/10.1364/OME.4.001601

[21] J. Fischer and M. Wegener, Three-dimensional optical laser lithography beyond the diffraction limit, Laser Photonics Rev. **7**(1), 22–44 (2013), http://dx.doi.org/10.1002/lpor.201100046

[22] V. Purlys, L. Maigyte, D. Gailevicius, M. Peckus, R. Gadonas, and K. Staliunas, Super-collimation by axisymmetric photonic crystals, Appl. Phys. Lett. **104**, 221108 (2014), http://dx.doi.org/10.1063/1.4881839

[23] L. Maigyte, V. Purlys, J. Trull, M. Peckus, C. Cojocaru, D. Gailevicius, M. Malinauskas, and K. Staliunas, Flat lensing in visible frequency range by woodpile photonic crystals, Opt. Lett. **38**(14), 2376–2378 (2013), http://dx.doi.org/10.1364/OL.38.002376

[24] L. Maigyte and K. Staliunas, Spatial filtering with photonic crystals, App. Phys. Rev. **2**, 011102 (2015), http://dx.doi.org/10.1063/1.4907345

[25] C. Malouin, A. Villeneuve, G. Vitrant, and R.A. Lessard, Degenerate four-wave mixing geometry in thin-film waveguides for nonlinear material characterization, Opt. Lett. **21**(1), 21–23 (1996), http://dx.doi.org/10.1364/OL.21.000021

[26] S. Nolte, M. Will, J. Burghoff, and A. Tuennermann, Femtosecond waveguide writing: a new avenue to three-dimensional integrated optics, Appl. Phys. A **77**(1), 109–111 (2003).

[27] H. Zhang, S.M. Eaton, and P.R. Herman, Single-step writing of Bragg grating waveguides in fused silica with an externally modulated femtosecond

fiber laser, Opt. Lett. **32**(17), 2559 (2007), http://dx.doi.org/10.1364/OL.32.002559

[28] M. Beresna, M. Gecevičius, P.G. Kazansky, and T. Gertus, Radially polarized optical vortex converter created by femtosecond laser nanostructuring of glass, Appl. Phys. Lett. **98**, 201101 (2011), http://dx.doi.org/10.1063/1.3590716

[29] M. Malinauskas, P. Danilevičius, and S. Juodkazis, Three-dimensional micro-/nano-structuring via direct write polymerization with picosecond laser pulses, Opt. Express **19**, 5602 (2011), http://dx.doi.org /10.1364/OE.19.005602

[30] S. Nisara, M.A. Sheikha, L. Lia, and S. Safdarb, Effect of thermal stresses on chip-free diode laser cutting of glass, Opt. Laser. Technol. **41**(3), 318–327 (2009), http://dx.doi.org/10.1016/j.optlastec.2008.05.025

[31] K.M. Davis, K. Miura, N. Sugimoto, and K. Hirao, Writing waveguides in glass with a femtosecond laser, Opt. Lett. **21**(21), 1729–1731 (1996), http://dx.doi.org/10.1364/OL.21.001729

[32] A.M. Streltsov and N.F. Borrelli, Fabrication and analysis of a directional coupler written in glass by nanojoule femtosecond laser pulses, Opt. Lett. **26**(1), 42–43 (2001), http://dx.doi.org/10.1364/OL.26.000042

[33] A.M. Streltsov and N.F. Borrelli, Study of femtosecond-laser-written waveguides in glasses, J. Opt. Soc. Am. B **19**(10), 2496–2504 (2002), http://dx.doi.org/10.1364/JOSAB.19.002496

[34] T.-C. Poon and T. Kim, *Engineering Optics with Matlab* (World Scientific, Singapore, 2006).

ERDVINIŲ FILTRŲ TIESIOGINIS LAZERINIS FORMAVIMAS FEMTOSEKUNDINIAIS IMPULSAIS NATRIO-KALCIO SILIKATINIAME STIKLE

D. Gailevičius [a], V. Purlys [a], L. Maigytė [b], E. Gaižauskas [a], M. Peckus [a], R. Gadonas [a], K. Staliūnas [b,c]

[a] *Vilniaus universiteto Lazerinių tyrimų centras, Vilnius, Lietuva*
[b] *Katalonijos politechnikos universiteto Fizikos ir branduolinės inžinerijos katedra, Terasa, Ispanija*
[c] *Katalonų tyrimų ir aukštųjų studijų institutas, Barselona, Ispanija*

Santrauka

Erdvinis filtravimas dažnai naudojamas lazerinių pluoštų erdvinei kokybei gerinti. Neseniai buvo parodytas erdvinis pluoštų filtravimas fotoniniais kristalais (FK) [24]. Šiame darbe tiriama šių naujo tipo FK erdvinių filtrų efektyvumo priklausomybė nuo FK įrašymo sąlygų. Fotoniniai dariniai suformuoti tiesioginio lazerinio rašymo būdu taikant pataškinį medžiagos lūžio rodiklio modifikavimą aštriai sufokusuotais femtosekundiniais impulsais natrio-kalcio silikatiniame stikle. Tokie FK yra apibūdinami panaudojus *s*-koeficientą – parametrą, skirtą apibrėžti FK filtro efektyvumą. Nagrinėjama filtravimo efektyvumo priklausomybė nuo skirtingų lazerinio įrašymo sąlygų, pavyzdžiui, smailinio spinduliuotės intensyvumo ir lazerio pluošto poliarizacijos. Parodoma, kad esant atitinkamoms įrašymo sąlygoms FK gali pasižymėti asimetriška vokselių sandara.

A3

PHOTONIC CRYSTAL MICROCHIP LASER

D. Gailevicius, V. Koliadenko, V. Purlys, M. Peckus, V.
Taranenko, and K. Staliunas

SCIENTIFIC REP⚙RTS

Photonic Crystal Microchip Laser

Darius Gailevicius[1], Volodymyr Koliadenko[2], Vytautas Purlys[1], Martynas Peckus[1], Victor Taranenko[2] & Kestutis Staliunas[3,4]

The microchip lasers, being very compact and efficient sources of coherent light, suffer from one serious drawback: low spatial quality of the beam strongly reducing the brightness of emitted radiation. Attempts to improve the beam quality, such as pump-beam guiding, external feedback, either strongly reduce the emission power, or drastically increase the size and complexity of the lasers. Here it is proposed that specially designed photonic crystal in the cavity of a microchip laser, can significantly improve the beam quality. Experiments show that a microchip laser, due to spatial filtering functionality of intracavity photonic crystal, improves the beam quality factor M^2 reducing it by a factor of 2, and increase the brightness of radiation by a factor of 3. This comprises a new kind of laser, the "photonic crystal microchip laser", a very compact and efficient light source emitting high spatial quality high brightness radiation.

The microchip lasers (and generally other micro- and millimeter size lasers such as edge-emitting or vertically-emitting semiconductor lasers) usually suffer from a low beam quality, especially in high power operation regimes. There have been proposed several techniques to improve the beam quality of microchip lasers, e.g. by using optical injection[1], external feedback[2], external gratings[3,4], external beam manipulation techniques[5] and others, however, this results in a loss of the main advantage–the compactness and simplicity of the laser design.

In order to obtain high beam quality in microchip lasers usually the emission area is confined in transverse space, localizing the fields by a defect[6] or by using a relatively narrow pump area. The restriction of the pump area and pump intensity enables a single-transverse mode emission, however, strongly reduces the emitted power (P_{out}). The increase of the pump power (either by increasing pump area or the pump intensity) results in multi-transverse mode emission, and therefore in a drastic reduction of the beam quality. The power of emitted radiation still increases with the increase of the pump power, however, the brightness ($B = P_{out}/A\Omega$, where A is the surface area of the beam cross-section, Ω is the solid angle of divergence) of the radiation saturates and does not increase.

Our idea, elaborated theoretically and proved experimentally in this letter, is that the specially designed intracavity Photonic Crystals (PhC) can solve the beam quality problem **for high pump power** decreasing the beam quality factor M^2. Photonic crystals, besides their celebrated properties in the frequency domain, such as frequency bandgaps and slow light effects[4,7,8], can also affect the spatial beam propagation, causing such peculiarities as the negative refraction[9,10], anomalous diffraction (flat lensing)[11,12], and importantly for the present work–spatial (angular) filtering. The spatial filtering by PhCs, is based on the angular band-gaps PhCs[13,14] and angular quasi-bandgaps PhCs[15,16], and does not require the access to the far field domain of resonating field like in conventional filtering techniques by confocal lens arrangement (see Supplementary Information for detailed description of PhC spatial filtering). The PhC spatial filters can provide efficient filtering in extremely short propagation distances (typically around $200\,\mu m$)[17]. The arrangement, therefore, comprises an efficient, compact laser source, which we named the microchip photonic crystal laser, able to emit powerful beams of good spatial quality (single transverse mode beams), and of high brightness.

Being specific, we consider a Nd: YAG based microchip laser, of cavity length 5 mm, and maximum emission power 900 mW (in multi-transverse mode regime). To ensure single transverse mode emission, the width of the pump beam is restricted (typically to $80\,\mu m$, depending on pump power). The use of broader pump area increases the Fresnel number, and results in multimode emission if no special means are taken. We propose to use the spatial PhC filters inside the cavity, in order to maintain a high beam quality while increasing the pump area and pump intensity.

[1]Laser Research Center, Department of Quantum Electronics, Vilnius University, Sauletekio Ave. 10, LT-10222, Vilnius, Lithuania. [2]International center "Institute of Applied Optics" NAS of Ukraine, Kudryavskaya Str. 10G, 04053, Kyiv, Ukraine. [3]Departament de Física i Enginyeria Nuclear, Universitat Politècnica de Catalunya, Colom 11, 08222 Terrassa, Spain. [4]Institucio Catalana de Reserca i Estudis Avançats (ICREA), passeig Lluis Companys 23, 08010 Barcelona, Spain. Correspondence and requests for materials should be addressed to D.G. (email: darius.gailevicius@ff.vu.lt)
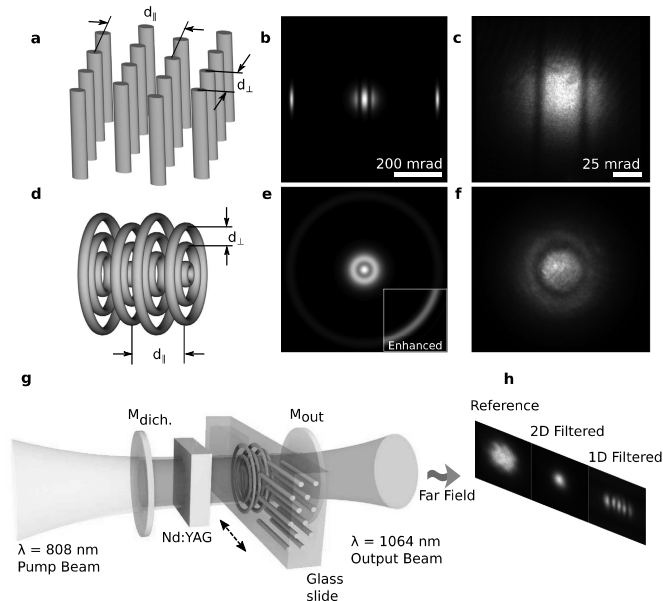
Figure 1. Filtering by one-dimensional and axisymmetric PhC filters. (**a**) Spatial PhC filter, consisting of periodic structure of parallel rods, results in one-dimensional filtering, as shown in single-pass angular far-field distribution, numerically (**b**) and experimentally (**c**). Respectively, PhCs of circular geometry (**d**) causes axisymmetric filtering (**e,f**). The (**g**) schematically shows the microchip laser structure, with inserted intracavity PhC filters (1D, axisymmetric and no filter), and (**h**) shows the experimentally measured far-field profiles in corresponding cases.

For that purpose we fabricated PhC filters of two different symmetries: the axisymmetric filter[18] (Fig. 1d) to achieve the main goal, i.e. the single-transverse mode emission; and also a one-dimensional (1D) spatial filter[17] (Fig. 1a), filtering in one transverse direction. The latter allows to convincingly demonstrate the appearance of a beneficial filtering effect, i.e. to have simultaneously a laser with- and without filtering in different directions in transverse space under identical conditions (the same pump power and the same losses for both field quadratures). We fabricated the PhCs using point-by-point direct laser writing technique, see the **Fabrication method**. The ratio between the longitudinal and transverse periods of the index modulation in the photonic crystal structure provides the angular position of the filtering range. For instance, the high angle pass filtering (removal of the axial mode) is obtained for $Q = 2d_\perp^2/(\lambda d_\parallel) = 1$ (see Supplementary Information for the calculation of the filtering angles in passive configuration). In order to obtain the low-angle pass filtering (transparent for the axial mode and opaque for small angle of-axis modes), which is the purpose of our work, the geometry parameter Q slightly deviates from unity.

The PhC filters were first tested in stand-alone configuration (see the experimentally measured transmission in Fig. 1c,f, also Supplementary Information), and then positioned inside the cavity of microchip laser. The experimental outcome is shown in Fig. 1h. The axisymmetric spatial filter in the cavity of microchip laser causes the narrowing of the far field radiation (decrease of angular spread of the beam) and formation of single-transverse-mode beam. For comparison 1D filter results in the decrease of the angular divergence along the filtering direction only (vertical direction in Fig. 1g) whereas the beam in unaffected (horizontal) direction remains largely diverging (containing higher order transverse modes).

Figure 2 summarizes the quantitative experimental results. Without the PhC filter the increasing pump power results in the increase of the emission power and of the divergence of the output beam, whereas the brightness of the radiation remains approximately constant. With the PhC filter in microcavity the divergence of the beam remains independent on the pump power (up to a particular pump level), and the brightness constantly increases with the pump. Note that the emission power in the presence of the PhC spatial filter just slightly decreases compared to the case without spatial filtering. The increase of brightness due to intracavity photonic crystal is 2.8 (maximum brightness)—3.1 times (at equal pumping) in this particular experimental measurement. Behind a particular threshold for the pump power the spatial filtering is no more sufficient, and the beam quality as well as brightness starts decreasing. Maximal power of single transverse mode beam was 88 mW without filtering and 335 mW with the PhC filter (area with divergence <9 mrad on Fig. 2). It depends on the efficiency of the spatial filtering (the width and the depth of filtered out area in angular domain). Speaking in numbers, the spatial quality factor of the beam from the PhC microchip laser remained $M^2 = 1.2$, for the emission power up to 300 mW,
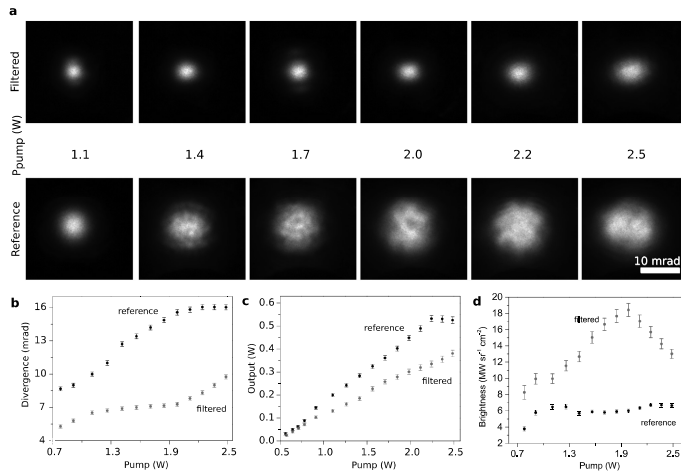
Figure 2. Experimental results. (a) Experimentally measured far-field distributions from the microchip laser without a PhC spatial filter (first column), and with (second column) axisymmetric intracavity spatial filter (Q = 1.18, N = 20). The width of the pump beam was 200 μm. Presence of the axisymmetric filter results in TEM00 mode of emitted radiation. (**b–d**) shows the beam divergence, output power, and brightness dependencies on the pump power respectively.

whereas the spatial quality factor of the beam from the laser without spatial filtering increased until $M^2 = 2.5$ for the same output power[19].

In order to justify the experimental observations, and also to show the potential of a photonic crystal microchip laser, we performed numerical simulations of the microchip laser with- and without the intracavity spatial filtering. The simulations are based on Maxwell-Bloch model, see *Numerical methods*. The results are summarized in Fig. 3, where series of calculation results are presented: one series (shown by red lines) approximately corresponds to the current experimental situation, and the other two series corresponding to the spatial filters of 2 and 4 times higher efficiency (beyond what our current technologies allow for today). The far field patterns without and with spatial filtering show the same qualitative features as in experiment (compare with Fig. 2). The qualitative characteristics of numerical simulations (dependence of power, divergence, and brightness of the emitted beam) are also well compatible with experimental observations in Fig. 2.

Note, that the inset in Fig. 3b (the averaged far field at the normalized pump intensity $D_0 = 6$) shows a dark ring. This happens when the PhC filtering efficiency is no more sufficient to ensure the single-transverse-mode emission. The PhC microchip laser starts emitting at the angles larger than the filtering area. This illustrates the limits of the applicability of spatial filtering for given filtering efficiency. The use of more efficient spatial filters, i.e. with a deeper/broader filtering angular range, would allow increasing the brightness of emitted radiation proportionally, as the Fig. 3b demonstrates.

Concluding, we show a substantial improvement of the spatial quality of the beam emitted by microchip laser due to the spatial filtering functionality of intracavity photonic crystals. Specifically, we were able to increase the power of single transverse mode emission from 90 mW without intracavity PhC, to 340 mW with intracavity PhC, i.e. almost 4 times. The brightness of the emitted radiation has been increased approximately by a factor of 3.

The performance can be strongly improved by advancing the angular transmission characteristics of the spatial filters. The angular filtering range is limited by the material characteristics of the filter (the amplitude of refraction index modulation, and the length of the PhC (the number of longitudinal periods). The performance of photonic crystal microchip laser is thus restricted by technological limitation (aberrations of femtosecond laser writing arrangement, available materials) of the PhC filters. With the future advance of microfabrication technologies and with new materials providing the larger refraction index modulation, the performance of the PhC microchip laser can be significantly improved. Technically, the idea can be brought to perfection by fabricating the PhC directly on the microchip active media using DLW techniques, resulting in a completely monolithic device[20]. The present work demonstrates the principle of intracavity spatial filtering by PhCs, and thus constitutes a new class of laser - the photonic crystal microchip laser. The numerical simulations shows huge potential of the photonic crystal microchip laser improved using advanced technologies. In particular, our numerics (not presented here) show that the concept is applicable for pulsed microchip lasers too (by numerically solving MBE Equations 1 with added saturable absorber).

Finally the proposed idea could be applied to the other types of microlasers, like semiconductor edge-emitting lasers, and vertical cavity semiconductor lasers, the VCSEL (in fact the VCSELS would convert into VECSELS,
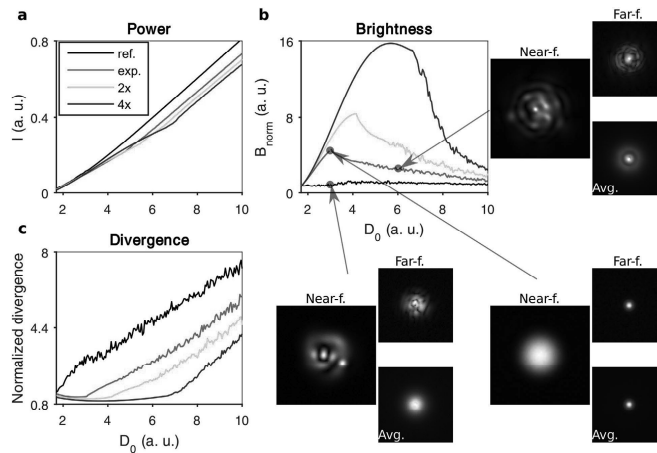
Figure 3. Numerical study. Summary of numerical simulations of photonic crystal microchip laser: (**a**) shows the emission power, (**b**) the brightness and (**c**) the angular divergence of the emitted beam, depending on the pump power, for three realizations of spatial filters. The black line depicts the reference case (no filter), the red line corresponds to the filter with transmission profile corresponding to the experimental situation (Figs 1 and 2), and the green and blue lines correspond to the filters with 2 and 4 times increased filtering performance (correspondingly increased width of the filtering area). The near- and far-field beam profiles as well as averaged far-field profiles are shown on insets: the near field window size is 2×2 mm, and far field windows size is 40×40 mrad.

the Vertical *External* Cavity Semiconductor Lasers, when one incorporates at approximately 200 μm length PhC filter inside the cavity).

Fabrication Method

We fabricated the PhCs using point-by-point direct laser writing technique (see Supplementary Information) in the bulk of standard soda-lime microscope glass slides ($n_{ref} = 1.52$) using direct laser writing technique. A femtosecond Yb:KGW laser beam (295 fs pulse duration at FWHM) was tightly focused into the sample using 40×0.95 NA microscope objective, and producing local modified refractive index areas at the vicinity of the focal point. Thus, by scanning the sample in respect to the focus, 3D PhCs are created. In particular, we used fundamental 1030 nm laser wavelength, 1 kHz pulse repetition rate, 432 nJ energy (246 TW/cm² peak intensity), and 800 μm/s writing speed.

The ratio between the longitudinal and transverse periods of the index modulation in the photonic crystal structure provides the angular position of the filtering range. For instance, the high angle pass filtering (removal of the axial mode) is obtained for $Q = 2d_\perp^2/(\lambda d_\parallel) = 1$ (see Supplementary Information for the calculation of the filtering angles in passive configuration). In order to obtain the low-angle pass filtering (transparent for the axial mode and opaque for small angle of-axis modes), which is the purpose of our work, the geometry parameter Q slightly deviates from unity. The transverse period was $d_\perp = 2$ μm, and longitudinal period was $d_\parallel = 9.4$ μm, corresponding to a geometry coefficient $Q \approx 1.18$ for a wavelength of $\lambda = 1064$ nm. The dimensions of PhC filters were restricted to fabrication time and the focal length of the objective. The lateral dimensions of both 1D and axisymmetric PhC filters were 200 μm, and the length was 188 μm, which corresponds to 40 layers or 20 periods. Each layer consists of parallel rod or concentric phase gratings, having an inverted pattern in respect to the neighboring layers, as conceptually shown in Fig. 1a,d.

We estimated the resulting scattering coefficient to be $s \approx 0.025$, by calibrating experimentally observed spatial transmittance spectra with numerically derived ones as in ref. 17. This value corresponds to about $s^2 \approx 0.6\%$ integral intensity scattering from one PhC layer.

Numerical methods. In order to justify the experimental observations, and also to show the potential of a photonic crystal microchip laser we performed numerical simulations of the microchip laser with- and without the intracavity spatial filtering. We numerically integrated the Maxwell-Bloch Equation (MBE) system:

$$\frac{\partial E}{\partial t} = [-(1 + i\omega_0) + ia\nabla_\perp^2 + iV(\mathbf{r}_\perp) + \hat{F}(\nabla_\perp)]E + P, \tag{1a}$$

$$\frac{\partial P}{\partial t} = -\gamma_\perp(P - ED), \tag{1b}$$

$$\frac{\partial D}{\partial t} = -\gamma_{\parallel}\left(D - D_0(\boldsymbol{r}_\perp) + \frac{EP^* + E^*P}{2}\right),$$

(1c)

where the envelope of the beam $E(\boldsymbol{r}_\perp, t)$, the field polarization $P(\boldsymbol{r}_\perp, t)$, and the population inversion $D(\boldsymbol{r}_\perp, t)$ are defined in two-dimensional transverse space $\boldsymbol{r}_\perp$, and evolving in time. $D_0(\mathbf{r})$ is the normalized pump profiled. Time is normalized to photon life time $\tau = \frac{Lf}{c}$, L being the full (round-trip) length of the resonator, and f is the cavity fines (in experiment $\tau \approx 0.1$ ns). Diffraction coefficient $a = \frac{L\lambda f}{2\pi}$ scales the transverse space (in experiment $a \approx 2 \times 10^3 \mu m^2$. ω_0 is the resonance detuning from the gain line center, $\gamma_\perp$ is the polarization relaxation rate, which is typically of order of 10, and $\gamma_\parallel$ is the inversion decay rate, typically of order of 10^{-6} (both normalized to photon relaxation rate). $V(\boldsymbol{r}_\perp)$ is the confining potential in transverse space (in microchip laser we considered thermal lensing, where refraction index follows pump profile $V(\boldsymbol{r}_\perp) = \alpha \cdot D_0(\boldsymbol{r}_\perp)$). The filtering function of intra-cavity PhC is introduced phenomenologically by the operator $\hat{F}(\nabla_\perp)$ providing the far-field transmission profile $\log(\hat{F}(k_\perp))$, and matching the experimentally measured angular transmission dependences of PhC filters.

References
1. Takimoto, S., Tachikawa, T., Shogenji, R. & Ohtsubo, J. Control of spatio-temporal dynamics of broad-area semiconductor lasers by strong optical injection. *IEEE Photonics Technol. Lett.* **21**, 1051–1053 (2009).
2. Mandre, S. K., Fischer, I. & Elssser, W. Control of the spatiotemporal emission of a broad-area semiconductor laser by spatially filtered feedback. *Opt. Lett.* **28**, 1135 (2003).
3. Martín-Regalado, J., van Tartwijk, G. H. M., Balle, S. & Miguel, M. S. Mode control and pattern stabilization in broad-area lasers by optical feedback. *Phys. Rev. A* **54**, 5386–5393 (1996).
4. Li, J., Ueda, K., Zhong, L., Musha, M., Shirakawa, A. & Sato, T. Efficient excitations of radially and azimuthally polarized Nd³⁻: YAG ceramic microchip laser by use of subwavelength multilayer concentric gratings composed of Nb₂O₅/SiO₂. *Opt. Express* **16(14)**, 10841 (2008).
5. Saikawa, J., Kurimura, S., Shoji, I. & Taira, T. Tunable frequency-doubled Yb:YAG microchip lasers. *Opt. Mater.* **19**, 160–174 (2002).
6. Song, D. S., Lee, Y. J., Choi, H. W. & Lee, Y. H. Polarization-controlled, single-transverse-mode, photonic-crystal, vertical-cavity, surface-emitting lasers. *Appl. Phys. Lett.* **82**, 3182–3184 (2003).
7. Baba, T. Slow light in photonic crystals. *Nat. Photonics* **2**, 465–473 (2008).
8. Gersen, H. *et al.* Real-space observation of ultraslow light in photonic crystal waveguides. *Phys. Rev. Lett.* **94**, 3–6 (2005).
9. Cubukcu, E., Aydin, K., Ozbay, E., Foteinopoulou, S. & Soukoulis, C. M. Electromagnetic waves: Negative refraction by photonic crystals. *Nature* **423**, 604–605 (2003).
10. Notomi, M. Manipulating light with strongly modulated photonic crystals. *Reports Prog. Phys.* **73**, 096501 (2010).
11. Parimi, P. V., Lu, W. T., Vodo, P. & Sridhar, S. Photonic crystals: imaging by flat lens using negative refraction. *Nature* **426**, 404 (2003).
12. Fang, N., Lee, H., Sun, C. & Zhang, X. Sub-diffraction-limited optical imaging with a silver superlens. *Science* **308**, 534–537 (2005).
13. Serebryannikov, A. E., Petrov, a. Y. & Ozbay, E. Toward photonic crystal based spatial filters with wide angle ranges of total transmission. *Appl. Phys. Lett.* **94**, 26–29 (2009).
14. Colak, E., Cakmak, A. O., Serebryannikov, A. E. & Ozbay, E. Spatial filtering using dielectric photonic crystals at beam-type excitation. *J. Appl. Phys.* **108**, 113106 (2010).
15. Maigyte, L. *et al.* Signatures of light-beam spatial filtering in a three-dimensional photonic crystal. *Phys. Rev. A* **82**, 043819 (2010).
16. Maigyte, L. & Staliunas, K. Spatial filtering with photonic crystals. *Appl. Phys. Rev.* **2**, 011102 (2015).
17. Purlys, V. *et al.* Spatial filtering by chirped photonic crystals. *Phys. Rev. A* **87**, 033805 (2013).
18. Purlys, V. *et al.* Spatial filtering by axisymmetric photonic microstructures. *Opt. Lett.* **39**, 929–932 (2014).
19. For measurement of beam quality factor we used the ISO 11146-1:2005 standard.
20. Salamu, G., Jipa, F., Zamfirescu, M. & Pavel, N. Laser emission from diode-pumped Nd:YAG ceramic waveguide lasers realized by direct femtosecond-laser writing technique, *Opt. Express* **22(5)**, 5177 –5182 (2014).

Author Contributions
D.G., V.P. and M.P designed, fabricated, and measured stand-alone PhC filters, V.K. and V.T. performed all measurements of microchip laser, K.S. performed numerical simulations, coordinated the research and wrote the manuscript. All authors were involved in discussions, and revisions of the manuscript.

Additional Information
Supplementary information accompanies this paper at http://www.nature.com/srep

Competing financial interests: The authors declare no competing financial interests.

How to cite this article: Gailevicius, D. *et al.* Photonic Crystal Microchip Laser. *Sci. Rep.* **6**, 34173; doi: 10.1038/srep34173 (2016).

A4

SPATIAL FILTERS ON DEMAND BASED ON APERIODIC PHOTONIC CRYSTALS

D. Gailevičius, V. Purlys, M. Peckus, R. Gadonas, and K. Staliunas

PAGE LEFT INTENTIONALLY
BLANK

A5

CHIRPED PHOTONIC CRYSTAL FOR SPATIALLY FILTERED OPTICAL FEEDBACK TO A BROAD-AREA LASER

C. Brée, **D. Gailevičius**, V. Purlys, G. G. Werner, K. Staliunas,
A. Rathsfeld, G. Schmidt, and M. Radziunas

PAGE LEFT INTENTIONALLY
BLANK

A6

ANGULAR FILTERING BY BRAGG PHOTONIC MICROSTRUCTURES FABRICATED BY PHYSICAL VAPOUR DEPOSITION

L. Grineviciute, C. Babayigit, **D. Gailevičius**, E. Bor, M. Turduev, V. Purlys, T. Tolenis, H. Kurt, and K. Staliunas

PAGE LEFT INTENTIONALLY
BLANK

A7

PHOTONIC CRYSTAL SPATIAL FILTERS FABRICATED BY FEMTOSECOND PULSED BESSEL BEAM

D. Gailevičius, V. Purlys, and K. Staliunas

Photonic Crystal Spatial Filters Fabricated by Femtosecond Pulsed Bessel Beam

DARIUS GAILEVIČIUS,[1,2]* VYTAUTAS PURLYS,[1,2] AND KESTUTIS STALIUNAS[3,4]

[1] *Vilnius University, Faculty of Physics, Laser Research Center, Sauletekio Ave. 10, Vilnius, Lithuania*
[2] *"Femtika", Saulėtekio al. 15, LT-10224, Vilnius, Lithuania*
[3] *Institució Catalana de Recerca i Estudis Avancats (ICREA), Passeig Lluís Companys 23, 08010, Barcelona, Spain*
[4] *Universitat Politècnica de Catalunya (UPC), Rambla Sant Nebridi 22, 08222, Terrassa (Barcelona) Spain*
*darius.gailevicius@ff.vu.lt

Abstract: We propose and experimentally demonstrate femtosecond direct laser writing with Bessel beams for the fabrication of photonic crystals with spatial filtering functionality. Such filters are mechanically stable, of small (of order of millimeter) size, do not require direct access to the far-field domain, and therefore are excellent candidates for intracavity spatial filtering applications in mini- and micro-lasers. The technique allows the fabrication of efficient photonic crystal spatial filters in glass, with a narrow angle (~1 degree) nearly 100%-transmission pass-band between broad angle (up to 10 degrees) nearly 0%-transmission angular stop-bands. We show, that this technique can not only significantly shorten the fabrication time, but also allows the fabrication of large-scale defect-free photonic crystal spatial filters with a wide filtering band.

1. Introduction

Spatial filtering is a general technique used to improve the spatial properties of the radiation of lasers. Typically, conventional lasers (e.g. solid-state lasers) contain low angle pass intracavity spatial filters in form of confocal arrangement of lenses with the circular diaphragm in the confocal plane. The diaphragm ensures the operation of the laser on the lowest possible order transverse mode [1]. However, such an arrangement is very inconvenient or even impossible in microlasers, such as microchip lasers, edge emitting semiconductor lasers, or VCSEL lasers. The millimeter-order length of the resonators does not allow the conventional confocal lens arrangement for the intracavity spatial filtering. This is possibly the main reason, why the radiation from many of microlasers suffers from the bad spatial beam quality, which is especially problematic in higher emission power regimes. Lifting the limitations of the beam spatial quality would allow to increase the brightness of the radiation of microlasers and would open new relevant areas of their technological application.

A promising solution of the beam spatial quality problem is the intracavity use of compact Photonic Crystal (PhC) spatial filters. The idea of PhC spatial filtering was proposed in [2,3], and subsequently experimentally demonstrated in [4–6] in different realizations. The idea is based on a selective diffraction of the angular components of the light propagating through the double-periodic photonic structure: the particular angular components of the incident light at a resonance with the transverse and longitudinal periodicities of the photonic structure diffract efficiently and are removed from the zero-diffraction order of the transmitted beam. The PhC spatial filtering, together with the super-collimation [7], already showed itself as a powerful tool to clean the spatial structure of the beams, which could be efficiently employed in microresonators, for instance in the microchip [8] and diode [9] lasers. For a detailed review on PhC spatial filtering see e.g. [10].

In practice, the fabricated PhC filters, especially those written by femtosecond pulses into inorganic materials using direct laser writing techniques, have a problem of a limited functionality of spatial filtering. Firstly, the rough estimations show [10], that the depth of

filtering band scales as $\Delta n \cdot l / \lambda$, where Δn is the refraction index modification (which in glasses is of the order of $10^{-3} - 10^{-2}$), l is the length of the written photonic crystal and λ is the wavelength. This means that the efficient filtering, with 100% depth of the filtering dips can be achieved for >100 μm length of the PhC. Moreover, the angular width of the filtering line is proportional to Δn, which is the fractions of degree for such low-index-contrast PhCs. For relevant applications the filtering line of several degrees is required (for instance the main technological challenge in edge emitting semiconductor lasers is to reduce the slow-axis divergence from ~ 5 degrees down to 1-2 degrees). The width of the filtering band is not a fundamental problem, since it can be substantially broadened using chirped photonic crystals [6,11], i.e. by sweeping the geometrical parameters along the photonic structure, which moves the relatively narrow filtering band through the broader area of angular transmission spectrum. Such sweep of the filtering band could cover larger angular ranges, see Fig.1(a) for the illustration, however, eventually would result in respectively longer crystals.

Thumb rule [10] says that the 100% filtering of the angular range $\Delta \varphi$ relates with the length l of the chirped photonic crystal as $l = \lambda \Delta \varphi / \Delta n$. For example, if Δn is small, of order of 10^{-2} and if the desired angular range of filtering is $\Delta \varphi \sim 0.1$ in radians, then one needs a crystal length of the order of 1 mm. Typically the PhCs are fabricated by direct laser writing using Gaussian beams, where tightly focused femtosecond laser beam induces local modification of refractive index in glass or other transparent materials [12–15]. The convenient transverse periodicity of the PhCs is in the range of 1-2 µm, which means that a relatively high numerical aperture (NA) focusing optics must be used (NA > 0.8), however, this contradicts with the required length of the PhC (> 1 mm). The existing variety of focusing optics forces to make a choice between high NA, but short working distance optics, and long working distance, but low NA optics. In addition, the deeper in the glass substrate is the focus, the more it is affected by the spherical aberrations. In practice, spherical aberrations and limited working distance limit the length of PhCs to appr. 0.3 mm.
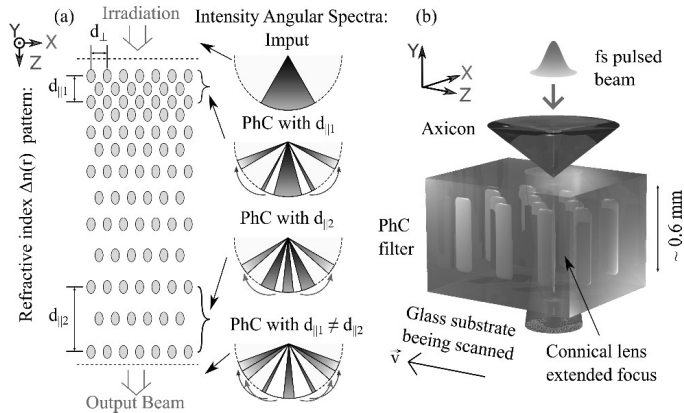
Fig. 1. (a) Illustration of broad band spatial filtering in chirped PhCs. (b) Principle scheme of direct laser writing using Bessel beams, illuminated in vertical Y-direction, whereas the filtering follows along the horizontal Z-direction.

For some applications the filtering along one direction is sufficient. For example, it is especially suitable for broad edge emitting semiconductor lasers, where only the slow-axis filtering is required [16,17]). In such case the PhCs of 2D geometry are needed. The idea

presented in this paper is to use the Bessel beams [18] for fabrication of such large longitudinal scale 2D PhC spatial filters.

Bessel beams can be generated by refractive, reflective or diffractive axicons and are characterized by a long and narrow high aspect ratio high intensity focusing area. This property is used for machining transparent materials [19–21], e.g. for fabrication of phase elements [22,23]. Due to very long and narrow area of refractive index modifications, the fabrication can be performed in a "horizontal geometry", see Fig.1(b). Then the length of the filtering structure is no longer a problem and in principle is limited only by the mechanical travel range of the fabrication stages. Although the vertical direction is still limited, it is at least by one order of magnitude longer compared to that using the Gaussian writing beam strategy.

The main message of the article is an experimental demonstration of a possibility to inscribe sufficiently long PhC crystals by using Bessel beams, which can ensure technologically relevant 1D spatial filtering. We show the efficient filters in the visible and in the near infrared range. The letter describes: Bessel beam writing setup; fabrication of the real structure; experimental observation of the light angular transmission characteristics through such PhC structures of different length.

2. Fabrication and characterization

The samples were fabricated using a direct laser writing setup, which is schematically shown in Fig. 2(a). The Bessel beam was generated using a UVFS ($n \approx 1.45$) conical lens (axicon) with a half angle of $\angle\alpha = 0.5°$ (cor. apex angle: 179°). The incoming beam was of a Gaussian profile with a diameter of $2w = 5.3$ mm at e^{-2} level. The center wavelength $\lambda = 1030$ nm, the pulse repetition rate 25 kHz and pulse duration approximately 200 fs. Such configuration led to an extended focal line (Bessel zone) length of approximately $Z_{BZ1} \approx 1.34$ m. In order to decrease its dimensions a demagnifying telescope was arranged from two lenses with the focal lengths of 500 mm and 9 mm, having a demagnification value of M~55.6. Pulse energy delivered to the sample corresponded to 8 µJ.

A polished N-BK7 ($n_{ref} \approx 1.51$) 4 mm thick rectangular substrate was used as a substrate and was mounted on a 3D positioning stage. After demagnification inside the substrate the Bessel zone length Z_{BZ2} was estimated to be around 600 µm (according Snell's law as in [24]). The sample was scanned at 2500 µm/s in a consecutive linear motion to produce the patterns shown in Fig. 2(b). The usable aperture of such PhCs is 0.6×1 mm^2 and can be extended in the horizontal (filtering) direction without limitation. We note that the usable aperture in the y-direction as shown in Fig. 2(b) is less than the estimated Bessel zone length Z_{BZ2}. Practically, Z_{BZ2} was expected to be longer since we did not use a spatial filter to correct the distortion by the axicon tip [25–27]. The oscillatory refractive index modifications seen at the bottom of the facet view are a result of this. For the exposure conditions used here, positive refractive index changes are induced during fabrication according to [28,29].

After fabrication we inspected the PhC samples with a transmission optical microscope, Fig. 2(b) and then probed them illuminating by focused Gaussian laser beam. We observed the angular filtering bands as shown in Fig. 2(c). To record the transmitted intensity pattern, we projected the beam directly on a CCD camera matrix placed at the far-field.
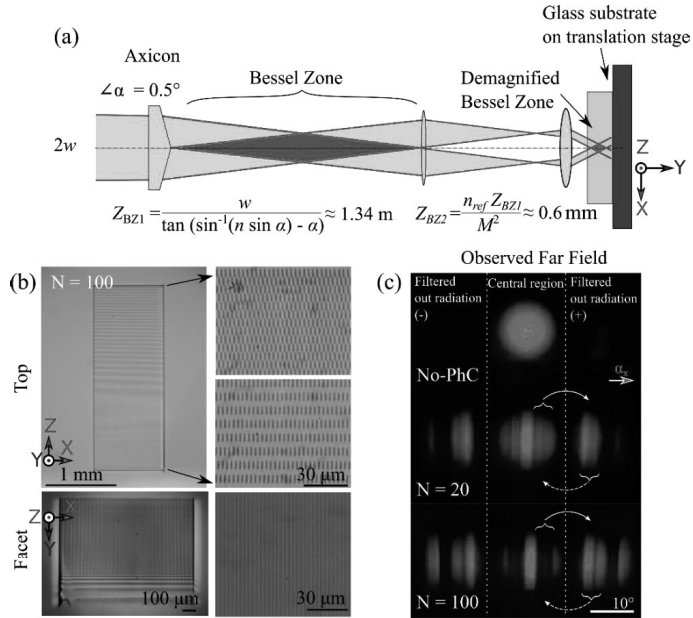
Fig. 2. Illustration of the fabrication arrangement (a), microscope-photos of the sample (b), and the 2D light transmission picture, showing the central beam region, from which radiation is filtered out (c). Arrows indicate resonant energy transfer between two coupled angular bands: outward and, also, inward to the central region.

The described fabrication scheme allowed us to achieve a minimum transverse period of 3 μm, accordingly by a ~1.5 μm transverse width of the inscribed voxels. The central filtering angle of non-chirped PhCs for a wavelength $\lambda = \lambda_{vac} \, n_{ref}$ in paraxial approximation reads: $\sin(\alpha_c) = \lambda(Q-1)/2d_\perp$, where Q is a geometry parameter, $Q = 2d_\perp^2/(\lambda d_\parallel)$, chosen according to the target filtering angle. For example, in order to have a central filtering angle of $\alpha_c = 1$ deg for $\lambda_{vac} = 633$ nm wavelength and $d_\perp = 3$ μm transverse period, the Q is ~1.25 ($d_\parallel$ ~34.4 μm respectively). For chirped PhCs the Q factor is varied along the structure. E.g. if the Q is varied from 1.2 to 1.4, the central filtering angle varies from 0.8 to 1.6 degrees.

3. Results

To explore the spatial filtering in regular (non-chirped) PhCs we fabricated several samples with different numbers of longitudinal periods N ($d_\parallel \approx 26.8$ μm). The target filtering wavelength was $\lambda_{HeNe} = 633$ nm. Experimentally measured transmission spectra are shown in Fig. 3(a). The filtering dips in the angular transmission function are getting deeper with increasing the PhC length until they reach the maximum depth at $N = 8$ periods. If the length of the PhC is further increased, the filtering regions become shallower again. This is due to the fact that the filtered radiation is propagating along the crystal couple back to the original modes. At $N = 14$ (approximately double the optimum length for filtering) almost no filtering regions are observed. These are so called Laue-Rabi oscillations, see [10] for a more detailed explanation, with the revival period of $N \approx 14$.
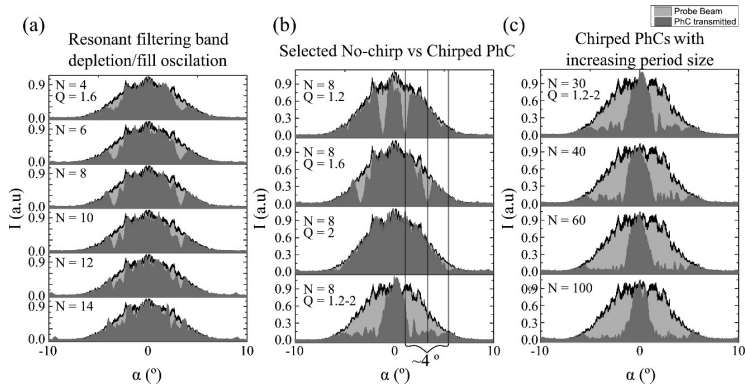
Fig. 3. Transmitted probe beam angular intensity spectra for different PhCs without (a,b) and with chirp (b,c) and for different crystal lengths (a,c) illuminated by $\lambda_{HeNe} = 633$ nm. (c) shows transmitted beams for increased PhC lengths for chirped case, where saturation of the filtering effect occurs.

Next, we selected several Q values $Q = 1.2$, 1.6, 2.0 (estimated central filtering angles: $\alpha_1 = 0.8°$, $\alpha_2 = 2.4°$, $\alpha_3 = 4°$) and fabricated three PhC samples with fixed longitudinal period and optimal length ($N = 8$ periods) in order to demonstrate the filtering angle dependence on the longitudinal period. The angular transmission spectra, Fig. 3(b), show that the filtering angles correspond reasonably well to the estimated values and were measured to be $\alpha_1 = 1.08°$, $\alpha_2 = 3.2°$, $\alpha_3 = 5.5°$. The discrepancy is due to paraxial approximation used to derive the angle *vs.* Q relation. The width of the filtering bands in all three cases was about $0.6°$.

In order to increase the width of the filtering band a chirped PhC geometry was used ($1.2 \leq Q \leq 2$). The $d_\parallel$ values were varied linearly in a range $21.5 \leq d_\parallel \leq 35.8$ µm. The bottom graph of Fig. 3(b). shows the corresponding angular transmission spectrum of such structure of $N = 30$ periods. The positive effect of chirping is obvious when comparing with Fig. 3(b) column. Although fabricated with the same conditions, the chirped PhCs exhibit much wider filtering band of $\Delta\alpha \approx 4°$, compared to $\Delta\alpha \approx 0.6°$ for non-chirped examples. The filtered angular bands are a bit shallower for $N = 30$ periods chirped crystals compared to the $N = 8$ periods non-chirped cases, however this can be corrected by increasing the number of periods as it is shown in Fig 3(c).

The geometry of the PhC can be tuned in order to match the target wavelength. In Fig. 4(a) the results for $\lambda_{IR} = 970$ nm and the same Q interval as previously are shown. In this case the longitudinal period was varied in $14 \leq d_\parallel \leq 23.35$ µm range. Here the filtering angle range is extended even further. We observed filtering for $2.2° \leq |\alpha| \leq 8.05°$, corresponding to the angular bandwidth of $\Delta\alpha \approx 5.8°$. In addition, we quantified the removed energy and the total incident energy ratio (Fig. 4(b)). As the PhC length (the number of longitudinal periods N) increases, the filtering performances increases also, and, opposite to the non-chirped case, saturates to the 100% filtering performance.

For comparison, the numerical simulations of the spatial filtering through the PhCs with varying refraction index contrast Δn were also performed and presented in Fig. 4(b). The simulations were performed using a beam propagation method approach, where a complex amplitude scattering efficiency parameter s was used [30] (the physical meaning is that for a plane-wave at resonant angle the s^2 represents the intensity scattered into one diffraction component per longitudinal half-period). The saturation to 100% filtering for smaller Δn occurs for longer PhCs, as expected. The simulations with $s = 0.14$ correspond well with experimental measurement data. Using this value, we determined the refraction index contrast in the

inscribed PhCs: $\Delta n \approx 2\lambda_0 s / \pi^{3/2} l_0 \approx 5 \cdot 10^{-3}$ ($l_0 \approx 6.9$ μm is the refractive index modified region length).

(a) (b)
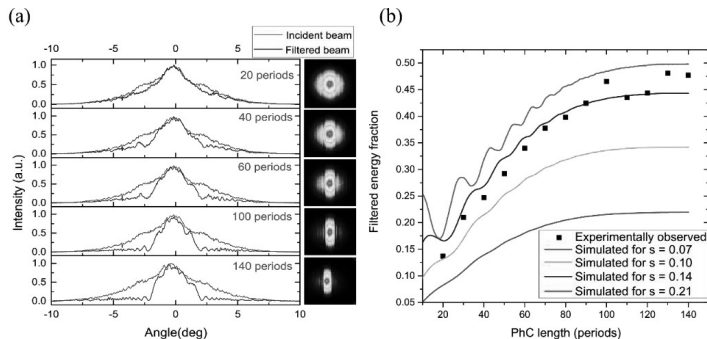
Fig. 4. (a) Experimentally measured angular transmission intensity spectra of PhCs designed for λ = 970 nm operating wavelength. Spatial filtering band is seen at $2.2° \leq |\alpha| \leq 8.05°$. (b) The corresponding data (black dots) for the change in total transmitted energy opposed to the PhC length and compared with four numeric cases (solid curves).

Judging from the examples in Fig. 3(c) and Fig. 4 the chirped PhCs provide a clear advantage over the non-chirped ones when a broad filtering band is required. The filtering band width can in principle be further extended by fabricating longer crystals using the described technique.

The total length of the filtering PhC structures was in the range of a few millimeters. For example, the PhC structures designed for both 633 nm and 970 nm wavelengths at N = 30 periods were of ~2 mm length. Such relatively high resolution ($d_\perp$ = 3 μm) and more importantly long structures are challenging to fabricate with the Gaussian beam point-by-point direct laser writing method because of the limited working distance and/or optical aberrations in the sample. Also, in practice their fabrication duration is relatively long. Let us make a simplified comparison. A PhC of an aperture of 600×600 μm^2 and 16 periods and Q = 1.2 takes around 3 minutes to produce using the Bessel technique. A PhC having the same aperture and transverse period using the reported scanning speed of v = 2.5 mm/s and a raster scan pattern would take around 30 minutes [6].

4. Conclusions

In this way we proposed new, efficient method for inscribing relatively long photonic crystal spatial filters. This technique, however, optimally works for the 2D photonic crystals, providing 1D spatial filtering, for the use, for instance, in broad area semiconductor lasers, where the slow-axis filtering is highly desired. The divergence of the beams along the slow axis is a real problem in such lasers, where typically, the divergences reach 3 to 10 degrees. The technique proposed by us provides the angular filtering range, sufficient for substantial improvement of the spatial structure in typical broad are semiconductor lasers.

Advanced chirping schemes could be applied to make use of the large number of periods to either extent the filtering range or to tune the filter angular transmission spectrum shape. Making a vertically stitched structure could increase the usable aperture by a factor of 2-5 times.

5. Funding, acknowledgments, and disclosures

5.1 Funding

5.3 Disclosures

The authors declare no conflicts of interest.

References

1. A. Bettinger, C. Charles, J. Osmalin, and J. G. Giraud, "Laser beam brightness improvement with high power spatial filtering," Opt. Commun. **18**, 176–177 (1976).
2. K. Staliunas and V. J. Sánchez-Morcillo, "Spatial filtering of light by chirped photonic crystals," Phys. Rev. A **79**, 053807 (2009).
3. E. Colak, A. O. Cakmak, A. E. Serebryannikov, and E. Ozbay, "Spatial filtering using dielectric photonic crystals at beam-type excitation," J. Appl. Phys. **108**, 113106 (2010).
4. Z. Luo, Z. Tang, Y. Xiang, H. Luo, and S. Wen, "Polarization-independent low-pass spatial filters based on one-dimensional photonic crystals containing negative-index materials," Appl. Phys. B **94**, 641–646 (2009).
5. L. Maigyte, T. Gertus, M. Peckus, J. Trull, C. Cojocaru, V. Sirutkaitis, and K. Staliunas, "Signatures of light-beam spatial filtering in a three-dimensional photonic crystal," Phys. Rev. A **82**, 043819 (2010).
6. V. Purlys, L. Maigyte, D. Gailevičius, M. Peckus, M. Malinauskas, and K. Staliunas, "Spatial filtering by chirped photonic crystals," Phys. Rev. A **87**, 033805 (2013).
7. V. Purlys, L. Maigyte, D. Gailevičius, M. Peckus, R. Gadonas, and K. Staliunas, "Super-collimation by axisymmetric photonic crystals," Appl. Phys. Lett. **104**, 221108 (2014).
8. D. Gailevicius, V. Koliadenko, V. Purlys, M. Peckus, V. Taranenko, and K. Staliunas, "Photonic Crystal Microchip Laser," Sci. Rep. **6**, 34173 (2016).
9. C. Brée, D. Gailevičius, V. Purlys, G. G. Werner, K. Staliunas, A. Rathsfeld, G. Schmidt, and M. Radziunas, "Chirped photonic crystal for spatially filtered optical feedback to a broad-area laser," J. Opt. **20**, 095804 (2018).
10. L. Maigyte and K. Staliunas, "Spatial filtering with photonic crystals," Appl. Phys. Rev. **2**, 011102 (2015).
11. D. Gailevicius, V. Purlys, L. Maigyte, M. Peckus, and K. Staliunas, "Chirped axisymmetric photonic microstructures for spatial filtering," J. Nanophotonics **8**, 084094 (2014).
12. K. M. Davis, K. Miura, N. Sugimoto, and K. Hirao, "Writing waveguides in glass with a femtosecond laser," Opt. Lett. **21**, 1729 (1996).
13. G. D. Marshall, A. Politi, J. C. F. Matthews, P. Dekker, M. Ams, M. J. Withford, and J. L. O'Brien, "Laser written waveguide photonic quantum circuits," Opt. Express **17**, 12546 (2009).
14. Y. Nasu, M. Kohtoku, and Y. Hibino, "Low-loss waveguides written with a femtosecond laser for flexible interconnection in a planar light-wave circuit," Opt. Lett. **30**, 723 (2005).
15. M. Malinauskas, A. Žukauskas, S. Hasegawa, Y. Hayasaki, V. Mizeikis, R. Buividas, and S. Juodkazis, "Ultrafast laser processing of materials: from science to industry," Light Sci. Appl. **5**, e16133–e16133 (2016).
16. H.-G. Treusch, A. Ovtchinnikov, X. He, M. Kanskar, J. Mott, and S. Yang, "High-brightness semiconductor laser sources for materials processing: stacking, beam shaping, and bars," IEEE J. Sel. Top. Quantum Electron. **6**, 601–614 (2000).
17. P. Shukla, J. Lawrence, and Y. Zhang, "Understanding laser beam brightness: A review and new prospective in material processing," Opt. Laser Technol. **75**, 40–51 (2015).
18. J. Durnin, J. J. Miceli, and J. H. Eberly, "Diffraction-free beams," Phys. Rev. Lett. **58**, 1499–1501 (1987).
19. A. Marcinkevicius, S. Juodkazis, S. Matsuo, V. Mizeikis, and H. Misawa, "Application of Bessel Beams for Microfabrication of Dielectrics by Femtosecond Laser," Jpn. J. Appl. Phys. **40**, L1197–L1199 (2001).
20. J. Amako, D. Sawaki, and E. Fujii, "Microstructuring transparent materials by use of nondiffracting ultrashort pulse beams generated by diffractive optics," J. Opt. Soc. Am. B **20**, 2562 (2003).
21. R. Stoian, M. K. Bhuyan, G. Zhang, G. Cheng, R. Meyer, and F. Courvoisier, "Ultrafast Bessel beams: Advanced tools for laser materials processing," Adv. Opt. Technol. **7**, 165–174 (2018).
22. M. Mikutis, T. Kudrius, G. Šlekys, D. Paipulas, and S. Juodkazis, "High 90% efficiency Bragg gratings formed in fused silica by femtosecond Gauss-Bessel laser beams," Opt. Mater. Express **3**, 1862 (2013).
23. A. Inyushov, P. Safronova, I. Trushnikov, A. Sarkyt, and V. Shandarov, "Formation of Photonic Structures

in Photorefractive Lithium Niobate by 1D and 2D Bessel-like Optical Fields," J. Phys. Conf. Ser. **867**, 012023 (2017).

24.   K. Liao, W. Wang, X. Mei, J. Cui, M. Li, and X. Li, "An analytical model to predict the sizes of modified layer in glass with femtosecond Bessel beam," Optik (Stuttg). **185**, 232–241 (2019).

25.   O. Brzobohatý, T. Čižmár, and P. Zemánek, "High quality quasi-Bessel beam generated by round-tip axicon," Opt. Express **16**, 12688 (2008).

26.   J. Dudutis, P. Gečys, and G. Račiukaitis, "Non-ideal axicon-generated Bessel beam application for intra-volume glass modification," Opt. Express **24**, 28433 (2016).

27.   J. Dudutis, R. Stonys, G. Račiukaitis, and P. Gečys, "Aberration-controlled Bessel beam processing of glass," Opt. Express **26**, 3627 (2018).

28.   P. K. Velpula, M. K. Bhuyan, F. Courvoisier, H. Zhang, J. P. Colombier, and R. Stoian, "Spatio-temporal dynamics in nondiffractive Bessel ultrafast laser nanoscale volume structuring," Laser Photon. Rev. **10**, 230–244 (2016).

29.   V. Garzillo, V. Jukna, A. Couairon, R. Grigutis, P. Di Trapani, and O. Jedrkiewicz, "Optimization of laser energy deposition for single-shot high aspect-ratio microstructuring of thick BK7 glass," J. Appl. Phys. **120**, 013102 (2016).

30.   D. Gailevičius, V. Purlys, M. Peckus, R. Gadonas, and K. Staliunas, "Spatial Filters on Demand Based on Aperiodic Photonic Crystals," Ann. Phys. **529**, 1700165 (2017).

A8

PHOTONIC CRYSTAL SPATIAL FILTERING IN BROAD APERTURE DIODE LASER

S. Gawali, **D. Gailevičius**, G. Gerre-Werner, V. Purlys, C. Cojocaru, J. Trull, J. Montiel-Ponsoda, and K. Staliunas

Photonic crystal spatial filtering in broad aperture diode laser

S.Gawali [1,a)], D. Gailevičius[2,3], G. Garre-Werner[1,4], V. Purlys[2,3], C. Cojocaru[1], J. Trull[1] J. Montiel-Ponsoda[4], and K. Staliunas[1,5]

[1]Universitat Politècnica de Catalunya (UPC), Physics Department, Rambla Sant Nebridi 22, 08222, Terrassa Barcelona, Spain

[2]Vilnius University, Faculty of Physics, Laser Research Center, Saulėtekio al. 10, LT-10223, Vilnius, Lithuania

[3]Femtika LTD, Saulėtekio al. 15, LT-10224, Vilnius, Lithuania

[4]Monocrom S.L, Vilanoveta, 6, 08800, Vilanova i la Geltrú, Spain

[5]Institució Catalana de Recerca i Estudis Avançats (ICREA), Passeig Lluís Companys 23, 08010, Barcelona, Spain

a) Author to whom correspondence should be addressed: sandeep.babu.gawali@upc.edu

ABSTRACT

Broad aperture semiconductor lasers usually suffer from low spatial quality of the emitted beams. Due to the highly compact character of such lasers the use of a conventional intra-cavity spatial filters is problematic. We demonstrate that extremely compact Photonic Crystal spatial filters, incorporated into the laser resonator, can improve the beam spatial quality, and correspondingly, increase the brightness of the emitted radiation. We report the decrease of the M^2 from 47 down to 28 due to Photonic Crystal spatial intra-cavity filtering, and the increase of the brightness by a factor of 1.5, giving a proof of principle of intra-cavity Photonic Crystal spatial filtering in broad area semiconductor lasers.

Broad Aperture Semiconductor (BAS) lasers usually suffer from the low spatial quality of the emitted beams, especially in high power emission regimes. This, among others, imposes limitations for tight focusing or coupling of its radiation into the optical fibers. The strong divergence of the beam in the fast-axis (y-axis) does not represent a problem since the single-transverse-mode-character of the radiation in this direction allows perfect collimation of the beam. Collimation in the slow-axis (x-axis) instead is quite problematic due to the intrinsic multi-transverse-mode emission along this axis. The absence of intra-cavity spatial filtering is the reason of the poor beam quality of other micro-laser types, such as microchip lasers, or Vertical Cavity Surface Emission Lasers (VCSELs). Conventional lasers (eg. solid state lasers) usually use intra-cavity spatial filters, typically using a confocal arrangement of lenses with a diaphragm in the confocal plane. This configuration allows direct access to the far field, where the diaphragm acts as a "low-pass" spatial filter blocking the higher angular components. This type of spatial filter has been demonstrated in an external resonator of diode laser array to improve the beam quality [1]. However, such a filtering

design is very inconvenient or even impossible for intra-cavity use in micro-lasers, such as microchip or semiconductor lasers, or VCSELs, since the lengths of the resonators typically lies in the millimeter range (in VCSELs case even in micrometer range) and provide no space for direct access to the far field. For the case of high power diode lasers, usually configured in an array of multiple emitters, the use of bulky lenses is impossible.

The quality of the BAS laser beams at low powers can be improved by several methods, for instance: (i) confining transversally the radiation by inscribing waveguide structure in the semiconductor material. This microstructured fabrication, however, severely restricts the amplification area, and thus reduces the emission power; (ii) by restricting the amplification/emission area through the use of apertures in VCSELs; or (iii) by accurate gain guiding in microchip lasers. None of these methods are useful to solve the problem of beam quality in high-emission-power regimes. For the BAS lasers, some other techniques have been proposed, like the use of tapered geometries, evanescent spatial filtering, and the use of external cavity [2-4]. However, these methods

1

have a limitation in terms of power achievable and the size of the device.

A promising idea to solve the beam quality problems of the microlasers in the high emission power regime is the use of intra-cavity Photonic Crystal (PhC) spatial filters integrated in the laser cavity. The concept of spatial filtering using PhCs was proposed in [5, 6], and subsequently experimentally demonstrated in [7-9]. The idea is based on a selective deflection of the angular components of the light propagating through a 2-D photonic structure: the angular components of the incident light resonant with the transverse and longitudinal periodicities of the photonic structure diffract efficiently and are deflected from the zero-diffraction order of the transmitted beam. The use of such PhC spatial filtering [10] was already proved as a powerful tool to clean the spatial structure of the beams, which could be efficiently employed for instance in the microchip lasers [11]. For more detailed theory on PhC spatial filtering see review [12].
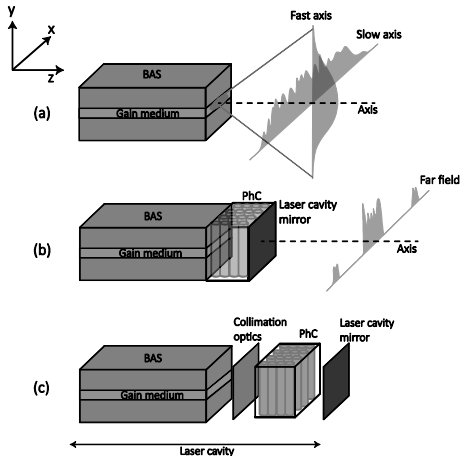
Fig. 1. (a) The illustration of the irregular beam structure emitted by typical BAS lasers (with partially reflective output facet mirror) in high power regimes. (b) The idea of spatial filtering by monolithically integrated PhCs in a compact configuration. While the lower angle modes propagate unaffected, as shown in a schematic far-field profile, the PhC diffracts and eliminates the higher angle modes. (c) The PhC placed inside an extended cavity resonator, which mimics the situation of the compact intra-cavity spatial filtering shown in (b).

The ultimate goal of the research reported in this article is the design of efficient intra-cavity PhC acting as a spatial filter in BAS lasers. The possible monolithic implementation scheme is illustrated in Fig. 1(b), showing how the PhC structure could be integrated directly between the active medium and the laser output cavity mirror. Such integration is, however, very challenging technologically. In order to show the reliability of the physical principle, i.e. to test the spatial filtering effect of the PhC, we propose in this article an extended-cavity configuration designed to mimic the

action of the more compact cavity. A low antireflective (AR) coating at the output facet of the semiconductor material prevents the lasing in the semiconductor gain medium alone, and enables building of the extended resonator by using external mirrors. Collimation optics and an external output cavity mirror provides the necessary feedback to achieve the laser action in this extended-cavity configuration, which allows placing the PhCs inside the laser cavity to test their filtering capabilities, as schematically depicted in Fig. 1(c).

The effect of the PhC filtering in BAS lasers has been numerically studied in extended cavity configuration [13]. In this article, we report the successful proof of the physical implementation of this idea, showing how the sub-millimeter length PhCs affects the emission of the BAS laser. The intra-cavity use of such filters allows an improvement of the beam spatial quality and an increase of brightness of the emitted radiation in high-power regimes. These results open the way for promising future goal i.e. the technological implementation of a compact (monolithic) intra cavity designed system for spatial filtering. This task is beyond the scope of the current letter due to technological challenges.
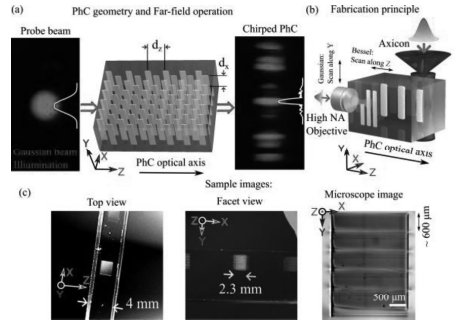
Fig. 2. (a) Illustration of the PhC, showing the architecture of index modulation inside the glass substrate and the expected effect on the Far-field intensity spectra of the beam, (b) Illustration of the PhC fabrication using femtosecond pulsed Bessel beam, and (c) photographs and microscope image of the fabricated structures. The images of the Far-field beam intensity profiles show the principle of angular filtering resulting in narrow angular transmission bands.

The PhC samples having a 2D periodic refractive index modulation (Fig. 2(a)) were fabricated via femtosecond laser writing technique in the bulk of glass substrate. The substrates were made from N-BK7 ($n_{ref} \approx 1.52$) glass with broadband antireflective coating on both facets. We fabricated two versions of PhC filters: the ones inscribed by Gaussian beam, and others inscribed using Bessel beam (Fig. 2(b)). For more details about the fabrication procedures and exposure parameters see [11] for Gaussian beam fabrication. The Gaussian beam fabrication strategy allows flexible 3D geometry but is limited by the working distance of high numerical aperture (NA) focusing (microscope) lens, therefore the maximal length of the PhC in our case was limited to < 375 µm. In addition, a significant amount of spherical aberration is present, which leads to defects and distortions of the PhC geometry. Moreover, the spatial filtering performance (the angular range of deflected

components) is proportional to the length of the PhC $\Delta\alpha = \Delta n\, l/\lambda$, where Δn is the change in refractive index, which is of the order of 10^{-3}. Due to the limited length of PhCs the Gaussian beam fabrication strategy allowed a filtering range of ~1 degree, which was not wide enough for BAS lasers (~ 5-10 degrees preferred).

The Bessel beam fabrication of PhCs [14] has practically no limits of longitudinal periods, due to the fact that the PhCs are fabricated by a beam illuminating along the perpendicular y-direction. Using this technique photonic structures of millimeters or even centimeters in length can be fabricated [15]. By scanning the sample as shown in Fig. 2(b), long (~ 600 μm) refractive index modified bulk structures were produced. We achieved this by taking a UVFS axicon with an apex angle of 179° and illiuminating it with a collimated Gaussian intensity profile pulsed (200 fs) laser beam with a diameter of $2w = 5.3$ mm ($1/e^2$), 1030 nm wavelength, pulse repetition rate of 25 kHz and 8 μJ pulse energy. We demagnified the resulting Bessel beam with a ~55× telescope producing a 600 μm length Bessel zone inside the substrate. Modified index areas were around half the d_x value wide and half of the minimum d_{zmin} value long (we scanned the substrate at a $v = 2500$ μm/s linear velocity while opening and closing the laser shutter to produce modifications of such length). The refractive index change is difficult to measure for such a closely packed structure, however we expect it to be near $\Delta n \lesssim 3 \cdot 10^{-3}$ [16, 17].

The geometry of the structures is characterized by the transverse and longitudinal lattice constants d_x and d_z. In order to increase the angular width of the filtering area, the longitudinal period can be "chirped", i.e. constantly varied along the propagation direction, as also described in [9,14]. The chirped structures are additionally characterized by the values of the longitudinal periods corresponding to the first, d_{z1}, and the last, d_{z2}, periods, with d_z values changing linearly along the structure. Following the previous references [12] we use the geometry factor Q to characterize our PhC structures. This parameter defines a relation between the transverse and longitudinal periods of the structure (not to be confused with resonator finess factor) and is defined as $Q = 2d_x^2 n_{ref}/\lambda d_z$, and can be used to estimate the filtering angle $\sin\alpha \approx \lambda(Q-1)/2d_x n_{ref}$. Small variation of the geometry factor result in a linear change of the central value of the filtering angle $\Delta Q \sim \Delta\alpha$.

Following this notation, the Gaussian-beam fabricated (non-chirped) structure was characterized by $d_x = 2$ μm, $\lambda = 970$ nm and $Q = 0.9$ with an aperture of 2x2 mm² and number of longitudinal periods $N_L = 10$. The Bessel-beam fabricated structure had a different transverse period $d_x = 3$ μm and was chirped along the z direction in the range of $1.15 \le Q \le 1.27$ with $N_L = 80$ and an aperture of 2.85 x 2.3 mm². In order to increase the height of the PhC aperture 5 layers of modified regions were stitched vertically. An example of this structure is shown in Fig. 2(c).

The filtering performance of the fabricated PhCs can be described through their transfer function, i.e. their diffracting action on the spatial modes, although for their proper operation these filters should be placed in the near field plane. The transmittance of the fabricated filters is shown in Fig. 2(a). When inserted inside the laser cavity, the diffracted modes do not contribute to the lasing action modifying the overall output of the system and the dynamics of the lasing operation.

For the experiments we used a BAS laser of 400 μm transverse width (along x-axis) and 1500 μm length (along z-axis), emitting 1.3 W in CW regime when operated at 3A at a wavelength of 970 nm. In the experiment we drove the laser at a repetition rate of 50 Hz with a 25% duty cycle. To operate this laser in the extended-cavity configuration the output facet of the laser was coated with a low AR coating ($R<0.01\%$) to prevent the emission of any optical mode above the lasing threshold level from the gain medium alone and a 4% reflectivity mirror was used as the output cavity laser mirror. The reflectivity of this external mirror is limited to 4% to avoid the possible damage of the emitter facets [18]. The extended cavity configuration, shown schematically in Fig. 3, was implemented using cylindrical lenses acting separately in the slow and fast axis. The fast axis emission was collimated by mounting a cylindrical lens of very short focal length of 590 μm, with a NA of 0.8. (FAC lens in Fig. 3). For the slow-axis direction, a double 4-f system was used to obtain two conjugated planes of the output facet of the active medium. In this way, the PhC could be inserted in the first conjugated plane, with 1:1 magnification, designated as B in Fig. 3. The PhC filters were mounted on a 3D translational stage, which allowed inserting it properly into the beam path. The size of the PhC 2x2 mm² for Gaussian beam fabricated crystal and 2.85x2.3 mm² for Bessel beam fabricated crystal, was large enough to allow the entire beam pass through the filter. The second 4f system provided a second near field plane, marked as D in Fig. 3, where the output laser-cavity mirror was placed and carefully aligned to obtain lasing action. All lenses were AR coated in order to prevent the appearance of multiple cavities effect within the setup.
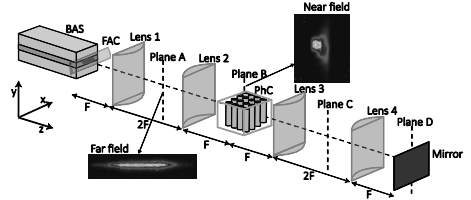
Fig. 3. Experimental setup of spatial filtering in extended-cavity configuration. BAS: Broad Area Semiconductor, FAC: fast-axis collimator. Lenses 1-4 with a focal length of 50.8 mm. Far-field areas are marked as (plane A) and (plane C). Near-field planes (images of the BAS output facets marked as B and D). The reflectivity of the mirror is 4%.

The emission characteristics of this extended laser when no PhC is inserted in the cavity shows a threshold at 1.3 A, and a spectral emission centered at 970 nm with a spectral bandwidth of 2.9 nm. The beam profile at the output of the laser (plane D in Fig. 3) was recorded by imaging this plane into a CCD camera (Spiricon SP620U) with proper magnification. The near-field profile recorded by this means has dimensions of 450 μm x 1.4 mm. The effect of the PhC filtering was observed experimentally by recording the far-

3

field distribution of the emitted radiation. The far-field pattern in our experiments was recorded using an external lens out of the cavity (not shown in Fig. 3) to image the rear focal plane into the CCD.

Fig. 4(a) shows the far-field profile of the laser emission when no filter and when the Gaussian-fabricated and Bessel-fabricated PhCs are placed within the laser cavity. The PhC effectively filters the beam along the slow-axis by selectively deflecting the higher-order modes in a given frequency range. The spectral selectivity of the filters is better seen by plotting the ratio between the far-field profile without and with filters inserted in the lasing cavity. This ratio, plotted on Fig. 4(b), indicates a clear filtering band between 1.5 and 2.5 degrees, with a more pronounced effect of the Bessel-fabricated PhC.
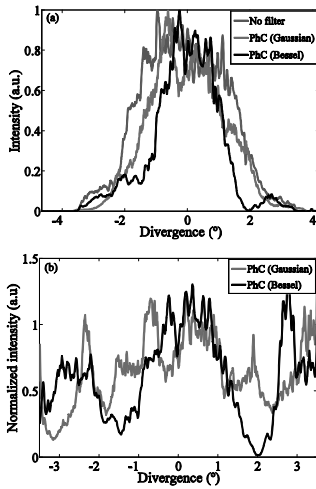
Fig. 4. (a) Measured Far-field profile without PhC (green), with PhC Gaussian beam (red) and Bessel beam fabricated (black) technique. (b) Reconstructed ratio between the far-field profiles in (a) without and with filters inserted in the lasing cavity.

The spatial quality of the beam is quantified by the measurement of the beam quality factor and brightness. The first is given by $M^2 \approx BPP_{actual\ beam}/BPP_{Gaussian\ beam}$, where BPP refers to beam parameter product and is given by $BPP = Beam\ waist \times Divergence\ angle$. The brightness, B is defined as $B = P_{opt}/\lambda^2 M^2_{slow} M^2_{fast}$ [19], where P_{opt} is the average optical power, M^2_{slow} and M^2_{fast} are the beam quality factors along slow and fast axis respectively and λ is the central wavelength.

In our setup, the M^2 factor was calculated by recording the profile of the beam as a function of propagation distance after being focused using an ancillary external lens of 100 mm focal length. The beam diameter, recorded independently in the fast and slow axis, was determined using the D4σ method (corresponding to 4 times the standard deviation of the energy distribution evaluated in the transverse direction over the beam intensity profile) [20]. From the diameter versus distance plot, the minimum spot size and divergence angle was measured to determine M^2. The initial M^2 factor measured from our laser with no filtering action was of $M^2_{slow} = 47$ and $M^2_{fast} = 3.3$. These large values obtained in the slow-axis (x-direction) indicate clearly the poor quality of the beam and are consistent with reported values in similar systems [21]. The unexpected large value of M^2 in the fast-axis (y-direction) is due to a small misalignment of the FAC lens in this particular sample available.

The spatial filtering effect of the PhCs in a single transmission when placed outside of the laser cavity has been proved in previous publications [8, 9]. However, this linear single-pass action, while improving the spatial quality of the beam (reducing M^2_{slow}), does not increase the brightness of the emitted radiation. Brightness enhancement is possible by intra cavity spatial filtering only. For instance, using conventional confocal lens arrangements, the suppression of the higher order transverse modes concentrates most of the pumping energy into the lowest order modes. The increase of brightness is obtained because closing the aperture has a weak effect on the total intensity, which decreases weakly, but a strong effect on the beam divergence, which can decrease considerably. If the aperture is too narrow, starting to affect the lowest transverse modes, the brightness starts decreasing as well.
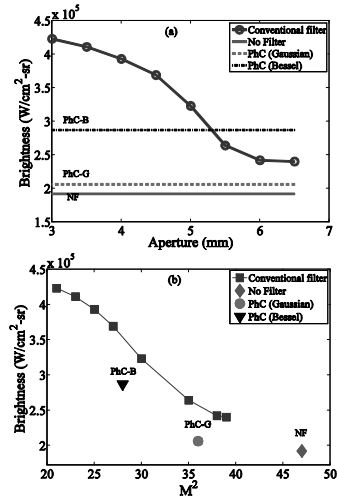
Fig. 5. (a) Shows the brightness of emission as a function of aperture (blue line) compared with PhC fabricated by Gaussian (PhC-G) and Bessel beam (PhC-B) and with No filter (NF). (b) Brightness versus M^2 along the slow axis.

Before exploring the effect of our fabricated PhC filters, we checked the spatial filtering properties using a variable thickness slit placed at the far field plane inside the

extended laser resonator (plane C shown in Fig. 3). This situation allows us to compare the action of the filters with respect to a more typical configuration. The initial value of M^2 and brightness of our laser without any type of filtering is shown as the green diamond in Fig. 5(b). The results of the brightness as a function of the aperture (width) of the slit are shown in Fig. 5(a). The horizontal green line indicates the value of the brightness for the case when no aperture was placed in the cavity. The calculated brightness as a function of aperture width, shows that the decrease in divergence is accompanied by brightness increase by a factor of almost 2.2.

While the aperture acts on the transverse modes when placed in the far-field plane, the PhC spatial filters work when placed inside the cavity at the near-field plane marked as B. This is achieved with the help of 4-f system configuration as shown in Fig. 3. This is a fundamental difference between the conventional far-field filtering, and the PhC near field filtering, since the filtering with the PhC, positioned in the near field domain, is the only option that could be implemented in a monolithic system. The brightness of the laser with PhCs intracavity filters are indicated by the horizontal (dashed and dashed-dot) lines in Fig. 5(a).

The measurements with the PhCs fabricated using the Gaussian beam technique show that the M^2_{slow} factor decreased from 47 to 36. As the output optical power dropped from 0.31 W to 0.230 W, the reduction of the divergence was not sufficient to compensate the loss of power and hence the brightness did not increase as indicated in Fig. 5(b) (red circle). Next, we explored the Bessel beam fabricated crystals. A clear modification of the emission pattern is observed (Fig. 4(a)). The change is observable with a slight loss in power. For the Bessel-beam fabricated PhCs, the M^2_{slow} reduced from 47 to 28 while brightness increased by a factor of 1.5 (black triangle in Fig. 5(b)).

The results of spatial filtering for conventional confocal filtering, PhC (Gaussian beam) and PhC (Bessel beam) compared with the situation without filtering are summarized in Fig. 5(b). Although the best performance was obtained for the conventional confocal filtering case, it is convincingly shown that the action of the improved PhCs filters tends towards the achievement of these optimal values.

Concluding, we have demonstrated spatial filtering in broad area semiconductor laser using a PhC spatial filter in extended cavity configuration, which mimics the compact cavity configuration. The main result was a decrease of M^2_{slow} and the brightness enhancement of the emitted radiation. Comparison with the conventional confocal filtering technique shows that by using PhCs filtering, one can achieve results approaching the same values of spatial beam quality improvement. This is the first test to demonstrate the working principle of spatial filtering in Broad Area Laser with single emitter with output power of the order of 1W. The same technique can be applied to high power diode laser bars. The advantage of the use of PhCs filtering comparing with the conventional technique is that it offers the possibility of integration of the PhC into the BAS leading to a serious breakthrough in regimes of high power emission. This article does not demonstrate such integration due to limited technologies, however, it shows the potential for such integration in near future, by proving the physical principles.

References

1. Su Zhouping, L. Qihong, D. Jingxing, Z. Jun, Wei Runrong, Optics express 12, 11776 (2007).
2. E. S. Kintzer, J. N. Walpole, S. R. Chinn, C. A. Wang, and L. J. Missaggia, IEEE Photonics Technology Letters 5, 605-608 (1993).
3. J. P. Leidner and J. R. Marciante, IEEE Journal of Quantum Electronics 48, 1269 – 1274 (2012).
4. M. Chi, N. Bøgh, B. Thestrup and P. Petersen, Applied Physics Letter 85, 1107 (2004).
5. K. Staliunas, V.J. Sánchez-Morcillo, Phys. Rev. A. 79, 053807 (2009).
6. E. Colak, A.O. Cakmak, A.E. Serebryannikov, E. Ozbay, J. Appl. Phys. 108, 113106 (2010).
7. Z. Luo, Z. Tang, Y. Xiang, H. Luo, S. Wen, Appl. Phys. B. 94, 641– 646 (2009).
8. L. Maigyte, T. Gertus, M. Peckus, J. Trull, C. Cojocaru, V. Sirutkaitis, K. Staliunas, Phys. Rev. A. 82, 043819 (2010).
9. V. Purlys, L. Maigyte, D. Gailevičius, M. Peckus, M. Malinauskas, K. Staliunas, Phys. Rev. A. 87, 033805,(2013).
10. V. Purlys, L. Maigyte, D. Gailevičius, M. Peckus, R. Gadonas, and K. Staliunas, Appl. Phys. Lett. 104, 221108 (2014).
11. D. Gailevicius, V. Koliadenko, V. Purlys, M. Peckus, V. Taranenko, K. Staliunas , Sci. Rep. 6, 34173 (2016).
12. L. Maigyte, K. Staliunas, Appl. Phys. Rev. 2, 011102 (2015).
13. C. Brée, D. Gailevičius, V. Purlys, G. G. Werner, K. Staliunas, A. Rathsfeld, G. Schmidt, M. Radziunas, J. Phys. A. 20, 095804 (2018).
14. D. Gailevicius et al. "Photonic Crystal Spatial Filter fabrication by fs-pulsed Bessel Beam", submitted (2019).
15. M. Mikutis, T. Kudrius, G. Šlekys, D. Paipulas, and S. Juodkazis, Opt. Mater. Express 3(11), 1862 (2013).
16. P. K. Velpula, M. K. Bhuyan, F. Courvoisier, H. Zhang, J. P. Colombier, and R. Stoian, Laser Photon. Rev. 10(2), 230–244 (2016).
17. V. Garzillo, V. Jukna, A. Couairon, R. Grigutis, P. Di Trapani, and O. Jedrkiewicz J. Appl. Phys. 120(1), 013102 (2016).
18. B. Leonhäuser, H. Kissel, A. Unger, B. Köhler, J. Biesenbach, Proc. SPIE 8965, 896506 (2014).
19. R. Diehl (Ed.), High-Power Diode Lasers: Fundamentals, Technology, Applications (Springer-Verlag, Berlin Heidelberg, 2000).
20. A. E. Siegman, Proc. SPIE 1868 (1993).
21. A. Jechow, V. Raab, and R. Menzel, Applied Optics. 45, 3545-3547 (2006).

Bibliography

[1] J. Zi, X. Yu, Y. Li, X. Hu, C. Xu, X. Wang, X. Liu, R. Fu, Coloration strategies in peacock feathers, Proceedings of the National Academy of Sciences **100**(22), 12576–12578 (2003).

[2] Y. Ding, S. Xu, Z. L. Wang, Structural colors from Morpho peleides butterfly wing scales, Journal of Applied Physics **106**(7), 074702 (2009).

[3] H. Gersen, T. J. Karle, R. J. P. Engelen, W. Bogaerts, J. P. Korterik, N. F. Van Hulst, T. F. Krauss, L. Kuipers, Real-space observation of ultraslow light in photonlc crystal waveguides, Phys. Rev. Lett. **94**(7), 3–6 (2005).

[4] T. Baba, Slow light in photonic crystals, Nat. Photonics **2**(8), 465–473 (2008).

[5] E. Cubukcu, K. Aydin, E. Ozbay, S. Foteinopoulou, C. M. Soukoulis, Negative refraction by photonic crystals, Nature **423**(6940), 604–605 (2003).

[6] M. Notomi, Manipulating light with strongly modulated photonic crystals, Reports Prog. Phys. **73**(9), 096501 (2010).

[7] P. V. Parimi, W. T. Lu, P. Vodo, S. Sridhar, Imaging by flat lens using negative refraction, Nature **426**(6965), 404–404 (2003).

[8] N. Fang, H. Lee, C. Sun, X. Zhang, Sub-diffraction-limited optical imaging with a silver superlens, Science **308**(5721), 534–537 (2005).

[9] A. E. Serebryannikov, A. Y. Petrov, E. Ozbay, Toward photonic crystal based spatial filters with wide angle ranges of total transmission, Appl. Phys. Lett. **94**(18), 181101 (2009).

[10] E. Colak, A. O. Cakmak, A. E. Serebryannikov, E. Ozbay, Spatial filtering using dielectric photonic crystals at beam-type excitation, J. Appl. Phys. **108**(11), 113106 (2010).

[11] L. Maigyte, T. Gertus, M. Peckus, J. Trull, C. Cojocaru, V. Sirutkaitis, K. Staliunas, Signatures of light-beam spatial filtering in a three-dimensional photonic crystal, Phys. Rev. A **82**(4), 043819 (2010).

[12] L. Maigyte, K. Staliunas, Spatial filtering with photonic crystals, Appl. Phys. Rev. **2**, 011102 (2015).

[13] L. Rayleigh, XXVI. On the remarkable phenomenon of crystalline reflexion described by Prof. Stokes, London, Edinburgh, Dublin Philos. Mag. J. Sci. **26**(160), 256–265 (1888).

[14] S. John, Strong localization of photons in certain disordered dielectric superlattices, Phys. Rev. Lett. **58**(23), 2486–2489 (1987).

[15] E. Yablonovitch, Inhibited Spontaneous Emission in Solid-State Physics and Electronics, Phys. Rev. Lett. **58**(20), 2059–2062 (1987).

[16] A. E. Siegman, Defining, measuring, and optimizing laser beam quality, in A. Bhowmik (ed.), *Proc. SPIE 1868* (1993), volume V, 2–12.

[17] J.-i. Kato, H. Tanaka, I. Yamaguchi, Nonlinear spatial filtering with a dye-doped liquid-crystal cell, Opt. Lett. **21**(11), 767 (1996).

[18] I. Moreno, J. J. Araiza, M. Avendano-Alejo, Thin-film spatial filters, Opt. Lett. **30**(8), 914 (2005).

[19] D. Schurig, D. R. Smith, Spatial filtering using media with indefinite permittivity and permeability tensors, Appl. Phys. Lett. **82**(14), 2215–2217 (2003).

[20] O. F. Siddiqui, G. V. Eleftheriades, Resonant modes in continuous metallic grids over ground and related spatial-filtering applications, J. Appl. Phys. **99**(8), 083102 (2006).

[21] Z. Tang, H. Zhang, Y. Ye, C. Zhao, S. Wen, D. Fan, Low-pass spatial filtering using optically thinner left-handed photonic crystals, in *Proc. Int. Symp. Biophotonics, Nanophotonics Metamaterials, Metamaterials 2006* (2006).

[22] Z. Luo, Z. Tang, Y. Xiang, H. Luo, S. Wen, Polarization-independent low-pass spatial filters based on one-dimensional photonic crystals containing negative-index materials, Appl. Phys. B **94**(4), 641–646 (2009).

[23] K. Staliunas, V. J. Sánchez-Morcillo, Spatial filtering of light by chirped photonic crystals, Phys. Rev. A **79**(5), 053807 (2009).

[24] V. Purlys, L. Maigyte, D. Gailevičius, M. Peckus, M. Malinauskas, K. Staliunas, Spatial filtering by chirped photonic crystals, Phys. Rev. A **87**(3), 033805 (2013).

[25] V. Purlys, L. Maigyte, D. Gailevičius, M. Peckus, M. Malinauskas, R. Gadonas, K. Staliunas, Spatial filtering by axisymmetric photonic microstructures, Opt. Lett. **39**(4), 929 (2014).

[26] D. Gailevicius, V. Purlys, L. Maigyte, M. Peckus, K. Staliunas, Chirped axisymmetric photonic microstructures for spatial filtering, J. Nanophotonics **8**(1), 084094 (2014).

[27] K. Staliunas, Removal of excitations of Bose-Einstein condensates by space- and time-modulated potentials, Phys. Rev. A **84**(1), 013626 (2011).

[28] B. K. Vainsthein, *Fundamentals of Crystals* (Springer Berlin Heidelberg, Berlin, Heidelberg, 1994).

[29] B. Brüser, I. Staude, G. von Freymann, M. Wegener, U. Pietsch, Visible light Laue diffraction from woodpile photonic crystals, Appl. Opt. **51**(28), 6732 (2012).

[30] W. H. Bragg, W. L. Bragg, The Reflection of X-rays by Crystals, Proc. R. Soc. A Math. Phys. Eng. Sci. **88**(605), 428–438 (1913).

[31] V. R. Bhardwaj, E. Simova, P. B. Corkum, D. M. Rayner, C. Hnatovsky, R. S. Taylor, B. Schreder, M. Kluge, J. Zimmer, Femtosecond laser-induced refractive index modification in multicomponent glasses, J. Appl. Phys. **97**(8), 083102 (2005).

[32] D. Paipulas, V. Kudriašov, K. Kuršelis, M. Malinauskas, V. Sirutkaitis, Manufacturing of diffractive elements in fused silica using high repetition rate femtosecond Yb:KGW laser pulses, Lith. J. Phys. **50**(1), 129–134 (2010).

[33] V. Purlys, L. Maigyte, D. Gailevičius, M. Peckus, R. Gadonas, K. Staliunas, Super-collimation by axisymmetric photonic crystals, Appl. Phys. Lett. **104**(22), 221108 (2014).

[34] L. Maigyte, V. Purlys, J. Trull, M. Peckus, C. Cojocaru, D. Gailevičius, M. Malinauskas, K. Staliunas, Flat lensing in the visible frequency range by woodpile photonic crystals, Opt. Lett. **38**(14), 2376 (2013).

[35] M. D. Feit, J. A. Fleck, Computation of mode properties in optical fiber waveguides by a propagating beam method, Appl. Opt. **19**(7), 1154 (1980).

[36] T.-C. Poon, T. Kim, The Split-Step Beam Propagation Method, in *Eng. Opt. with MATLAB ®* (WORLD SCIENTIFIC, Singapore, 2006), chapter 3.4.

[37] M. Peckus, R. Rogalskis, M. Andrulevicius, T. Tamulevicius, A. Guobiene, V. Jarutis, V. Sirutkaitis, K. Staliunas, Resonators with manipulated diffraction due to two- and three-dimensional intracavity photonic crystals, Phys. Rev. A **79**(3), 033806 (2009).

[38] T.-C. Poon, T. Kim, *Engineering Optics with MATLAB ®* (WORLD SCIENTIFIC, 2006).

[39] M. Guizar-Sicairos, J. C. Gutiérrez-Vega, Computation of quasi-discrete Hankel transforms of integer order for propagating optical wave fields, J. Opt. Soc. Am. A **21**(1), 53 (2004).

[40] A. Taflove, S. Hagness, *Computational Electrodynamics* (Artech House, Norwood, 2005), third edit edition.

[41] Talbot, Neuer Interferenzversuch, Ann. der Phys. und Chemie **118**(10), 234–234 (1837).

[42] L. Rayleigh, XXV. On copying diffraction-gratings, and on some phenomena connected therewith, London, Edinburgh, Dublin Philos. Mag. J. Sci. **11**(67), 196–205 (1881).

[43] M. L. Ng, D. Chanda, P. R. Herman, Coherent stitching of light in multilayered diffractive optical elements., Opt. Express **20**(21), 23960–70 (2012).

[44] L. Li, J. Hirsh, All-dielectric high-efficiency reflection gratings made with multilayer thin-film coatings, Opt. Lett. **20**(11), 1349 (1995).

[45] T. Clausnitzer, E.-B. Kley, A. Tünnermann, A. Bunkowski, O. Burmeister, K. Danzmann, R. Schnabel, S. Gliech, A. Duparré, Ultra low-loss low-efficiency diffraction gratings, Opt. Express **13**(12), 4370 (2005).

[46] N. Destouches, J.-C. Pommier, O. Parriaux, T. Clausnitzer, N. Lyndin, S. Tonchev, Narrow band resonant grating of 100% reflection under normal incidence, Opt. Express **14**(26), 12613 (2006).

[47] D. Voronov, E. Anderson, R. Cambie, S. Cabrini, S. Dhuey, L. Goray, E. Gullikson, F. Salmassi, T. Warwick, V. Yashchuk, H. Padmore, A 10,000 groove/mm multilayer coated grating for EUV spectroscopy, Opt. Express **19**(7), 6320 (2011).

[48] Q. Huang, V. Medvedev, R. van de Kruijs, A. Yakshin, E. Louis, F. Bijkerk, Spectral tailoring of nanoscale EUV and soft x-ray multilayer optics, Appl. Phys. Rev. **4**(1), 011104 (2017).

[49] V. Purlys, *Trimačiai fotoniniai kristalai: formavimas ir taikymas chromatinių bei erdvinių šviesos savybių valdymui.*, Ph.D. thesis, Vilnius University (2015).

[50] V. Purlys, *Three-dimensional photonic crystals: fabrication and applications for control of chromatic and spatial light properties. Summary of doctoral dissertation.*, Ph.D. thesis, Vilnius university (2015).

[51] J. E Shelby, *Introduction to Glass Science and Technology* (Royal Society of Chemistry, Cambridge, 2005).

[52] A. M. Kowalevicz, V. Sharma, E. P. Ippen, J. G. Fujimoto, K. Minoshima, Three-dimensional photonic devices fabricated in glass by use of a femtosecond laser oscillator., Opt. Lett. **30**(9), 1060–1062 (2005).

[53] Y. Li, Y. Dou, R. An, H. Yang, Q. Gong, Permanent computer-generated holograms embedded in silica glass by femtosecond laser pulses, Opt. Express **13**(7), 2433 (2005).

[54] K. Suzuki, V. Sharma, J. G. Fujimoto, E. P. Ippen, Y. Nasu, Characterization of symmetric [3 x 3] directional couplers fabricated by direct writing with a femtosecond laser oscillator, Opt. Express **14**(6), 2335 (2006).

[55] J.-H. Chung, Y. Gu, J. G. Fujimoto, Submicron-Period Waveguide Bragg Gratings Direct Written by an 800-nm Femtosecond Oscillator, in *2007 Conf. Lasers Electro-Optics* (IEEE, 2007), 1–2.

[56] https://www.carlroth.com/downloads/allgemein/en/ Tables_and_general_information.pdf 2019-06-06.

[57] P. Docker, J. Teng, P. Prewett, K. Jiang, Fabrication of nano-dimensional features in FOTURAN using focused ion beam technology, in *4M 2006 - Second Int. Conf. Multi-Material Micro Manuf.* (Elsevier, 2006), volume II, 217–219.

[58] Z. L. Li, D. K. Y. Low, M. K. Ho, G. C. Lim, K. J. Moh, Fabrication of waveguides in Foturan by femtosecond laser, J. Laser Appl. **18**(4), 320–324 (2006).

[59] K. Vishnubhatla, S. V. Rao, R. S. S. Kumar, M. Ferrari, D. N. Rao, Optical studies of two dimensional gratings in fused silica, GE 124, and Foturan™ glasses fabricated using femtosecond laser pulses, Opt. Commun. **282**(23), 4537–4542 (2009).

[60] A. Q. Wu, I. H. Chowdhury, X. Xu, Femtosecond laser absorption in fused silica: Numerical and experimental investigation, Phys. Rev. B **72**(8), 085128 (2005).

[61] B. Poumellec, M. Lancry, A. Chahid-Erraji, P. G. Kazansky, Modification thresholds in femtosecond laser processing of pure silica: review of dependencies on laser parameters [Invited], Opt. Mater. Express **1**(4), 766 (2011).

[62] C. Fourment, B. Chimier, F. Deneuville, D. Descamps, F. Dorchies, G. Duchateau, M.-C. Nadeau, S. Petit, Ultrafast changes in optical properties of SiO2 excited by femtosecond laser at the damage threshold and above, Phys. Rev. B **98**(15), 155110 (2018).

[63] N. M. Ravindra, J. Narayan, Optical properties of amorphous silicon and silicon dioxide, J. Appl. Phys. **60**(3), 1139–1146 (1986).

[64] R. Boscaino, E. Vella, G. Navarra, Absorption edge in silica glass, in *Proc. 2005 IEEE/LEOS Work. Fibres Opt. Passiv. Components, 2005.* (IEEE, 2005), volume 2005, 318–322.

[65] G. L. Tan, M. F. Lemon, D. J. Jones, R. H. French, Optical properties and London dispersion interaction of amorphous and crystalline SiO2 determined by vacuum ultraviolet spectroscopy and spectroscopic ellipsometry, Phys. Rev. B **72**(20), 205117 (2005).

[66] M. H. Mohd Zaid, K. A. Matori, S. H. Abdul Aziz, A. Zakaria, M. S. Mohd Ghazali, Effect of ZnO on the Physical Properties and Optical Band Gap of Soda Lime Silicate Glass, Int. J. Mol. Sci. **13**(6), 7550–7558 (2012).

[67] Y. Kondo, K. Miura, T. Suzuki, H. Inouye, T. Mitsuyu, K. Hirao, Three-dimensional arrays of crystallites within glass by using non-resonant femtosecond pulses, J. Non. Cryst. Solids **253**(1-3), 143–156 (1999).

[68] Y. Kondo, H. Inouye, S. Fujiwara, T. Suzuki, T. Mitsuyu, T. Yoko, K. Hirao, Wavelength dependence of photoreduction of Ag+ ions in glasses through the multiphoton process, J. Appl. Phys. **88**(3), 1244–1250 (2000).

[69] B. Fisette, M. Meunier, Femtosecond laser three-dimensional microstructuring inside photosensitive glasses, in J. C. Armitage, R. A. Lessard, G. A. Lampropoulos (eds.), *Photonics North 2004 Photonic Appl. Astron. Biomed. Imaging, Mater. Process. Educ.* (2004), volume 5578, 677.

[70] B. Fisette, F. Busque, J.-Y. Degorce, M. Meunier, Three-dimensional crystallization inside photosensitive glasses by focused femtosecond laser, Appl. Phys. Lett. **88**(9), 091104 (2006).

[71] B. T. Do, M. C. Phillips, P. A. Miller, M. W. Kimmel, J. Britsch, S.-H. Cho, Properties of optical breakdown in BK7 glass induced by an extended-cavity femtosecond laser oscillator, Opt. Express **17**(4), 2739 (2009).

[72] D. J. Little, M. Ams, M. J. Withford, Influence of bandgap and polarization on photo-ionization: guidelines for ultrafast laser inscription [Invited], Opt. Mater. Express **1**(4), 670 (2011).

[73] D. Paipulas, *Lūžio rodiklio modifikavimas stikluose ir kristaluose veikiant ultratrumpaisiais lazerio impulsais*, Ph.D. thesis, Vilnius University (2011).

[74] C. B. Schaffer, A. Brodeur, E. Mazur, Laser-induced breakdown and damage in bulk transparent materials induced by tightly focused femtosecond laser pulses, Meas. Sci. Technol. **12**(11), 1784–1794 (2001).

[75] S. M. Eaton, H. Zhang, P. R. Herman, F. Yoshino, L. Shah, J. Bovatsek, A. Y. Arai, Heat accumulation effects in femtosecond laser-written waveguides with variable repetition rate, Opt. Express **13**(12), 4708 (2005).

[76] M. Sakakura, M. Terazima, Oscillation of the refractive index at the focal region of a femtosecond laser pulse inside a glass, Opt. Lett. **29**(13), 1548 (2004).

[77] M. Sakakura, M. Terazima, Y. Shimotsuma, K. Miura, K. Hirao, Elastic and Thermal Dynamics in Femtosecond Laser-Induced Structural Change Inside Glasses Studied by the Transient Lens Method, Laser Chem. **2010**, 1–15 (2010).

[78] K. Bergner, B. Seyfarth, K. A. Lammers, T. Ullsperger, S. Döring, M. Heinrich, M. Kumkar, D. Flamm, A. Tünnermann, S. Nolte, Spatio-temporal analysis of glass volume processing using ultrashort laser pulses, Appl. Opt. **57**(16), 4618 (2018).

[79] L. Keldysh, Ionization in the field of a strong electromagnetic wave, Sov. Phys. JEPT **20**(5), 1307–1314 (1965).

[80] B. Rethfeld, Unified Model for the Free-Electron Avalanche in Laser-Irradiated Dielectrics, Phys. Rev. Lett. **92**(18), 187401 (2004).

[81] R. W. Boyd, *Nonlinear Optics, Third Edition* (Academic Press, Inc., Orlando, FL, USA, 2008), 3rd edition.

[82] S. Quan, J. Hong-Bing, L. Yi, Z. Yong-Heng, Y. Hong, G. Qi-Huang, Relaxation of dense electron plasma induced by femtosecond laser in dielectric materials, Chin. Phys. Lett. **23**(1), 189–192 (2006).

[83] A. Horn, E. Kreutz, R. Poprawe, Ultrafast time-resolved photography of femtosecond laser induced modifications in BK7 glass and fused silica, Appl. Phys. A **79**(4-6), 923–925 (2004).

[84] C. Mauclair, A. Mermillod-Blondin, K. Mishchik, J. Bonse, A. Rosenfeld, J. P. Colombier, R. Stoian, Excitation and relaxation dynamics in ultrafast laser irradiated optical glasses, High Power Laser Sci. Eng. **4**, e46 (2016).

[85] J. W. Chan, T. Huser, S. Risbud, D. M. Krol, Structural changes in fused silica after exposure to focused femtosecond laser pulses, Opt. Lett. **26**(21), 1726 (2001).

[86] S. M. Eaton, G. Cerullo, R. Osellame, Fundamentals of Femtosecond Laser Modification of Bulk Dielectrics, in *Femtosecond Laser Micromach.* (Springer, Berlin, Heidelberg, 2012), 3–18.

[87] W. Reichman, C. A. Click, D. M. Krol, Femtosecond laser writing of waveguide structures in sodium calcium silicate glasses, in J. Neev, C. B. Schaffer, A. Ostendorf, S. Nolte (eds.), *Proc. SPIE* (2005), volume 5714, 238.

[88] S. Matsuo, H. Sumi, S. Kiyama, T. Tomita, S. Hashimoto, Femtosecond laser-assisted etching of Pyrex glass with aqueous solution of KOH, Appl. Surf. Sci. **255**(24), 9758–9760 (2009).

[89] N. Varkentina, T. Cardinal, F. Moroté, P. Mounaix, P. André, Y. Deshayes, L. Canioni, Examination of femtosecond laser matter interaction in multipulse regime for surface nanopatterning of vitreous substrates, Opt. Express **21**(24), 29090 (2013).

[90] D. Gailevicius, V. Purlys, L. Maigyte, E. Gaizauskas, M. Peckus, R. Gadonas, K. Staliunas, Asymmetric 2D spatial beam filtering by photonic crystals, in H. Thienpont, J. Mohr, H. Zappe, H. Nakajima (eds.), *Micro-Optics 2016* (2016), volume 9888, 98880O.

[91] K. Hirao, K. Miura, Writing waveguides and gratings in silica and related materials by a femtosecond laser, J. Non. Cryst. Solids **239**(1-3), 91–95 (1998).

[92] M. Sakakura, K. Yoshimura, T. Kurita, M. Shimizu, Y. Shimotsuma, N. Fukuda, K. Hirao, K. Miura, Condensation of Si-rich region inside soda-lime glass by parallel femtosecond laser irradiation, Opt. Express **22**(13), 16493 (2014).

[93] K. M. Davis, K. Miura, N. Sugimoto, K. Hirao, Writing waveguides in glass with a femtosecond laser, Opt. Lett. **21**(21), 1729 (1996).

[94] G. D. Marshall, A. Politi, J. C. F. Matthews, P. Dekker, M. Ams, M. J. Withford, J. L. O'Brien, Laser written waveguide photonic quantum circuits, Opt. Express **17**(15), 12546 (2009).

[95] Y. Nasu, M. Kohtoku, Y. Hibino, Low-loss waveguides written with a femtosecond laser for flexible interconnection in a planar light-wave circuit, Opt. Lett. **30**(7), 723 (2005).

[96] H.-G. Treusch, A. Ovtchinnikov, X. He, M. Kanskar, J. Mott, S. Yang, High-brightness semiconductor laser sources for materials processing: stacking, beam shaping, and bars, IEEE J. Sel. Top. Quantum Electron. **6**(4), 601–614 (2000).

[97] P. Shukla, J. Lawrence, Y. Zhang, Understanding laser beam brightness: A review and new prospective in material processing, Opt. Laser Technol. **75**, 40–51 (2015).

[98] J. Durnin, J. J. Miceli, J. H. Eberly, Diffraction-free beams, Phys. Rev. Lett. **58**(15), 1499–1501 (1987).

[99] A. Marcinkevicius, S. Juodkazis, S. Matsuo, V. Mizeikis, H. Misawa, Application of Bessel Beams for Microfabrication of Dielectrics by Femtosecond Laser, Jpn. J. Appl. Phys. **40**(Part 2, No. 11A), L1197–L1199 (2001).

[100] J. Amako, D. Sawaki, E. Fujii, Microstructuring transparent materials by use of nondiffracting ultrashort pulse beams generated by diffractive optics, J. Opt. Soc. Am. B **20**(12), 2562 (2003).

[101] R. Stoian, M. K. Bhuyan, G. Zhang, G. Cheng, R. Meyer, F. Courvoisier, Ultrafast Bessel beams: Advanced tools for laser materials processing, Adv. Opt. Technol. **7**(3), 165–174 (2018).

[102] M. Mikutis, T. Kudrius, G. Šlekys, D. Paipulas, S. Juodkazis, High 90% efficiency Bragg gratings formed in fused silica by femtosecond Gauss-Bessel laser beams, Opt. Mater. Express **3**(11), 1862 (2013).

[103] A. Inyushov, P. Safronova, I. Trushnikov, A. Sarkyt, V. Shandarov, Formation of Photonic Structures in Photorefractive Lithium Niobate by 1D and 2D Bessel-like Optical Fields, J. Phys. Conf. Ser. **867**(1), 012023 (2017).

[104] P. K. Velpula, M. K. Bhuyan, F. Courvoisier, H. Zhang, J. P. Colombier, R. Stoian, Spatio-temporal dynamics in nondiffractive Bessel ultrafast laser nanoscale volume structuring, Laser Photon. Rev. **10**(2), 230–244 (2016).

[105] V. Garzillo, V. Jukna, A. Couairon, R. Grigutis, P. Di Trapani, O. Jedrkiewicz, Optimization of laser energy deposition for single-shot high aspect-ratio microstructuring of thick BK7 glass, J. Appl. Phys. **120**(1), 013102 (2016).

[106] S. Maruo, O. Nakamura, S. Kawata, Three-dimensional microfabrication with two-photon-absorbed photopolymerization, Opt. Lett. **22**(2), 132 (1997).

[107] G. D. Marshall, M. Ams, M. J. Withford, Femtosecond inscription of wavelength specific features in optical waveguide structures, in G. C. Righini (ed.), *Integr. Opt. Silicon Photonics, Photonic Integr. Circuits* (2006), volume 6183, 61830Q.

[108] M. Malinauskas, A. Žukauskas, S. Hasegawa, Y. Hayasaki, V. Mizeikis, R. Buividas, S. Juodkazis, Ultrafast laser processing of materials: from science to industry, Light Sci. Appl. **5**(8), e16133–e16133 (2016).

[109] M. Campbell, D. N. Sharp, M. T. Harrison, R. G. Denning, A. J. Turberfield, Fabrication of photonic crystals for the visible spectrum by holographic lithography, Nature **404**(6773), 53–56 (2000).

[110] C. K. Ullal, M. Maldovan, E. L. Thomas, G. Chen, Y.-J. Han, S. Yang, Photonic crystals through holographic lithography: Simple cubic, diamond-like, and gyroid-like structures, Appl. Phys. Lett. **84**(26), 5434–5436 (2004).

[111] S. Wilbrandt, O. Stenzel, N. Kaiser, Experimental determination of the refractive index profile of rugate filters based on in situ measurements of transmission spectra, J. Phys. D. Appl. Phys. **40**(5), 1435–1441 (2007).

[112] R. J. Martín-Palma, C. G. Pantano, A. Lakhtakia, Replication of fly eyes by the conformal-evaporated-film-by-rotation technique, Nanotechnology **19**(35), 355704 (2008).

[113] L. Jonušauskas, D. Gailevičius, S. Rekštytė, T. Baldacchini, S. Juodkazis, M. Malinauskas, Mesoscale laser 3d printing, Opt. Express **27**(11), 15205–15221 (2019).

[114] https://www.lumerical.com/products/fdtd/ Retrieved 2019-06-09 (2019).

[115] J. Chandezon, G. Raoult, D. Maystre, A new theoretical method for diffraction gratings and its numerical application, J. Opt. **11**(4), 235–241 (1980).

[116] J. Chandezon, M. T. Dupuis, G. Cornet, D. Maystre, Multicoated gratings: a differential formalism applicable in the entire optical region, J. Opt. Soc. Am. **72**(7), 839 (1982).

[117] L. Li, Multilayer-coated diffraction gratings: differential method of Chandezon et al. revisited: errata, J. Opt. Soc. Am. A **13**(3), 543 (1996).

[118] L. Li, J. Chandezon, G. Granet, J.-P. Plumey, Rigorous and efficient grating-analysis method made easy for optical engineers, Appl. Opt. **38**(2), 304 (1999).

[119] https://www.microresist.de/sites/default/files/download/ PI_OrmoComp_OrmoClearFX_2015_0.pdf Retrieved 2019-06-09.

[120] K. S. Harsha (ed.), *Principles of Vapor Deposition of Thin Films* (Elsevier, 2006).

[121] T. Tolenis, L. Grinevičiūtė, R. Buzelis, L. Smalakys, E. Pupka, S. Melnikas, A. Selskis, R. Drazdys, A. Melninkaitis, Sculptured anti-reflection coatings for high power lasers, Opt. Mater. Express **7**(4), 1249 (2017).

[122] T. Tolenis, L. Grineviciute, L. Mažule, A. Selskis, R. Drazdys, Low-stress phase plates produced by serial bideposition of TiO 2 thin films, J. Nanophotonics **10**(3), 036003 (2016).

[123] L. Grinevičiūtė, M. Andrulevičius, A. Melninkaitis, R. Buzelis, A. Selskis, A. Lazauskas, T. Tolenis, Highly Resistant Zero-Order Waveplates Based on All-Silica Multilayer Coatings, Phys. status solidi **214**(12), 1700764 (2017).

[124] T. Tolenis, L. Grinevičiūtė, L. Smalakys, M. Ščiuka, R. Drazdys, L. Mažulė, R. Buzelis, A. Melninkaitis, Next generation highly resistant mirrors featuring all-silica layers, Sci. Rep. **7**(1), 10898 (2017).

[125] A. Balcytis, T. Tolenis, X. Wang, G. Seniutinas, R. Drazdys, P. R. Stoddart, S. Juodkazis, Percolation threshold gold films on columnar coatings: characterisation for SERS applications, Appl. Surf. Sci. **481**(February), 353–359 (2016).

[126] T. Tolenis, S. E. Swiontek, A. Lakhtakia, Structural colours of nickel bioreplicas of butterfly wings, J. Mod. Opt. **64**(8), 781–786 (2017).

[127] J. J. Zayhowski, Microchip lasers, Opt. Mater. (Amst). **11**(2-3), 255–267 (1999).

[128] R. M. e. Rainer Michalzik (auth.), *VCSELs: Fundamentals, Technology and Applications of Vertical-Cavity Surface-Emitting Lasers*, Springer Series in Optical Sciences 166 (Springer-Verlag Berlin Heidelberg, 2013), 1 edition.

[129] V. Purlys, L. Maigyte, D. Gailevičius, M. Peckus, M. Malinauskas, K. Staliunas, Spatial filtering by chirped photonic crystals, Phys. Rev. A **87**(3), 033805 (2013).

[130] D. Gailevicius, V. Koliadenko, V. Purlys, M. Peckus, V. Taranenko, K. Staliunas, Photonic Crystal Microchip Laser, Sci. Rep. **6**(1), 34173 (2016).

[131] E. Popov, Chapter 7: Differential theory of periodic structures, in E. Popov (ed.), *Gratings: Theory and Numerical Applications* (Presses Universitaires de Provence, Aix Marseille Université, Institut Fresnel UMR 7249, 2014), chapter 7.

[132] M. G. Moharam, T. K. Gaylord, Rigorous coupled wave analysis of planar-grating diffraction, J. Opt. Soc. Amer. **71**, 811–818 (1981).

[133] M. Nevieère, E. Popov, *Light propagation in periodic media* (Marcel Dekker, Inc., New York, Basel, 2003).

[134] D. Grobnic, S. Mihailov, C. Smelser, H. Ding, Sapphire Fiber Bragg Grating Sensor Made Using Femtosecond Laser Radiation for Ultrahigh Temperature Applications, IEEE Photonics Technol. Lett. **16**(11), 2505–2507 (2004).

[135] M. Malinauskas, A. Žukauskas, S. Hasegawa, Y. Hayasaki, V. Mizeikis, R. Buividas, S. Juodkazis, Ultrafast laser processing of materials: from science to industry, Light: Science & Applications **5**(8), e16133 (2016).

[136] S. Juodkazis, K. Yamasaki, V. Mizeikis, S. Matsuo, H. Misawa, Formation of embedded patterns in glasses using femtosecond irradiation, Appl. Phys. A **79**(4-6), 1549–1553 (2004).

[137] J. Li, B. Jia, G. Zhou, M. Gu, Fabrication of three-dimensional woodpile photonic crystals in a PbSe quantum dot composite material, Opt. Express **14**(22), 10740 (2006).

[138] Y. Shimotsuma, P. G. Kazansky, J. Qiu, K. Hirao, Self-Organized Nanogratings in Glass Irradiated by Ultrashort Light Pulses, Phys. Rev. Lett. **91**(24), 247405 (2003).

[139] D.-M. Song, Z.-X. Tang, L. Zhao, Z. Sui, S.-C. Wen, D.-Y. Fan, Experimental demonstration of a low-pass spatial filter based on a one-dimensional photonic crystal with a defect layer, Chin. Phys. Lett. **30**(4), 044206 (2013).

[140] S. Takimoto, T. Tachikawa, R. Shogenji, J. Ohtsubo, Control of Spatio-Temporal Dynamics of Broad-Area Semiconductor Lasers by Strong Optical Injection, IEEE Photonics Technol. Lett. **21**(15), 1051–1053 (2009).

[141] S. K. Mandre, I. Fischer, W. Elssser, Control of the spatiotemporal emission of a broad-area semiconductor laser by spatially filtered feedback, Opt. Lett. **28**(13), 1135 (2003).

[142] J. Martín-Regalado, G. H. M. van Tartwijk, S. Balle, M. S. Miguel, Mode control and pattern stabilization in broad-area lasers by optical feedback, Phys. Rev. A **54**(6), 5386–5393 (1996).

[143] J.-l. Li, K.-i. Ueda, L.-x. Zhong, M. Musha, A. Shirakawa, Efficient excitations of radially and azimuthally polarized Nd^3+:YAG ceramic microchip laser by use of subwavelength multilayer concentric gratings composed of Nb_2O_5/SiO_2, Opt. Express **16**(14), 16841 (2008).

[144] J. Saikawa, S. Kurimura, I. Shoji, T. Taira, Tunable frequency-doubled Yb:YAG microchip lasers, Opt. Mater. (Amst). **19**(1), 169–174 (2002).

[145] D.-S. Song, Y.-J. Lee, H.-W. Choi, Y.-H. Lee, Polarization-controlled, single-transverse-mode, photonic-crystal, vertical-cavity, surface-emitting lasers, Appl. Phys. Lett. **82**(19), 3182–3184 (2003).

[146] G. Salamu, F. Jipa, M. Zamfirescu, N. Pavel, Laser emission from diode-pumped Nd:YAG ceramic waveguide lasers realized by direct femtosecond-laser writing technique, Opt. Express **22**(5), 5177 (2014).

[147] M. Nixon, B. Redding, A. A. Friesem, H. Cao, N. Davidson, Efficient method for controlling the spatial coherence of a laser, Opt. Lett. **38**(19), 3858 (2013).

[148] T. Yu, F. Gao, X. Zhang, X. Yuan, B. Xiong, The design of two-lens slit spatial filter for high power laser system, in Y. Yang (ed.), *Tenth Int. Conf. Inf. Opt. Photonics* (SPIE, 2018), November 2018, 118.

[149] S. Zhouping, L. Qihong, D. Jingxing, Z. Jun, W. Runrong, Beam quality improvement of laser diode array by using off-axis external cavity, Opt. Express **15**(19), 11776 (2007).

[150] E. Kintzer, J. Walpole, S. Chinn, C. Wang, L. Missaggia, High-power, strained-layer amplifiers and lasers with tapered gain regions, IEEE Photonics Technol. Lett. **5**(6), 605–608 (1993).

[151] J. P. Leidner, J. R. Marciante, Beam Quality Improvement in Broad-Area Semiconductor Lasers via Evanescent Spatial Filtering, IEEE J. Quantum Electron. **48**(10), 1269–1274 (2012).

[152] M. Chi, N.-S. Bøgh, B. Thestrup, P. M. Petersen, Improvement of the beam quality of a broad-area diode laser using double feedback from two external mirrors, Appl. Phys. Lett. **85**(7), 1107–1109 (2004).

[153] B. Leonhäuser, H. Kissel, A. Unger, B. Köhler, J. Biesenbach, Feedback-induced catastrophic optical mirror damage (COMD) on 976nm broad area single emitters with different AR reflectivity, in M. S. Zediker (ed.), *SPIE Proc. Vol. 8965* (2014), 896506.

[154] R. Diehl (ed.), *High-Power Diode Lasers*, volume 78 of *Topics in Applied Physics* (Springer Berlin Heidelberg, Berlin, Heidelberg, 2000).

[155] A. Jechow, V. Raab, R. Menzel, High cw power using an external cavity for spectral beam combining of diode laser-bar emission, Appl. Opt. **45**(15), 3545 (2006).

NOTES

NOTES

NOTES